Interval Approximations for Fully Commutative Quivers and Their Applications
完全可換クイバーの区間近似とその応用

by

Chenguang Xu / 許 晨光

A Doctoral Thesis

Thesis Supervisor: Yasuaki Hiraoka / 平岡 裕章
Professor of Kyoto University Institute for Advanced Study

京都大学
KYOTO UNIVERSITY

Abstract

The study of multiparameter persistent homology, a central concept in topological data analysis, has seen significant advancements in recent years. However, a key challenge in this domain is the lack of a complete and discrete invariant that effectively encapsulates the topological persistence information of data. To address this challenge, our research proposes an enriched framework for investigating representations of a fully commutative quiver. This approach utilizes interval subquivers, employing a synthesis of interpretations derived from using these interval subquivers to query an arbitrary representation. By doing so, it allows for a holistic understanding of the original representation. Within this framework, we introduce the concept of "partial interval approximation". This invariant allows us to tune the balance between approximation resolution and computational complexity. This balance is crucial for handling complex data sets where a balance between computational efficiency and in-depth analytical precision is under concern. We evaluate this framework on commutative ladders of both finite-type and infinite-type. For finite-type commutative ladders, our approach successfully identifies an efficient method for computing the indecomposable decomposition of an arbitrary representation. This method leverages zigzag representations, which determine the multiplicity functions of both intervals and non-intervals in finite-type commutative ladders using only one-parameter persistent homology. For infinite-type commutative ladders, we introduce a new invariant that reveals persistence in the second parameter by connecting two standard persistence diagrams using interval approximations. This discovery opens a new avenue in the visualization of topological persistence that was previously challenging to express. Building on these insights, we subsequently present several models for constructing commutative ladder filtrations. These models provide a flexible way for a wide range of applications to adapt. We then demonstrate computational examples of random filtrations and point cloud data, offering fresh insights and showcasing the potential of our toolkit's effectiveness in analyzing the topology of data.

Acknowledgements

First and foremost, I extend my deepest gratitude to my supervisor, Professor Yasuaki Hiraoka, for his invaluable guidance, unwavering support, and insightful critiques throughout my research journey. His expertise and mentorship have been pivotal in shaping the direction and quality of this thesis. Professor Hiraoka's dedication to excellence, combined with his patient and encouraging approach, has significantly contributed to my professional and personal growth. His ability to challenge my ideas while providing constructive feedback has been instrumental in refining my research methodologies and thought processes.

I am extremely grateful for the insightful suggestions and constructive comments from Doctor Ken Nakashima and Professor Ippei Obayashi. Their comprehensive reviews and critical perspectives have been beneficial in refining my work, enhancing its quality, and ensuring its academic rigor. The collaborative sessions and in-depth discussions with them have opened new avenues of thought and have been essential in advancing my thesis to its current state.

I am also grateful to both the current and past members, as well as the administrative staff, of the Hiraoka Laboratory. The camaraderie and collaborative atmosphere within the lab have created a rich and stimulating environment for academic growth. The teamwork, shared experiences, and intellectual exchanges have broadened my horizons and contributed to a dynamic and productive research environment.

I am deeply indebted to Professor Kathryn Hess Bellwald for her invaluable support and guidance during my studies at EPFL. Her extensive knowledge, innovative thinking, and passion for research have been a great source of inspiration. Her encouragement to pursue challenging topics and advice on academic choices have been invaluable in shaping my academic direction.

I wish to extend my gratitude for the financial support that contributed to my doctoral studies. This includes the Institute of Physical and Chemical Research's Junior Research Associate Program, the Japan Science and Technology Agency's Support for Pioneering Research Initiated by the Next Generation, and the Kyoto University Science and Technology Innovation Creation Fellowship.

Completing this thesis has been a transformative journey, and I am deeply grateful to my family and friends, and everyone who has been a part of it for their support and encouragement throughout this endeavor. The knowledge gained, the challenges overcome, and the people I have met along the way have all enriched my life in immeasurable ways. This journey has not only contributed to my academic growth but has also profoundly impacted my personal development, instilling in me values such as perseverance, critical thinking, and a deep appreciation for collaborative learning and intellectual diversity.

Contents

Notations

$\mathsf{CL}(n)$ equi-oriented commutative ladder of length n

$\mathsf{Course}(G)$ set of all courses on G

δ_M^ξ interval approxmiation of M via ξ-compressed multiplicity functions

$\underline{\dim}$ dimension vector of a representation

$\vec{G}_{p,q}$ equi-oriented commutative grid

$\mathbb{I}_G$ set of interval subquivers of a quiver G

$\mathbf{rep}(Q, R)$ category of representations of (Q, R)

$\mathcal{L}$ complete set of representatives of isomorphism classes of indecomposable representations of a quiver with relations

$\mathfrak{h}$ Hasse quiver operation

$\mathsf{n\text{-}Score}'_c$ inferred non-interval score with the constant weight function

$\mathsf{n\text{-}Score}_c$ non-interval score with the constant weight function

$\mathsf{n\text{-}Score}_l$ non-interval score with the logistic weight function

τ_n orientation of arrows in a type A_n quiver

$\mathsf{tour}_{(C,F)}(G)$ tour on a course (C, F) in G

$\vec{A}_n$ equi-oriented type $\mathbb{A}_n$ quiver

ξ essential assignment

A_n type $\mathbb{A}_n$ quiver

$c_M^\xi(I)$ ξ-compressed multiplicity of M on the interval I

d multiplicity function in the Krull-Schmidt theorem

$E(I)$ set of essential vertices of an interval representation I

$G_{p,q}$ commutative grid $A_p \otimes A_q$

R_Q^{fc} set of full commutativity relations of a quiver Q

V_I interval representation associated with an interval subquiver I

1 Introduction

1.1 A Brief History

The journey of Topological Data Analysis (TDA) dates back to the ancient roots of topology itself, the name of which originates from the Greek words *topos* (place) and *logos* (study), reflecting an early philosophical underpinnings that laid the groundwork for a more rigorous mathematical exploration.

Like many other mathematical disciplines, the Renaissance era stands as a pivotal formal initialization phase of topology. Heralded by René Descartes's introduction of the Cartesian coordinate system along with the advent of analytic geometry, the way people understand geometric objects is revolutionized. This integration of algebra into geometry profoundly influenced the development of mathematical concepts and methodologies, laying a crucial foundation for advancements in topology and beyond. One of this era's most influential figures was Leonhard Euler, whose work on the Seven Bridges of Königsberg abstracting the city's bridges and landmasses into a graph and a question about connectivity is often regarded as a foundational milestone in the history of topology [19]. Euler later introduced the concept of Euler characteristic in his famous polyhedron formula $\chi = V - E + F$, a topological invariant still widely used today. The term *topology* itself was coined in the 1840s by German mathematician Johann Benedict Listing in his seminal work *Vorstudien zur Topologie*(1847) [34], which focused on the study of geometric properties that are preserved under continuous deformations. Later, in the 1850s, Bernhard Riemann defined the genus as a way to classify Riemann surfaces by counting the number of handles [47]. The word "genus" is borrowed from biology, meaning "kind or class of things" in Latin, which captures the idea of classifying surfaces by their topological types. Another key concept in this fast-evolving era is Betti numbers, firstly introduced by Enrico Betti in his 1871 paper [6], offered a method to distinguish topological spaces by examining the connectivity of n-dimensional holes. This innovative idea was a precursor to the more complex homology theories, which is credited to Henri Poincaré in his groundbreaking work *Analysis Situs* [43] published in 1895, which laid the foundation of algebraic topology, where he introduced the concept of homotopy and homology to distinguish topological spaces. Poincaré is also the first person to use the term "homology", which is also borrowed from biology and means "the study of the same" in Greek.

Fast-forward to the 1990s, the development of algebraic topology has been significantly influenced by the advent of computers. This period saw a surge in data availability, necessitating new methods for its analysis. Computational topology, thus, evolved in response to these demands, marking a shift towards more data-driven approaches in the field. This era signaled a convergence of traditional topology with modern computational techniques, enriching the discipline with enhanced analytical capabilities and broader applicability in various data-intensive domains. Object recognition in computer vision is such an example in the pre-deep learning era. Research in this period, constrained by computational power, primarily focused on feature engineering. In the 1992 paper *Measuring shapes by size functions* by Patrizio Frosini [20], "size functions" were introduced for recognizing similar objects. Although the word persistent was not used in this paper, his idea is equivalent to the concept of 0-dimensional persistent homology. The first known usage of the term *persistent* in the context of studying topological spaces is in the 1999 paper *Towards Computing Homology from Finite Approximations* by Vanessa Robins [48]. This paper introduced the concept of persistent Betti numbers for analyzing the topological structure of dynamical systems. This term is derived from its verb form *persist*, where the author mentioned that

> "... We show that the inclusion maps are necessary to identify topological features in an ϵ-neighborhood that **persist** in the limit as $\epsilon \to 0$."

The etymology of "persist", combining the Latin words "per" (thoroughly) and "sistere" (to stand), aptly highlights the idea of catching topological features that are robust and enduring.

The historical arc reaches a pivotal point with the paper *Topological Persistence and Simplification* by Edelsbrunner, Letscher, and Zomorodian [14]. This work introduced the concept of persistence independently from Robins' work [48] [1], formalized the notion of filtration as a growing simplicial complex, firstly used the term persistent homology in mathematics, provided an algorithm to compute it, and visualized the results using k-intervals (known as barcodes today). The speed of the development of TDA has been accelerating since then. The paper *Computing Persistent Homology* by Zomorodian and Carlsson is a significant milestone in the development of TDA [52]. This work placed persistent homology within the classical framework of algebraic topology by building a single structure that contains all the elements in a filtration of modules. Specifically, they reveal a key correspondence between the persistence module $\mathcal{M} := \{ M^i, \varphi^I \}_{i \geq 0}$ over a ring R and the graded module $\alpha(\mathcal{M}) := \bigoplus_{i=0}^{\infty} M^i$ over the polynomial ring $R[z]$, where the action of the indeterminate z is given by $t \cdot (m^0, m^1, \dots) := (0, \varphi^0(m^0), \varphi^1(m^1), \dots)$, effectively shifting up the grading of each element by one using the morphism $\varphi^i \colon M^i \to M^{i+1}$. In particular, if R is a field, then $R[z]$ is a principal ideal domain (PID). Then the structure theorem for finitely generated modules over a PID applies to $\alpha(\mathcal{M})$, which states that

$$\alpha(\mathcal{M}) \cong \bigoplus_{s=1}^{m} R[z](i_s) \oplus \bigoplus_{t=1}^{n} \big(R[z]/\langle z^{l_t} \rangle\big)(j_t),$$

[1] "Finally, we note that Robins has independently formulated an alternate but equivalent definition of persistence ..." [14].

where the notation $\square(i)$ means the module $\square$ is shifted up by i. An immediate consequence of this theorem is a discrete complete invariant for persistence modules over a field, which can be expressed in the form of birth-death pairs as $\{ [i_s, \infty) \}_{s=1}^{m} \cup \{ [j_t, j_t + l_t) \}_{t=1}^{n}$. Building on the foundations of one-parameter persistence, the concept of persistence was further generalized to multiparameter filtrations by Carlsson and Zomorodian in their 2007 paper *The theory of multidimensional persistence* [9] [2]. Parallel to the one-parameter case, they identified a multiparameter persistence module as a finitely generated graded module over a multivariate polynomial ring. Then, they show that this structure can be classified using a set of orbit spaces, which does not have a precise parameterization. This challenging outcome has been stimulating ongoing research efforts in TDA, driving advancements and deeper exploration. This result highlighted the significant distinction between one-parameter and multiparameter persistence, underscoring the complexity and the potential of multiparameter persistence, encouraging further research in this area. The 2008 paper *TOPOLOGY AND DATA* by Gunnar Carlsson [7], a cornerstone in the field, established the connection between persistent homology and data analysis. It elaborated on various topology-inspired methods for interpreting data, showcasing their applications in areas like image processing and neuroscience. This work not only underscores the relevance of topological techniques in data analysis but also broadens the scope of their practical utility in diverse scientific domains. Almost concurrently, Carlsson and de Silva's paper *Zigzag Persistence* introduced quiver representation theory to the study of persistence modules [8], making the theory of TDA accessible to Gabriel's theorem — a fundamental result in the representation theory of quivers. In addition, this work enhances the scope of one-parameter persistence modules by allowing the arrows to go in either direction, making the theory of TDA more versatile and is crucial for the research of this thesis.

Advancing to the 2010s, research in the TDA community has rapidly expanded across various subfields, including but not limited to the stability theory, multiparameter persistence, topological machine learning, and applications in various domains. Moving forward, we will focus on several key publications that are directly aligned with our research interests. A pioneering work in providing a comprehensible toolkit for multiparameter persistent homology is the 2015 paper *Interactive Visualization of 2-D Persistence Modules* by Lesnick and Wright [31]. Aimed at making multiparameter persistent homology more accessible to data practitioners, it developed the theory and implemented the algorithm to explore a 2-D persistence module by taking 1-D slices and visualizing via persistence diagrams. Escolar and Hiraoka's work *Persistence Modules on Commutative Ladders of Finite Type* introduced a structure called *commutative ladders* to compare two one-parameter persistence modules [18]. They conducted a study of persistence modules on this structure using the Auslander-Reiten theory, and also defined a generalized form of persistence diagrams using Auslander-Reiten quivers.

There are multiple works on generalizing persistence diagrams to diverse settings, with the hope of extending both the theoretical framework and the applicability of TDA to a broader range of problems. Amit Patel's work *Generalized Persistence Diagrams* gener-

[2] Originally termed "multidimensional persistence", this concept has later been renamed as "multiparameter persistence", avoiding potential confusion with "dimension" in homology dimension.

alizes persistence diagrams to constructible persistence modules valued in a symmetric monoidal category and demonstrates the feasibility of using Möbius inversion to compute them [42]. As an approach to address the challenge of studying multiparameter persistence modules, Asashiba and collaborators resorted to the representation theory of quivers and algebras and focused on interval representations, which is a subclass of persistence modules that are easier to study. In their 2018 work *On interval decomposability of 2D persistence modules*, finer classification of interval representations was proposed, and a criterion for determining whether a persistence module is interval indecomposable or not without computing its decomposition is provided [1]. Their 2019 work *On approximation of 2D persistence modules by interval-decomposables* introduced the concept of interval approximation as an invariant for 2D persistence modules, which serves as a building component for crafting several invariants in multiparameter persistence, and is going to be generalized in this thesis [3]. In *Approximation by interval-decomposables and interval resolutions of persistence modules*, the authors studied persistence modules using interval resolutions and show that the interval resolution global dimension is finite for finite posets [2]. Comparable work has also been done mainly from the perspective of the representation theory of posets. Kim et al. proposed the generalized rank invariant in *Generalized persistence diagrams for persistence modules over posets* [28] and demonstrated how it could be computed using zigzag persistence in *Computing Generalized Rank Invariant for 2-Parameter Persistence Modules via Zigzag Persistence and Its Applications* [12]. In the paper *Bigraded Betti numbers and Generalized Persistence Diagrams* [29], Kim et al. showed how the bigraded Betti numbers can be calculated from the generalized rank invariants. The paper *Signed Barcodes for Multi-Parameter Persistence via Rank Decompositions and Rank-Exact Resolutions* by Botnan et al. introduced the concept of signed barcodes as a new visual representation for multiparameter persistence modules.

Applications

The success of one-parameter persistent homology is evident in its fruitful applications across diverse domains where data are abundant. In the field of cosmology, [51] uses persistent homology to find homology generators from dimension 0 to 2 in cosmological datasets, which can provide valuable information on the sum of neutrino masses; [45] introduces a multiscale topological description of the cosmic matter distribution, providing a powerful tool to describe the rich connectivity structure in the cosmic web; [44] studies the topology of the cosmic microwave background radiation and shows that a significant difference exists between the observed data and the theoretical model. TDA also finds extensive usage in medical imaging, attributed to the rich sources of imaging data. The work [10] initializes the usage of persistence diagrams in medical imaging by showing that the homological structures are distinct over cortical thickness data from different groups; [37] identifies a subgroup of breast cancers using a tool from TDA called Mapper; [41] compares the results of TDA and texture analysis when used in the classification of hepatic tumors based on imaging data. Material science, a domain where point cloud data in rich supply, has witnessed a wide range of successful TDA applications. The study [22] proposes a topological method that classifies the one-dimensional homology structures in atomic configurations of amorphous solids into different orders; [27] combines TDA

and molecular dynamics to study and distinguish amorphous ices of different densities; [49] uses persistent homology to identify the contributions of different medium-range order structures in amorphous materials to the first sharp diffraction peak.

This is far from an exhaustive list. TDA also finds applications in fields as diverse as botany [32], protein structure analysis [50], genomics [46], and quantitative biology [35]. Additionally, the Database of Original & Non-Theoretical Uses of Topology (DONUT) [13] provides a rich repository of TDA applications across various domains. These applications underscore the transformative impact of TDA and persistent homology, reflecting their broad impact and utility in various scientific and engineering fields.

1.2 Contributions and Thesis Structure

In this thesis, we introduce a refined theoretical framework for the study of multiparameter persistence modules via the language of the representations of fully commutative quivers. We formulate the concept of "tours" and "courses", which serve as innovative tools for tracing selected compositions of paths within a quiver. Building on this, we generalize the idea of boundary compression and enrich the established concept of interval approximation proposed in [3] as a linear combination of these courses. Our approach offers heightened flexibility and precision in extracting information from a representation using intervals compared with existing methods. As we apply the new framework to two-dimensional commutative grids, a challenge arises: the exponential growth in the number of intervals makes the computation of interval approximations impractical. To address this, we introduce the concept of "partial interval approximation", an invariant designed to tune the balance between the number of examined intervals and the resolution of the approximation reached.

We then validate our new framework on a specific family of fully commutative quivers known as commutative ladders [18], characterized by a two-parameter configuration where the second parameter changes only once (see Figure 1.1). Commutative ladders provide a feasible and valuable testbed for our framework. When the ladder length of it is equal to or below four, it possesses a finite representation type, and we can maintain a complete discrete invariant, analogous to the scenario in one-parameter persistent homology. In this scenario, our framework simplifies the computation of indecomposable decomposition, leveraging one-parameter zigzag persistence and circumventing the complexities associated with 2D representation calculations. This streamlined process unveils new types of courses and opens a new door for exploring non-interval representations, a hitherto under-investigated aspect of multiparameter persistence modules. When the ladder length is above four, we have infinite-type commutative ladders. For them, we propose a new invariant: the connected persistence diagram. It visualizes persistence in both directions by combining two standard persistence diagrams and then connects homology generators according to their non-horizontal persistence measured by an interval approximation.

The two approaches above enable the exploration of topological structures in datasets that can be fitted to a commutative ladder filtration. To complete the picture and facilitate applicability, we present several models tailored for constructing commutative lad-

der filtrations of simplicial complexes, illustrating new techniques to create filtrations from point cloud data or random simplicial complexes. We then showcase the versatility of our toolkit through a series of computational demonstrations. Specifically, we study the topological structures of random simplicial complexes and atomic arrangements using commutative ladder configurations. Our computational outcomes highlight the effectiveness of the new framework and commutative ladders as a tool for studying complex data structures. Notably, non-interval components exhibit a markedly lower proportion in configurations derived from point cloud data.

Overall, our contributions provide a deeper, more comprehensive, and computationally accessible approach to understanding representations of fully commutative quivers. Our research not only provides a framework in the theoretical study of representations but also stands as an effective tool in the analysis of complex datasets.

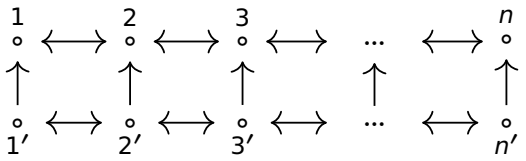

Figure 1.1: A length-n commutative ladder. The symbol $\leftrightarrow$ means either $\leftarrow$ or $\rightarrow$. Orientations in the two rows are assumed to be identical, and each square commutes.

The main result of this thesis is based on [24].

Outline

This thesis is organized as follows. Chapter 2 establishes the relevant background and notations used throughout this paper. Chapter 3 refines interval approximations, proposes partial interval approximations, and demonstrates how our framework can be used to construct persistence diagrams of a slice in a 2D persistence module as proposed in RIVET [31]. In Chapter 4, we apply our framework to finite-type commutative ladders, yielding an efficient method for computing any indecomposable decomposition; and to infinite-type commutative ladders, defining a new diagram to visualize the interval approximations. Chapter 5 introduces several models for building up commutative ladder filtrations. In Chapter 6, we employ the new toolkit to analyze the topological properties of filtrations generated from the models above. We conclude with an overview of our advancements and future research directions in Chapter 7.

The source code, along with the associated data, can be accessed through the dedicated webpage referenced in [23].

2 Preliminaries

This section reviews key concepts in quiver representations and persistent homology and fixes conventions. Details and proofs can be found in [5], [3] and [40]. We adhere to a fixed base field $\Bbbk$ throughout this paper.

2.1 Representations of Quivers with Relations

Definition 2.1.

- A *quiver* $Q = (Q_0, Q_1, \mathfrak{s}, \mathfrak{t})$ is a directed multigraph consisting of a vertex set Q_0, an arrow set Q_1 and two maps $\mathfrak{s}, \mathfrak{t} \colon Q_1 \to Q_0$ assigning the start and target for each arrow in Q_1. This quiver is called *finite* if both Q_0 and Q_1 are finite sets.
- A vertex $u \in Q_0$ is referred to as a *source* if it has no arrows pointing toward it, and a *sink* if it has no arrows originating from it.
- A *path* p from vertex u to vertex v is a finite sequence of concatenable arrows in Q_1, written as $p = (v|\alpha_l \cdots \alpha_1|u)$, where $\mathfrak{s}(\alpha_1) = u$, $\mathfrak{t}(\alpha_i) = \mathfrak{s}(\alpha_{i+1})$ for $i = 1, \ldots, l-1$, and $\mathfrak{t}(\alpha_l) = v$. Following the function composition convention, the arrows are ordered from right to left. If the starting vertex and the target vertex are clear from the context, they are omitted, and the path is written as $\alpha_l \cdots \alpha_1$. The maps $\mathfrak{s}$ and $\mathfrak{t}$ can be extended to the set of paths, by defining $\mathfrak{s}(p) = \mathfrak{s}(\alpha_1)$ and $\mathfrak{t}(p) = \mathfrak{t}(\alpha_l)$.
- A path's *length* is the number of arrows it contains.
- Paths p_1 and p_2 are *parallel*, denoted by $p_1 /\!/ p_2$, if they share the same starting and target vertices.
- Every vertex $u \in Q_0$ is associated with a unique length-zero path, called the *trivial path*, denoted as $\varepsilon_u = (u||u)$. Each vertex and its trivial path can be regarded as equivalent.
- For a non-negative integer l, define Q_l as the set of paths in Q of length l, and $Q_{\geq n} := \bigcup_{l \geq n} Q_l$.

- We can construct a unital associative $\Bbbk$-algebra with the underlying vector space being the free $\Bbbk$-module generated by $Q_{\geq 0}$, and the product is given by the concatenation of paths. This associative algebra is called the *path algebra* $\Bbbk Q$ of Q. Also, from the concatenation of paths, a quiver can be naturally regarded as a category.
- A quiver Q is said to be *acyclic* if it does not contain any cycles, *i.e.*, a non-trivial path that starts and ends at the same vertex.

Example 2.2. A quiver is of *type* $\mathbb{A}_n$ if its underlying graph is a linear graph with n vertices. The orientation of arrows in a type $\mathbb{A}_n$ quiver is specified by a string τ_n consisting of $n-1$ letters f and b, where f stands for a forward arrow and b a backward arrow (see Figure 2.1). We represent a type $\mathbb{A}_n$ quiver with its orientation τ_n as the pair (A_n, τ_n). When the orientation is implicit, we may simply write A_n. An *equi-oriented* type $\mathbb{A}_n$ quiver has all of its arrows pointing in the same direction, denoted as $\vec{A}_n$.

Figure 2.1: A type $\mathbb{A}_3$ quiver with orientation $\tau_3 = (fb)$.

Definition 2.3. Let Q be a quiver. A *relation* ρ in Q with coefficients in $\Bbbk$ is a linear combination of parallel paths, written as

$$\rho = \sum_{i=1}^{m} \lambda_i p_i,$$

where $\lambda_i \in \Bbbk$, $p_i \in Q_{\geq 1}$, and $p_i \mathbin{/\!\!/} p_j$ for $i, j \in \{1, \ldots, m\}$. For a set $R := \{\rho_j\}_{j \in J}$ of relations, the pair (Q, R) is called a *quiver with relations*.

Given a set of relations $\{\rho_j\}_{j \in J}$, one can generate a two-sided ideal $\mathcal{I} = \langle \rho_j \mid j \in J \rangle$ in the path algebra $\Bbbk Q$, and also define the quotient algebra $\Bbbk Q/\mathcal{I}$.

Remark 2.4. The relation $\rho = 0$ is regarded as the *trivial relation*, and it holds that $\Bbbk Q \cong \Bbbk Q/\langle 0 \rangle$. A relation of the form $\rho = \lambda p_1$ with $\lambda \neq 0$ is referred to as a *zero relation*. A relation of the form $p_1 - p_2$ is called a *commutativity relation*.

Definition 2.5. Let Q be a quiver. Its *full commutativity relations* is a set R_Q^{fc} defined as:

$$R_Q^{\mathrm{fc}} = \{ p_1 - p_2 \mid p_1, p_2 \in Q_{\geq 1} \text{ and } p_1 \mathbin{/\!\!/} p_2 \}.$$

A quiver with these relations is called a *fully commutative quiver*.

Remark 2.6. Throughout this paper, we will focus exclusively on quivers with relations that are finite, acyclic, and fully commutative unless otherwise specified.

Definition 2.7. Let $Q = (Q_0, Q_1, \mathfrak{s}, \mathfrak{t})$ be a quiver.

- A *subquiver* of Q is a quiver $Q' = (Q'_0, Q'_1, \mathfrak{s}', \mathfrak{t}')$ such that $Q'_0 \subseteq Q_0$, $Q'_1 \subseteq Q_1$, $\mathfrak{s}'$ and $\mathfrak{t}'$ are the restrictions of $\mathfrak{s}$ and $\mathfrak{t}$ to Q'_1 respectively.
- A subquiver Q' is *full* if every arrow $\alpha \in Q_1$ with its start and target in Q'_0 also belongs to Q'_1.
- A full subquiver Q' of Q is said to be *convex* if, for any path in Q that starts and ends in Q', all intermediate vertices also belong to Q'.
- The *convex hull* of a set $S \subseteq Q_0$, denoted by $\mathsf{Conv}(S)$, is the full subquiver of Q whose vertices are all the vertices that lie on a path starting and ending with vertices in S.
- A subquiver is said to be *connected* if its underlying graph is connected.

The notions of convexity and convex hull can be naturally extended to quivers with relations.

Definition 2.8. Let (Q, R) be a quiver with relations and Q' be a subquiver of Q. The set of induced relations R' on Q' consists of elements $\rho \in R$ such that all paths p_i in $\rho = \sum_{i=1}^{m} \lambda_i p_i$ are in Q'. We say (Q', R') is *convex* if for any non-zero path p in (Q, R) with its start and target in Q', all vertices of the path are also in Q'. The convex hull of a set $S \subseteq Q_0$ is then the full subquiver of Q whose vertices are all the vertices that lie on a non-zero path in (Q, R) starting and ending with vertices in S.

Definition 2.9. Let $G = (Q, R)$ be a quiver with relations. An induced subquiver with relations $G' = (Q', R')$ is called an *interval subquiver (with relations)*, or simply an *interval* of G, if Q' is a connected convex subquiver, and R' does not contain any zero relations. The set of all interval subquivers of G is denoted as $\mathbb{I}_G$. It forms a partially ordered set by containment of the corresponding vertex sets. Specifically, for two interval subquivers I and J, $I \leq J$ if and only if $I_0 \subseteq J_0$.

Remark 2.10. This paper's definition of an interval differs slightly from [3, Definition 2.4]. The cited paper defines an interval for quivers without relations, requiring only two conditions: convexity and connectedness. However, our research engages with quivers with relations, and we accommodate quivers with zero relations for generality. As a result, a new condition "does not contain any zero relations" is added.

Remark 2.11. Incorporating zero relations offers several benefits. Firstly, it extends the applicability of our approach and enables us to tackle infinite representation problems by reducing them to finite representation. Secondly, the adoption of quiver representation theory over the poset configuration setting is further justified. Unlike the latter, quiver representations possess the inherent capacity to accommodate zero relations, thus providing a more versatile framework for our analysis.

Example 2.12. Consider a quiver with relations $Q := \clubsuit \xrightarrow{\alpha} \blacklozenge \xrightarrow{\beta} \spadesuit$ and $R := \{ \beta\alpha \}$. Then, the set of all interval subquivers of Q is $\mathbb{I}_Q = \{ \clubsuit, \blacklozenge, \spadesuit, \clubsuit \xrightarrow{\alpha} \blacklozenge, \blacklozenge \xrightarrow{\beta} \spadesuit \}$. Notice

that $\clubsuit \xrightarrow{\alpha} \blacklozenge \xrightarrow{\beta} \spadesuit$ does not qualify as an interval subquiver as it encompasses the zero relation $\beta\alpha$.

Next, we introduce representations of quivers and quivers with relations. The category of finite-dimensional $\Bbbk$-vector spaces is denoted as $\mathbf{vect}_{\Bbbk}$. For brevity, $\mathbf{vect}$ is used since we are working over a fixed field.

Definition 2.13. Let Q be a quiver and $G = (Q, R)$ be a quiver with relations.

- A (finite-dimensional) *representation* of Q is a functor M from Q to $\mathbf{vect}$. We denote the associated vector spaces as M_u for $u \in Q_0$, and the morphisms as $M(\alpha)$ for $\alpha \in Q_1$.
- A *representation* of G is a representation M of the underlying quiver Q satisfying the additional condition that the evaluation of M on each relation $\rho \in R$ vanishes.
- The category of representations of G is denoted as $\mathbf{rep}(G)$.
- The vector $\underline{\dim}\, M := (\dim_{\Bbbk} M_u)_{u \in Q_0}$ is called the *dimension vector* of M
- If the associated $\Bbbk$-algebra $\Bbbk Q/\langle R \rangle$ is a representation-finite algebra, G is said to have a *finite type*.

Definition 2.14. Let G be a quiver with relations, M be a representation in $\mathbf{rep}(G)$, and G' be an induced subquiver with relations. A representation in $\mathbf{rep}(G')$ can be derived from M by restricting M to the vertices and arrows of the induced subquiver. This restricted representation is denoted as $M|_{G'}$.

Definition 2.15. Consider a quiver with relations G and M as a representation of G. The *support* of M, denoted as $\mathsf{supp}(M)$, is the full subquiver of Q consisting of vertices u for which $M_u \neq 0$.

Definition 2.16. Given a quiver with relations G and an interval subquiver I, the associated interval representation V_I is defined as follows:

$$(V_I)_u := \begin{cases} \Bbbk & u \in I_0 \\ \mathbf{0} & \text{otherwise;} \end{cases} \qquad V_I(\alpha) := \begin{cases} \mathrm{id}_{\Bbbk} & \text{both } \mathfrak{s}(\alpha) \text{ and } \mathfrak{t}(\alpha) \text{ are in } I_0 \\ \mathbf{0} & \text{otherwise.} \end{cases}$$

Example 2.17. Consider the following fully commutative quiver and interval subquiver:

$$G := \begin{array}{ccccccc} 5 & \longrightarrow & 6 & \longrightarrow & 7 & \longrightarrow & 8 \\ \uparrow & \circlearrowleft & \uparrow & \circlearrowleft & \uparrow & \circlearrowleft & \uparrow \\ 1 & \longrightarrow & 2 & \longrightarrow & 3 & \longrightarrow & 4 \end{array}, \qquad I := \begin{array}{ccccc} 5 & \longrightarrow & 6 & \longrightarrow & 7 \\ & & \uparrow & \circlearrowleft & \uparrow \\ & & 2 & \longrightarrow & 3 \end{array}.$$

The associated interval representation V_I is $\begin{array}{ccccccc} \Bbbk & \xrightarrow{\mathrm{id}} & \Bbbk & \xrightarrow{\mathrm{id}} & \Bbbk & \to & \mathbf{0} \\ \uparrow & & \uparrow_{\mathrm{id}} & & \uparrow_{\mathrm{id}} & & \uparrow \\ \mathbf{0} & \to & \Bbbk & \xrightarrow[\mathrm{id}]{} & \Bbbk & \to & \mathbf{0} \end{array}$. Notice that a bijective correspondence exists between an interval representation and its dimension vector. Therefore, we can represent V_I by its dimension vector $\underline{\dim}\, V_I = \begin{pmatrix} 1 & 1 & 1 & 0 \\ 0 & 1 & 1 & 0 \end{pmatrix}$.

Definition 2.18. Let G be a quiver with relations. A representation $M \in \mathbf{rep}(G)$ is said to be *interval-decomposable* if it is isomorphic to a direct sum of interval representations of G.

When we are working with a finite acyclic quiver Q with a set of relations R, both the path algebra $\Bbbk Q$ and its quotient algebra $\Bbbk Q/\langle R\rangle$ have finite dimensions. As a result, the representation category of (Q, R) satisfies the unique decomposition theorem, also known as the Krull-Schmidt theorem.

Theorem 2.19. *Let $\mathcal{L}$ be a complete set of representatives of the isomorphism classes of indecomposable representations of a quiver with relations $G = (Q, R)$. For each representation $M \in \mathbf{rep}(G)$, there exists a unique function $d_M \colon \mathcal{L} \to \mathbb{Z}_{\geq 0}$ such that*

$$M \cong \bigoplus_{L \in \mathcal{L}} L^{d_M(L)}. \tag{2.1}$$

The function d_M is referred to as the multiplicity function *of M, and the value $d_M(L)$ is called the* multiplicity *of the indecomposable L in M. This isomorphism is referred to as the* indecomposable decomposition *of M. Moreover, M is uniquely determined by d_M up to isomorphism.*

2.2 Commutative Grids and Commutative Ladders

Definition 2.20. Let $Q = (Q_0, Q_1, \mathfrak{s}, \mathfrak{t})$ and $Q' = (Q'_0, Q'_1, \mathfrak{s}', \mathfrak{t}')$ be two quivers. Their *Cartesian product* $Q \times Q'$ is a quiver defined as follows:

- The vertex set is the Cartesian product $Q_0 \times Q'_0$.
- There exists an arrow from (u, u') to (v, v') if and only if either:
  - $u = v$ and there exists an arrow α' from u' to v', denoted by $(u, \alpha') \in Q_0 \times Q'_1$;
  - $u' = v'$ and there exists an arrow α from u to v, denoted by $(\alpha, u') \in Q_1 \times Q'_0$.

The *tensor product* of Q and Q', denoted by $Q \otimes Q'$, is the quiver $Q \times Q'$ with the following relations:

$$\Big((v, v') \mid (\alpha, v')(u, \alpha') \mid (u, u')\Big) - \Big((v, v') \mid (v, \alpha')(\alpha, u') \mid (u, u')\Big)$$

for all $\alpha \colon u \to v \in Q_1$ and $\alpha' \colon u' \to v' \in Q'_1$ (see Figure 2.2).

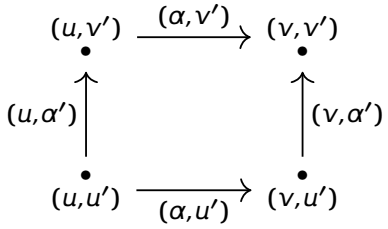

Figure 2.2: Illustration of a relation in the tensor product construction.

Definition 2.21. A *two-dimensional fully commutative grid with orientation* (τ_p, τ_q) is the tensor product of quivers (A_p, τ_p) and (A_q, τ_q), written as $G_{p,q} := A_p \otimes A_q$ (See Figure 2.3). We often refer to $G_{p,q}$ simply as a *commutative grid* or a *grid*. If both A_p and A_q are equi-oriented, we have the *equi-oriented commutative grid*, represented as $\vec{G}_{p,q} := \vec{A}_p \otimes \vec{A}_q$.

The vertices of $G_{p,q}$ can be depicted as a rectangular lattice with p columns and q rows, with edges connecting vertically or horizontally adjacent vertices. For equi-oriented grids, we will draw horizontal arrows pointing rightwards and vertical ones upwards without loss of generality.

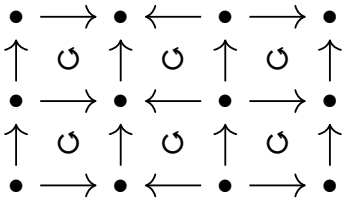

Figure 2.3: Commutative grid $G_{4,3}$ with orientation (τ_4, τ_3) where $\tau_4 = (fbf)$ and $\tau_3 = (ff)$.

Intervals in $\vec{G}_{p,q}$ exhibit staircase shapes, and they can be parameterized as discussed above [1, Proposition 21]. To simplify the notation, we use $\mathbb{I}_{p,q}$ to represent $\mathbb{I}_{\vec{G}_{p,q}}$.

$$\mathbb{I}_{p,q} = \left\{ \bigsqcup_{i=s}^{t} [b_i, d_i]_i \;\middle|\; \begin{array}{l} b_i, d_i, s, t \in \mathbb{Z}, 1 \le b_i \le d_i \le p,\ 1 \le s \le t \le q, \\ \text{if } t > s, \text{ then } 1 \le b_{i+1} \le b_i \le d_{i+1} \le d_i \le p\ \forall\, i \in \{ s, \dots, t-1 \} \end{array} \right\}. \tag{2.2}$$

Definition 2.22. A *commutative ladder* $\mathsf{CL}(\tau_n)$ is a commutative grid $G_{n,2}$ with orientation (τ_n, τ_2). We can use just τ_n to represent its orientation since the value of τ_2 is inconsequential in this context. An *equi-oriented commutative ladder* of length n is denoted as $\mathsf{CL}(n)$.

Commutative ladders are of significant interest in the transition from one-parameter to two-parameter persistence modules. Under specific conditions, these ladders exhibit representation-finiteness, unlocking the possibility of computing all multiplicity functions. On the other hand, they remain representation-infinite in general situations, driving the need for new approaches. A criterion for representation-finiteness of commutative ladders is given in [18].

Theorem 2.23. *For an arbitrary orientation τ_n, the commutative ladder $\mathsf{CL}(\tau_n)$ is*

1. *representation-finite if $n \leq 4$;*
2. *representation-infinite if $n \geq 5$.*

2.3 Persistent Homology

Persistent homology stands as a cornerstone of topological data analysis, bridging the gap between abstract mathematical theory and practical data interpretation. It extracts and analyzes topological features from data that can be adapted as a filtration of simplicial complexes by scanning over the entire range of parameters to study how topological features evolve, instead of relying on the manipulation of parameters

To illustrate the concept of persistent homology, consider a point cloud sampled from an ∞-shaped figure (see Figure 2.5). Intuitively, we discern two connected loops (or holes). To confirm this observation in an algebraic way, we use the ball model, associating each point with a disk of radius r and letting it grow from zero to see how the topological space formed by the union of balls evolves. Since the point set is finite, the number of radii at which the topology changes is also finite and discrete. Such a radius is called a critical radius. In such a way, we obtain an A_n-filtration of topological spaces, assuming the number of critical radii is n. We note that each topological space can be represented by a simplicial complex to facilitate the computation of homology. The sequence of four snapshots illustrates the evolution of the topological space with the associated simplicial complex. The first frame captures the original point cloud as a discrete topological space. As we advance to the second frame, a slight increment in the radius parameter causes the expanding disks around proximate points to contact, and some small holes appear. Progressing to the third frame, a further increase in the radius gives rise to a complex network of edges and triangles, but holistically, we see the merging of individual disks into a two-hole structure that persists over a wide range of radii. The final frame shows that as the radius continues to increase, the previously observed holes become filled, indicating a point at which further growth of the radius does not alter the topological structure.

Applying a homology functor to the filtration of simplicial complexes above yields a sequence of homology modules M that can be viewed as an object in $\mathbf{rep}(\vec{A}_n)$. It encodes the topological features of the data by tracking the birth and death of topological features. Using homology functors at different dimensions, we can track features like connected components and holes for the example shown and voids or higher-dimensional homology generators for the general cases. The persistence of these features across the filtration offers a detailed portrait of the data's intrinsic topology.

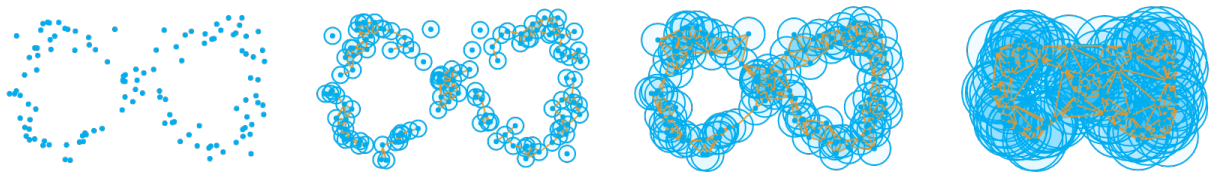

Figure 2.4: Evolution of a simplicial complex from a point cloud. The sequence from left to right shows the point cloud at critical radii, where each point is associated with a disk of increasing radius r.

The diagram in Figure 2.5 visually encapsulates the topological features in the example revealed by applying the H_0 and H_1 functors. It suffices to stop at dimension one because all higher dimensional homologies are trivial for a point cloud embedded in $\mathbb{R}^2$. Each point on this diagram represents a feature, with its x-coordinates indicating the feature's birth radius, and y-coordinate indicating the death radius within the filtration. Their difference, which is proportional to the distance to a point's distance to the diagonal line, is the lifespan of the corresponding feature. Hence, points near the diagonal — indicating shorter lifespans — may be regarded as noise, while those distant from the diagonal line can be considered signals. Let us begin our analysis by examining the result from H_0, which effectively captures the clustering within the point cloud. Initially, each point serves as an isolated connected component. However, as the radius increases, many disks are connected together, reducing the number of connected components. Eventually, this process leads to a single connected component corresponding to the top red point in the diagram. For H_1, we observe the presence of two holes in the point cloud, which corresponds to the two green points away from the diagonal line. As we gradually increase the radius, cycles form among adjacent points. Still, these cycles will soon be filled, resulting in the emergence of many green points near the diagonal line. This graphical representation, known as a *persistence diagram*, serves as a succinct summary of the topological persistence within the data. It effectively highlights features that are significant across scales.

In general, consider a quiver A_n represented as $\bullet_1 \hookleftarrow \bullet_2 \hookleftarrow \cdots \hookleftarrow \bullet_n$ and a representation M of A_n. According to Gabriel's theorem, M is interval-decomposable [21]. Then by Theorem 2.19, M is isomorphic to $\bigoplus_{I \in \mathbb{I}_{A_n}} V_I^{d_M(V_I)}$.

Definition 2.24. Given a one-parameter persistence module M and its associated multiplicity function d_M, the persistence diagram of M, denoted as $\mathfrak{Dgm}(M)$, visualizes d_M as a multiset of points in the two-dimensional integer lattice $\mathbb{Z}^2$. Here, the multiplicity for (x, y) with $x < y$ is $d_M(V_{[x,y-1]})$.

Remark 2.25. For any point (b, d) in the persistence diagram, we adopt the following conventions:

- The birth coordinate b is inclusive, meaning the generator emerges at value b.

- The death coordinate d is exclusive, indicating that value d is the earliest point at which the generator vanishes.

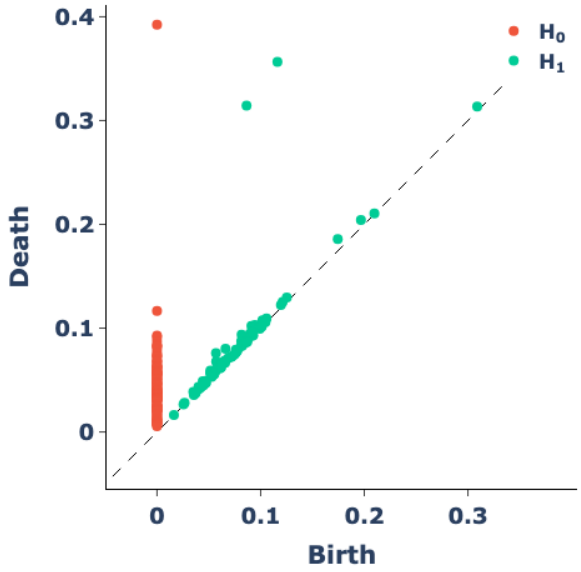

Figure 2.5: The persistence diagram of the point cloud in Figure 2.4.

Our mixed usage of the term "module" and "representation" is justified by [5, Theorem 7.2], which establishes an equivalence between the module category and the representation category, offering multiple perspectives for analyzing and visualizing the persistence of topological features in data. Below, we introduce standard terms of persistence modules. Each module offers a lens through which the underlying topological features of a dataset can be viewed and understood.

Definition 2.26. A *persistence module* refers to a representation of a quiver with relations $G = (Q, R)$. This corresponds to a module over the quotient algebra $\Bbbk Q/\langle R\rangle$. Several common families have established nomenclature as below.

- A *one-parameter persistence module* is a representation of a quiver A_n.
- A *zigzag persistence module* designates a one-parameter persistence module, highlighting that the underlying quiver A_n may not be equi-oriented.
- A *two-parameter persistence module* is a representation of a commutative grid $G_{p,q}$.
- A *persistent homology* is a persistence module obtained by taking a homology functor on a filtration of topological spaces.

3 Refining Interval Approximations

In the study of multiparameter persistence modules, we aim to obtain the indecomposable decomposition of a given representation M, equivalent to the computation of the multiplicity function d_M. However, direct computation is extremely challenging, especially when M is not interval-decomposable. To overcome this difficulty, we turn to the interval approximation method, first proposed in [3], which approximates the rank invariant of a representation M via those of interval representations.

A crucial quantity in defining the interval approximation is compression. It provides a lossy yet more manageable way to define invariants on M. This section presents a new mechanism for handling various types of compressions in a more general and flexible way. We then stratify intervals within a general two-dimensional commutative grid, proposing the partial interval approximation to address the issue of an exponentially growing number of intervals. Moreover, we show how the interactive visualization of a 2-D persistence module [31] can be reformulated using the interval approximation. Throughout this section, we consider a finite fully commutative acyclic quiver $G = (Q, R)$.

3.1 Courses and Tours

Definition 3.1 (Course)**.** A *course* on G is a pair (C, F) with $C := (C_0, C_1, \mathfrak{s}, \mathfrak{t})$ being a connected quiver and $F\colon C_0 \to Q_0$ acting as a *labeling map*, such that for any arrow $\alpha \in C_1$, there exists a path from $F(\mathfrak{s}(\alpha))$ to $F(\mathfrak{t}(\alpha))$ in G. The set of all courses on G is denoted by $\mathsf{Course}(G)$.

Example 3.2. Consider the fully commutative quiver $\vec{G}_{3,3}$ and a connected quiver $C := \underset{1}{\bullet} \to \underset{2}{\bullet} \leftarrow \underset{3}{\bullet}$. We define two labeling maps F and F' as shown in Figure 3.1.

Definition 3.3 (Essential Vertex)**.** Let I be an interval subquiver of G. A vertex $v \in I_0$ is called *essential* if v is either a source or a sink in I (see Figure 3.2). The set of all essential vertices of I is denoted by $E(I)$.

Remark 3.4. We note that the essential vertices defined here are called the "source-sink-essential vertices" in [3, Definition 4.1], and they are the minimal information required

(a) (b)

Figure 3.1: (a) Labeling map $F\colon C_0 \to \left(\vec{G}_{3,3}\right)_0$. (b) Another labeling map F'. Notice that the vertex in the center is not in the image of F'.

to recover an interval subquiver. Specifically, an interval subquiver I is the convex hull of $E(I)$.

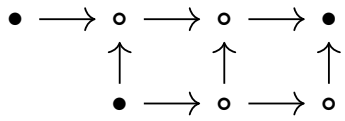

Figure 3.2: A visual representation of essential vertices. The interval I comprises all vertices shown, where essential vertices are depicted as solid dots and non-essential vertices are shown as hollow dots.

The concept of essential vertices provides a criterion to determine the containment relations between two intervals in $\mathbb{I}_G$. The following proposition justifies their name as being "essential".

Proposition 3.5. *Let I, J be intervals of G. If $E(I)$ is contained in J_0, then $I \leq J$.*

Proof. This statement can be proved similarly as in [3, Lemma 4.3]. □

Within an interval I, courses that visit all $E(I)$ are of particular importance.

Definition 3.6 (Essential Course)**.** Let (C, F) be a course on G. For an interval $I \in \mathbb{I}_G$, the course (C, F) is said to be:

- a *course in I* if the image of F is contained in I_0.
- an *essential course in I*, or *essential in I*, if it is a course in I and all essential vertices of I are contained in the image of F, *i.e.*, $E(I) \subseteq F(C_0) \subseteq I_0$.

Proposition 3.7. *Consider a course* (C, F) *on* G*. If there exists an interval* $I \in \mathbb{I}_G$ *for which* (C, F) *serves as an essential course, then* I *is unique.*

Proof. Suppose (C, F) is an essential course in both I and J. By definition, we have $E(I) \subseteq F(C_0) \subseteq I_0$ and $E(J) \subseteq F(C_0) \subseteq J_0$, thus $E(I) \subseteq J_0$ and $E(J) \subseteq I_0$. Then it follows from Proposition 3.5 that $I = J$. □

Remark 3.8. The converse statement is generally not true, as multiple essential courses can be defined within a fixed interval. Figure 4.1 provides such an example.

Definition 3.9 (Essential Assignment)**.** An *essential assignment* is a map that assigns each interval $I \in \mathbb{I}_G$ an essential course in I. This can be formally expressed as:

$$\begin{aligned} \xi \colon \mathbb{I}_G &\to \mathsf{Course}(G) \\ I &\mapsto \xi(I) \text{ is an essential course in } I. \end{aligned}$$

Definition 3.10 (Tour)**.** A *tour* on a course (C, F) in G is an additive functor $\mathsf{tour}_{(C,F)}(-)$ that maps a representation $M \in \mathbf{rep}(G)$ to an object in $\mathbf{rep}(C)$ specified as below:

$$\begin{aligned} \mathsf{tour}_{(C,F)}(-) : \mathbf{rep}(G) &\to \mathbf{rep}(C) \\ M &\mapsto \left(M_{F(\mathfrak{s}(\alpha))} \xrightarrow{M\left(F(\mathfrak{s}(\alpha)) \to F(\mathfrak{t}(\alpha))\right)} M_{F(\mathfrak{t}(\alpha))} \right)_{\alpha \in C_1}, \end{aligned}$$

where $M\big(F(\mathfrak{s}(\alpha)) \to F(\mathfrak{t}(\alpha))\big)$ represents the evaluation of M on a path in G from $F(\mathfrak{s}(\alpha))$ to $F(t(\alpha))$, which is well-defined by the full commutativity of G. For a morphism $\varphi \colon M \to N$ in $\mathbf{rep}(G)$, a morphism $\mathsf{tour}_{(C,F)}(\varphi)$ in $\mathbf{rep}(C)$ is given by $(M_{F(v)} \xrightarrow{\varphi(F(v))} N_{F(v)})$ for each $v \in C_0$.

Remark 3.11. Consider a representation $M \in \mathbf{rep}(G)$. The choice of a quiver C and a labeling map F can significantly impact the analysis's feasibility. Using $C = A_n$ will place the tour defined above in the category $\mathbf{rep}(A_n)$, which usually makes the situation more tractable than working directly with a representation in $\mathbf{rep}(G)$. This process, however, can lead to information loss of M. To compensate for it, we employ a set of tours to probe M, with each tour offering partial information about M from different perspectives. Collectively, they provide a more complete understanding of M, where the amount of information loss varies and is based on the particular choice of courses and the method by which the tours are combined. For instance, in the context of $\mathsf{CL}(n)$, an essential assignment (referred to as a quiver morphism in the cited paper below) that exhibits several appealing properties is demonstrated in [2, Section 5.1], highlighting the value of this approach.

We introduce the Hasse quiver as an analog to the Hasse diagram in quivers, facilitating the characterization of the transitive reduction of paths.

Definition 3.12 (Hasse Quiver)**.** Let $Q = (Q_0, Q_1)$ be an acyclic quiver and let $S \subseteq Q_0$ be a subset of its vertices. The *Hasse quiver* $\mathfrak{h}(S, Q)$ is a quiver derived from S and Q as follows:

- The vertex set of $\mathfrak{h}(S, Q)$ is S.
- For each pair of distinct vertices $u, v \in S$, an arrow is drawn from u to v if there is a path from u to v in Q, and there is no third vertex $w \in S \setminus \{ u, v \}$ in any path from u to v in Q.

Example 3.13. We illustrate the concept of the Hasse quiver by capturing the idea of a "compressed category" within the context of $\vec{G}_{p,q}$, as described in [3]. Given an interval subquiver $I \in \mathbb{I}_{p,q}$, the selection of different subsets $S \subseteq I_0$ can lead to a variety of Hasse quivers. Consider the following three possibilities:

1. $S_1 := I_0$;
2. $S_2 := E(I)$;
3. $S_3 := \mathsf{CC}(I)$, where CC is an operation that identifies "corner-complete" vertices. This subset of I_0 includes all vertices present in both a row and a column with essential vertices. Note that all essential vertices are corner-complete.

As an example, consider $\vec{G}_{4,3}$ and an interval $I \in \mathbb{I}_{4,3}$ in Figure 3.3. The Hasse quivers on $E(I)$ and $\mathsf{CC}(I)$ are shown in (b) and (c), respectively. Notice that $\mathfrak{h}(S_1, I)$ equals I, emphasizing that the Hasse quiver is equal to the original quiver when all vertices are considered.

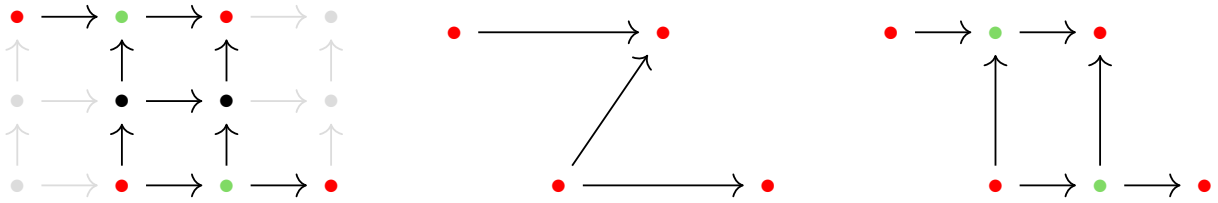

(a) (b) (c)

Figure 3.3: (a) A visual representation of the interval I. Vertices and arrows outside the interval I are grayed out for clarity. Essential vertices of I are marked red, while corner-complete vertices that are not essential are colored in green. (b) The Hasse quiver of the essential vertices. (c) The Hasse quiver of the corner-complete vertices.

We now show two examples demonstrating the adaptability and versatility of the concept of essential assignment. These examples highlight how it serves as a unified framework for incorporating related definitions from existing literature.

Example 3.14. The three types of compressions (ss, cc, and tot) introduced in [3] can be expressed as different essential assignments. Consider $\vec{G}_{p,q}$ and the following maps de-

fined on its set of intervals:

$$\begin{aligned} & \mathbb{I}_{p,q} \to \mathsf{Course}(\vec{G}_{p,q}) \\ \xi^{\mathsf{tot}}\colon \quad & I \mapsto \big(\mathfrak{h}(I_0, I), \mathsf{id}\big), \\ \xi^{\mathsf{ss}}\colon \quad & I \mapsto \big(\mathfrak{h}(E(I), I), \mathsf{id}\big), \\ \xi^{\mathsf{cc}}\colon \quad & I \mapsto \big(\mathfrak{h}(\mathsf{CC}(I), I), \mathsf{id}\big). \end{aligned}$$

With these constructions, we can verify that $\mathsf{tour}_{\xi^*(I)}(-) = \mathsf{Comp}^*_I(-)$ for $* = \mathsf{ss}, \mathsf{cc}, \mathsf{tot}$ as defined in the reference.

Example 3.15. We demonstrate how the concept of boundary cap from [12, Definition 19] fits within our framework. Consider the interval I depicted in Figure 3.4. Its boundary cap, denoted by ∂I, can be regarded as a type $\mathbb{A}_n$ quiver. It is constructed from all vertices in $E(I)$ and intermediate vertices on the boundary of I to ensure connectivity. Therefore, ∂I can be expressed as an essential course in I. As a result, we can reproduce it using an essential assignment that follows the same pattern.

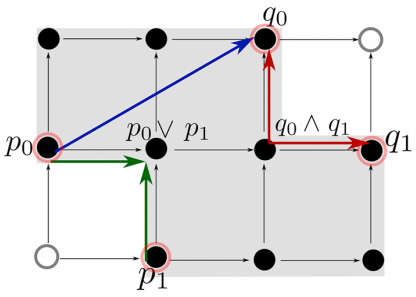

Figure 3.4: An example of a boundary cap ∂I from [12, Figure 2]. The gray area represents the interval I, with essential vertices encircled. The sequence of arrows from p_1 to q_1 represents the boundary cap ∂I.

3.2 ξ-compressed Multiplicities and Interval Approximations

We are ready to introduce the concept of ξ-compressed multiplicity. This quantity captures the multiplicity of an interval representation V_I within a representation M relative to the designated tour $\xi(I)$.

Definition 3.16 (ξ-compressed Multiplicity)**.** Let M be a representation of G and ξ be an essential assignment. For an interval $I \in \mathbb{I}_G$, we define the *ξ-compressed multiplicity of M on the interval I* as follows:

$$c^{\xi}_M(I) := d_{\mathsf{tour}_{\xi(I)}(M)}\big(\mathsf{tour}_{\xi(I)}(V_I)\big),$$

where d is the multiplicity function as in (2.1).

Remark 3.17. Consider an $I \in \mathbb{I}_G$ with $\xi(I) = (C, F)$. Using the definition of V_I and noting that C is a connected quiver, we can easily verify that $\mathsf{tour}_{\xi(I)}(V_I)$ is an indecomposable representation. In particular, if C is a type $\mathbb{A}_n$ quiver, then all indecomposable representations of it are interval representations. The longest one among them can be represented as:

$$\mathsf{tour}_{(C,F)}(V_I) \cong \underset{1}{\Bbbk} \overset{\mathsf{id}}{\longleftrightarrow} \underset{2}{\Bbbk} \overset{\mathsf{id}}{\longleftrightarrow} \cdots \overset{\mathsf{id}}{\longleftrightarrow} \underset{n}{\Bbbk}$$

with $n = |C_0|$, which we denote as $V_{\xi(I)}$ or V_C.

Example 3.18. Consider the essential assignment ξ^{tot} in Example 3.14. Then $c_M^{\xi^{\mathsf{tot}}}(I) = \underline{d}_M^{\mathsf{tot}}(I)$ in [3, Remark 4.13], which is shown to be equal to the generalized rank invariant of [28].

Proposition 3.19. *Let ξ be an essential assignment. For any $I, J \in \mathbb{I}_G$ satisfying $I \leq J$, the following holds:*

$$\mathsf{tour}_{\xi(I)}(V_J) = \mathsf{tour}_{\xi(I)}(V_I).$$

Proof. This equality is straightforward, as when we compute the value on the left-hand side, any vertices not included within I can be ignored. □

Proposition 3.20. *Let ξ be an essential assignment and I be an interval in $\mathbb{I}_G$. For any $M, N \in \mathbf{rep}(G)$, we have:*

$$c^{\xi}_{M\oplus N}(I) = c^{\xi}_M(I) + c^{\xi}_N(I).$$

Proof. Starting from the definition of the ξ-compressed multiplicity, we obtain

$$c^{\xi}_{M\oplus N}(I) = d_{\mathsf{tour}_{\xi(I)}(M\oplus N)}\big(\mathsf{tour}_{\xi(I)}(V_I)\big).$$

Using the additivity of the tour functor with respect to direct sums and the additivity of the multiplicity function d with respect to direct sums of representations in the subscript, the expression expands to:

$$d_{\mathsf{tour}_{\xi(I)}(M)\oplus\mathsf{tour}_{\xi(I)}(N)}\big(\mathsf{tour}_{\xi(I)}(V_I)\big) = d_{\mathsf{tour}_{\xi(I)}(M)}\big(\mathsf{tour}_{\xi(I)}(V_I)\big) + d_{\mathsf{tour}_{\xi(I)}(N)}\big(\mathsf{tour}_{\xi(I)}(V_I)\big),$$

substituting back the definition of ξ-compressed multiplicity completes the proof. □

Proposition 3.21. *Let ξ be an essential assignment and $I, J \in \mathbb{I}_G$. The ξ-compressed multiplicity function $c^{\xi}_{V_J}$ evaluates as:*

$$c^{\xi}_{V_J}(I) = \begin{cases} 1 & I \leq J \\ 0 & \textit{otherwise.} \end{cases}$$

Proof. By definition, $c^{\xi}_{V_J}(I) = d_{\mathsf{tour}_{\xi(I)}(V_J)}\big(\mathsf{tour}_{\xi(I)}(V_I)\big)$.
Case 1: If $I \leq J$, then Proposition 3.19 asserts that $d_{\mathsf{tour}_{\xi(I)}(V_I)}\big(\mathsf{tour}_{\xi(I)}(V_I)\big) = 1$.
Case 2: Otherwise, there exists an essential vertex u of I but not in J, as guaranteed by Proposition 3.5. This implies that $(V_J)_u = \mathbf{0}$. Given that $\xi(I)$ is an essential course in I, u is visited by $\xi(I)$. As a result, the associated vector space of u in $\mathsf{tour}_{\xi(I)}(V_J)$ is zero, but it is nonzero in $\mathsf{tour}_{\xi(I)}(V_I)$. This leads to the zero multiplicity for $\mathsf{tour}_{\xi(I)}(V_I)$ in $\mathsf{tour}_{\xi(I)}(V_J)$. □

The following lemma is intended to serve as a counterpart to [3, Lemma 4.21].

Lemma 3.22. *Let ξ be an essential assignment and $I \in \mathbb{I}_G$. If M is an interval-decomposable representation in $\mathbf{rep}(G)$, then the following equation holds:*

$$c_M^\xi(I) = \sum_{I \le J \in \mathbb{I}_G} d_M(V_J).$$

Proof. By replacing M in the subscript of $c_M^\xi(I)$ with its indecomposable decomposition $\bigoplus_{J \in \mathbb{I}_G} V_J^{d_M(V_J)}$ and using the additivity property from Proposition 3.20, we can express the left-hand side as $\sum_{J \in \mathbb{I}_G} d_M(V_J) \cdot c_{V_J}^\xi(I)$. Then, by applying Proposition 3.21, we obtain the desired result. □

Definition 3.23 (Cover and Join)**.** Consider $\mathbb{I}_G$ as a partially ordered set. The *cover* of an interval $I \in \mathbb{I}_G$, denoted $\mathsf{Cov} I$, is the set of intervals $J \in \mathbb{I}_G$ satisfying $I < J$ and there is no interval L such that $I < L < J$. The *join* of a subset $S \subseteq \mathbb{I}_G$, denoted $\bigvee S$, is the supremum of S provided that it exists.

When $G = \vec{G}_{p,q}$, for each $I \in \mathbb{I}_G$, the join operation is well-defined for every subset $S \subseteq \mathsf{Cov} I$, as shown in the discussion above [3, Example 3.7]. Here, $\bigvee S$ equals the minimum interval containing the union of intervals in S. For simplicity, we use the convention $\bigvee \emptyset = I$ for $\emptyset \subseteq \mathsf{Cov} I$.

Theorem 3.24. *Consider an equi-oriented commutative grid $\vec{G}_{p,q}$. Let ξ be an essential assignment and $I \in \mathbb{I}_{p,q}$. If M is an interval-decomposable representation of $\vec{G}_{p,q}$, then*

$$d_M(V_I) = \sum_{S \subseteq \mathsf{Cov} I} (-1)^{\#S} \cdot c_M^\xi(\textstyle\bigvee S).$$

Proof. This follows directly from the Möbius inversion theorem, as detailed in [3, Section 5]. □

The definition of interval approximation below is motivated by the Möbius inversion of the formula above, where we define it for more general quivers and remove the interval-decomposable condition.

Definition 3.25 (Interval Approximation)**.** Let M be a representation of G and ξ be an essential assignment on $\mathbb{I}_G$. The *interval approximation of M by $\mathbb{I}_G$ via ξ-compressed multiplicity functions* is an integer-valued function δ_M^ξ that satisfies

$$c_M^\xi(I) = \sum_{I \le J \in \mathbb{I}_G} \delta_M^\xi(J) \tag{3.1}$$

for any $I \in \mathbb{I}_G$. When the choice of ξ is clear from the context, we refer to δ_M^ξ as the *interval approximation*.

Remark 3.26. A function δ_M^ξ can always be constructed as follows. First, we define $\delta_M^\xi(J) := c_M^\xi(J)$ for each maximal J in $\mathbb{I}_G$. Then, we iteratively trace down along the cover relations and set $\delta_M^\xi(J) := c_M^\xi(J) - \sum_{J<I\in\mathbb{I}_G} \delta_M^\xi(I)$. However, if the join operation is well-defined for any subset $S \subseteq \mathrm{Cov}\, I$ for all $I \in \mathbb{I}_G$, we can apply the Möbius transform to (3.1) and obtain

$$\delta_M^\xi(I) = \sum_{S\subseteq \mathrm{Cov}\, I} (-1)^{\#S} \cdot c_M^\xi(\bigvee S).$$

To conclude this subsection, we prove a theorem establishing that the interval approximation accurately recovers the rank function, thereby justifying its name as an approximation.

Lemma 3.27. *Let ξ be an essential assignment and p be a non-zero path in G starting from vertex s and ending at vertex t. Let B denote the convex hull of vertices $\{s, t\}$. If M is a representation of G, then the following equation holds:*

$$\sum_{I\in\mathbb{I}_G} \delta_M^\xi(I) \cdot \mathrm{rank}\big(V_I(p)\big) = c_M^\xi(B).$$

Proof. For any $I \in \mathbb{I}_G$, the rank of the morphism $V_I(p)$ satisfies

$$\mathrm{rank}\big(V_I(p)\big) = \begin{cases} 1 & V_I(p) = \mathrm{id} \iff \text{each vertex of } p \text{ is in } I \\ 0 & \text{otherwise.} \end{cases}$$

Since the convex hull B is the unique minimum interval subquiver that contains each vertex of p, we can reformulate the left-hand side as

$$\sum_{I\in\mathbb{I}_G} \delta_M^\xi(I) \cdot \mathrm{rank}\big(V_I(p)\big) = \sum_{\substack{I\in\mathbb{I}_G \\ V_I(p)=\mathrm{id}}} \delta_M^\xi(I) = \sum_{B\le I\in\mathbb{I}_G} \delta_M^\xi(I) = c_M^\xi(B),$$

where the last equality is obtained by Definition 3.25. □

Lemma 3.28. *Assume the same conditions as in the previous lemma. Then the following equality holds:*

$$c_M^\xi(B) = \mathrm{rank}\big(M(p)\big).$$

Proof. Consider the following restrictions:

- Restrict $M \in \mathbf{rep}(G)$ to $M|_B \in \mathbf{rep}(B)$.
- Use the symbol $\widetilde{B}$ when we view B as an interval subquiver of $\mathbb{I}_B$.
- Restrict $V_B \in \mathbf{rep}(G)$ to $V_B|_B \in \mathbf{rep}(B)$, which equals $V_{\widetilde{B}}$
- Restrict $\xi\colon \mathbb{I}_G \to \mathsf{Course}(G)$ to $\widetilde{\xi}\colon \mathbb{I}_B \to \mathsf{Course}(B)$.

The ξ-compressed multiplicity on the left-hand side can be reformulated as follows:

$$c_M^{\xi}(B) = d_{\mathsf{tour}_{\xi(B)}(M)}\big(\mathsf{tour}_{\xi(B)}(V_B)\big) = d_{\mathsf{tour}_{\widetilde{\xi}(B)}(M|_B)}\big(\mathsf{tour}_{\widetilde{\xi}(B)}(V_B\big|_B)\big) = c_{M|_B}^{\widetilde{\xi}}(\widetilde{B}). \quad (3.2)$$

We will show that the right-hand side above is equal to $r := \mathsf{rank}\big(M(p)\big)$.

First we prove that $d_{M|_B}(V_{\widetilde{B}}) = r$. While our proof is similar to the discussion in [3, Section 4.3], we articulate the details in our terminology here for clarity. Let A denote the quotient algebra $\Bbbk\widetilde{B}/R_{\widetilde{B}}^{\mathsf{fc}}$. Notice that $V_{\widetilde{B}}$ is an indecomposable projective-injective representation, thus by [4, Theorem 3.4], the multiplicity of $V_{\widetilde{B}}$ in $M|_B$ can be expressed as:

$$d_{M|_B}(V_{\widetilde{B}}) = \dim_{\Bbbk} \mathsf{Hom}_A(V_{\widetilde{B}}, M\big|_B) - \dim_{\Bbbk} \mathsf{Hom}_A\left(V_{\widetilde{B}}/\,\mathsf{soc}(V_{\widetilde{B}}), M\big|_B\right). \quad (3.3)$$

As a left A-module, the interval representation $V_{\widetilde{B}}$ is isomorphic to $P(s) = Ae_s$, where $P(s)$ denotes the indecomposable projective A-module associated with vertex s and e_s is the corresponding primitive idempotent (see [5] for details). An isomorphism $\mathsf{Hom}_A(P(s), M|_B) \cong M|_B(s)$ can be established via

$$\begin{aligned} \mathsf{Hom}_A(P(s), M\big|_B) &\cong M\big|_B(s) \\ f &\mapsto f(e_s) \\ (e_s a \mapsto e_s m a) &\hookleftarrow e_s m, \end{aligned}$$

which implies that $\dim_{\Bbbk} \mathsf{Hom}_A(V_{\widetilde{B}}, M|_B) = \dim_{\Bbbk} M|_B(s)$. For computing the subtrahend, consider the short exact sequence below:

$$\mathbf{0} \longrightarrow \mathsf{soc}(V_{\widetilde{B}}) \xrightarrow{\mu} V_{\widetilde{B}} \xrightarrow{\epsilon} V_{\widetilde{B}}/\,\mathsf{soc}(V_{\widetilde{V}}) \longrightarrow \mathbf{0}.$$

Applying $\mathsf{Hom}_A(-, M|_B)$, a contravariant left-exact functor, yields

$$\begin{aligned} \mathbf{0} \longrightarrow \mathsf{Hom}_A(V_{\widetilde{B}}/\,\mathsf{soc}(V_{\widetilde{B}}), M\big|_B) &\xrightarrow{\mathsf{Hom}_A(\epsilon, M|_B)} \\ \mathsf{Hom}_A(V_{\widetilde{B}}, M\big|_B) &\xrightarrow{\mathsf{Hom}_A(\mu, M|_B)} \mathsf{Hom}_A(\mathsf{soc}(V_{\widetilde{B}}), M\big|_B). \end{aligned}$$

Using the property of exact sequence and noticing that $\mathsf{soc}(V_{\widetilde{B}})$ is equal to the simple module $\Bbbk p$, we obtain

$$\begin{aligned} \mathsf{Hom}_A(V_{\widetilde{B}}/\,\mathsf{soc}(V_{\widetilde{B}}), M\big|_B) &\cong \mathsf{Im}(\mathsf{Hom}_A(\epsilon, M\big|_B)) \\ &\cong \mathsf{Ker}\,\mathsf{Hom}_A(\mu, M\big|_B) \\ &= \left\{ f \in \mathsf{Hom}_A(V_{\widetilde{B}}, M\big|_B) \,\middle|\, f \circ \mu = 0 \right\} \\ &= \left\{ f \in \mathsf{Hom}_A(V_{\widetilde{B}}, M\big|_B) \,\middle|\, f(\mathsf{soc}(V_{\widetilde{B}})) = 0 \right\} \\ &= \left\{ f \in \mathsf{Hom}_A(V_{\widetilde{B}}, M\big|_B) \,\middle|\, f(p) = 0 \right\} \\ &= \left\{ m \in M\big|_B(s) \,\middle|\, M\big|_B(p)(m) = 0 \right\} \\ &= \mathsf{Ker}(M\big|_B(p)), \end{aligned}$$

where the isomorphism $\mathsf{Hom}_A(V_{\widetilde{B}}, M|_B) \cong \mathsf{Hom}_A(P(s), M|_B) \cong M|_B(s)$ proved above is used in the penultimate step. Combining computations so far and applying the rank-nullity theorem to the dimension of the final kernel above, we can reduce (3.3) as

$$\begin{aligned} d_{M|_B}(V_{\widetilde{B}}) &= \dim_{\Bbbk} M\big|_B(s) - \Big(\dim_{\Bbbk} M\big|_B(s) - \mathsf{rank}\big(M\big|_B(p)\big)\Big) \\ &= \mathsf{rank}\big(M\big|_B(p)\big) \\ &= \mathsf{rank}\big(M(p)\big) \\ &= r. \end{aligned}$$

As a result, $M|_B$ decomposes as $M|_B = V_{\widetilde{B}}^{\oplus r} \oplus N$, with $N \in \mathbf{rep}(B)$ not having $V_{\widetilde{B}}$ as a direct summand. By applying the additivity (Proposition 3.20) to this decomposition, we have

$$c^{\widetilde{\xi}}_{M|_B}(\widetilde{B}) = c^{\widetilde{\xi}}_{V_{\widetilde{B}}^{\oplus r} \oplus N}(\widetilde{B}) = r \cdot c^{\widetilde{\xi}}_{V_{\widetilde{B}}}(\widetilde{B}) + c^{\widetilde{\xi}}_{N}(\widetilde{B}) \geq r.$$

Next we show the reverse inequality $c^{\widetilde{\xi}}_{M|_B}(\widetilde{B}) \leq r$. We break down the proof into the following steps.

1. First we observe that s is the only source of B. If s were not a source, there would be a vertex $t \neq u \in B_0$ with an arrow from u to s. By B's defining property, there would be a path from s to t passing through u, leading to a cycle containing s, contradicting G's acyclicity. The definition of the convex hull immediately implies its uniqueness. Similarly, t is the only sink of B.

2. Consider the essential course $\widetilde{\xi}(B) := (C, F)$, where C is a connected quiver and $F\colon C_0 \to B_0$ is the labeling map. Since this is an essential course in B, and s, t are essential vertices of B, there exists vertices $c_s, c_t \in C_0$ such that $F(c_s) = s$ and $F(c_t) = t$. As C is connected, we can find a subquiver W of C of type $\mathbb{A}_n$, which starts from c_s and ends at c_t. This subquiver induces a type $\mathbb{A}_n$ course $\omega := (W, F|_W)$ in B, where $F|_W$ denote the restriction of F to W_0. Observe that vertices in $\mathsf{Im}(F|_W)$ together with arrows between each adjacent pair can be expressed as

$$\underset{s}{\bullet} \to \underset{2}{\bullet} \leftrightarrow \underset{3}{\bullet} \leftrightarrow \cdots \leftrightarrow \underset{n-1}{\bullet} \to \underset{t}{\bullet}, \tag{3.4}$$

   where the directions of the first and last arrows are fixed, as shown in the first step above. Since W is a subquiver of C, the following inequality holds:

$$\begin{aligned} c^{\widetilde{\xi}}_{M|_B}(\widetilde{B}) &= d_{\mathsf{tour}_{\widetilde{\xi}(B)}(M|_B)}\big(\mathsf{tour}_{\widetilde{\xi}(B)}(V_{\widetilde{B}})\big) \\ &\leq d_{\mathsf{tour}_{\omega}(M|_B)}\big(\mathsf{tour}_{\omega}(V_{\widetilde{B}})\big) \\ &=: x. \end{aligned}$$

   Therefore, it suffices to show that $x \leq r$. By definition, $\mathsf{tour}_\omega(V_{\widetilde{B}})^{\oplus x}$ is a summand of $\mathsf{tour}_\omega(M|_B)$, thereby we have the following section and retraction, where $\pi \circ \sigma =$

id:

$$\begin{array}{c} \mathsf{tour}_\omega(M|_B) \\ \sigma \overrightarrow{\uparrow} \quad \downarrow \pi \\ \mathsf{tour}_\omega(V_{\widetilde{B}})^{\oplus x} \end{array} .$$

We can explicitly represent the sections and retractions between vector spaces using the labels in (3.4) as the two commutative diagrams below, where the orientation of horizontal arrows is identical to those in (3.4):

$$\begin{array}{ccccccccccc} M_s & \longrightarrow & M_2 & \longleftarrow & M_3 & \longleftarrow & \cdots & \longleftarrow & M_{n-1} & \longrightarrow & M_t \\ {\scriptstyle\sigma_s}\uparrow & & {\scriptstyle\sigma_2}\uparrow & & {\scriptstyle\sigma_3}\uparrow & & & & {\scriptstyle\sigma_{n-1}}\uparrow & & {\scriptstyle\sigma_t}\uparrow \\ \Bbbk^x & \xrightarrow[\mathsf{id}]{} & \Bbbk^x & \xleftarrow[\mathsf{id}]{} & \Bbbk^x & \xleftarrow[\mathsf{id}]{} & \cdots & \xleftarrow[\mathsf{id}]{} & \Bbbk^x & \xrightarrow[\mathsf{id}]{} & \Bbbk^x \end{array} ,$$

$$\begin{array}{ccccccccccc} M_s & \longrightarrow & M_2 & \longleftarrow & M_3 & \longleftarrow & \cdots & \longleftarrow & M_{n-1} & \longrightarrow & M_t \\ {\scriptstyle\pi_s}\downarrow & & {\scriptstyle\pi_2}\downarrow & & {\scriptstyle\pi_3}\downarrow & & & & {\scriptstyle\pi_{n-1}}\downarrow & & {\scriptstyle\pi_t}\downarrow \\ \Bbbk^x & \xrightarrow[\mathsf{id}]{} & \Bbbk^x & \xleftarrow[\mathsf{id}]{} & \Bbbk^x & \xleftarrow[\mathsf{id}]{} & \cdots & \xleftarrow[\mathsf{id}]{} & \Bbbk^x & \xrightarrow[\mathsf{id}]{} & \Bbbk^x \end{array} .$$

Since each morphism in the lower row is bijective, we can reorient all arrows to be forward-going. With this adjustment, we formulate the following commutative diagram by selecting sections from σ_s to σ_{n-1} together with retraction π_t, and identity maps are also indexed for clarity:

$$\begin{array}{ccccccccccc} M_s & \longrightarrow & M_2 & \longleftarrow & M_3 & \longleftarrow & \cdots & \longleftarrow & M_{n-1} & \longrightarrow & M_t \\ {\scriptstyle\sigma_s}\uparrow & & {\scriptstyle\sigma_2}\uparrow & & {\scriptstyle\sigma_3}\uparrow & & & & {\scriptstyle\sigma_{n-1}}\uparrow & & {\scriptstyle\pi_t}\downarrow \\ \Bbbk^x & \xrightarrow[\mathsf{id}_x(s\to 2)]{} & \Bbbk^x & \xrightarrow[\mathsf{id}_x(2\to 3)]{} & \Bbbk^x & \xrightarrow[\mathsf{id}_x(3\to 4)]{} & \cdots & \xrightarrow[\mathsf{id}_x(n-2\to n-1)]{} & \Bbbk^x & \xrightarrow[\mathsf{id}_x(n-1\to t)]{} & \Bbbk^x \end{array} .$$

Let $\mathsf{id}_x(s \to t)$ denote the composition of all identity maps in the lower row. If we can prove $\pi_t \circ M(p) \circ \sigma_s = \mathsf{id}_x(s \to t)$, then it would follow that $r = \mathsf{rank}\big(M(p)\big) \geq \mathsf{rank}\big(\mathsf{id}_x(s \to t)\big) = x$.

3. Now, we prove the aforementioned equation in the second step. Let $M_1 := M_s$, $p_1 := p$, $\sigma_1 := \sigma_s$ and $M_n := M_t$, $p_n := \mathsf{id}_{M_t}$, $\sigma_n := \sigma_t$ for easier indexing. By the definition of the convex hull $B = \mathsf{Conv}(\{ s, t \})$, each vertex in it lies on a path from s to t. Hence the following commutative diagram exists for $i = 2, 3, \ldots, n$:

$$\begin{array}{ccccc} & & {\scriptstyle M(p_{i-1})}\frown & & \\ M_{i-1} & \xleftarrow[M(i-1\leftrightarrow i)]{} & M_i & \xrightarrow[M(p_i)]{} & M_t. \end{array}$$

We follow the procedures below to reduce the map $M(p_{i-1}) \circ \sigma_{i-1}$ for $i = 2, 3, \ldots, n-1$.

- If the arrow from M_{i-1} to M_i goes forward, then by the commutative diagram

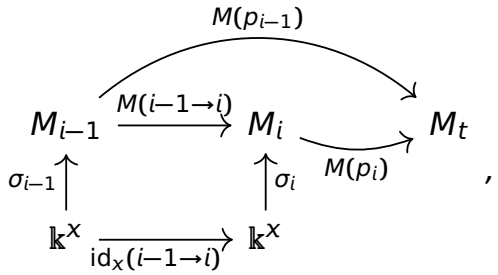

,

  we have

$$M(p_{i-1}) \circ \sigma_{i-1} = M(p_i) \circ M(i-1 \to i) \circ \sigma_{i-1} = M(p_i) \circ \sigma_i \circ \mathrm{id}_x(i-1 \to i).$$

- If the arrow from M_{i-1} to M_i goes backward, then by the commutative diagram

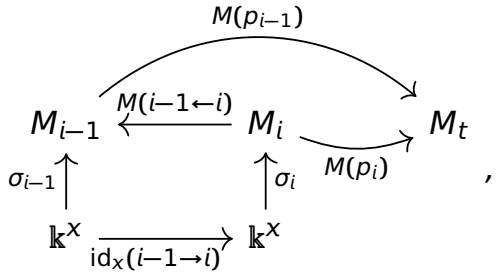

,

  we have

$$\begin{aligned} M(p_{i-1}) \circ \sigma_{i-1} &= M(p_{i-1}) \circ M(i-1 \leftarrow i) \circ \sigma_i \circ \mathrm{id}_x(i-1 \to i) \\ &= M(p_i) \circ \sigma_i \circ \mathrm{id}_x(i-1 \to i). \end{aligned}$$

Applying this reduction iteratively, we obtain

$$\begin{aligned} \pi_t \circ M(p) \circ \sigma_s &= \pi_t \circ M(p_1) \circ \sigma_1 \\ &= \pi_t \circ M(p_2) \circ \sigma_2 \circ \mathrm{id}_x(1 \to 2) \\ &\vdots \\ &= \pi_t \circ M(p_n) \circ \sigma_n \circ \mathrm{id}_x(n-1 \to n) \circ \cdots \circ \mathrm{id}_x(2 \to 3) \circ \mathrm{id}_x(1 \to 2) \\ &= \pi_t \circ \sigma_t \circ \mathrm{id}_x(s \to t) \\ &= \mathrm{id}_x(s \to t). \end{aligned}$$

This concludes the proof.

□

Theorem 3.29. *Let ξ be an essential assignment on G, M be a representation in $\mathbf{rep}(G)$, and p be a path in G. Then the following equation holds:*

$$\mathrm{rank}\big(M(p)\big) = \sum_{I \in \mathbb{I}_G} \delta_M^{\xi}(I) \cdot \mathrm{rank}\big(V_I(p)\big).$$

Proof. If p is a zero path, then both sides are equal to zero. For non-zero paths, the result follows directly from the two preceding lemmas. □

3.3 Approximation Series in 2D Grids

In this subsection, we focus on the computation of interval approximations in a two-dimensional commutative grid $\vec{G}_{p,q}$. Even though the number of interval representations in $\mathbb{I}_{p,q}$ is finite, it increases exponentially with the size of $\vec{G}_{p,q}$. To address this problem, we define a series of partial approximations, each one necessitating more computational demands but also providing incrementally details. Additionally, we demonstrate that the interactive visualization of a 2D persistence module by the barcodes of 1D affine slices in [31] can be reformulated using an approximation in the series developed.

Theorem 3.30. *[1, Theorem 31] The number of interval representations of $\vec{G}_{p,q}$ is given by*

$$\#\mathbb{I}_{p,q} = \sum_{h=1}^{q}\sum_{w=1}^{p} \frac{(q-h+1)(p-w+1)}{h+w-1} \cdot \binom{h+w-1}{h-1} \cdot \binom{h+w-1}{w-1}.$$

In particular, $\#\mathbb{I}_{p,q}$ is $O(p^{2q})$ for $p \geq q$.

We can stratify intervals by enumerating the number of essential vertices since an interval is fully determined by its essential vertices. As a result, the number of essential vertices serves as an indicator of the interval's complexity.

Definition 3.31 (k-essential Interval)**.** Given a positive integer k, the set of *k-essential intervals* $\mathbb{E}_k$ of $\vec{G}_{p,q}$ is a subset of $\mathbb{I}_{p,q}$ that includes all intervals with exactly k essential vertices, expressed as:

$$\mathbb{E}_k = \left\{ I \in \mathbb{I}_{p,q} \;\middle|\; \#E(I) = k \right\}.$$

Furthermore, we use $\mathbb{E}_{\leq k}$ to represent the disjoint union of all i-essential intervals for $i \leq k$:

$$\mathbb{E}_{\leq k} := \bigcup_{i \leq k} \mathbb{E}_i.$$

Example 3.32. The description and cardinality of $\mathbb{E}_k$ for $k = 1, 2, 3$ are detailed as follows:

$$\mathbb{E}_1 = \left\{ I \in \mathbb{I}_{p,q} \;\middle|\; I \text{ is a vertex} \right\}, \qquad \#\mathbb{E}_1 = p \cdot q,$$

$$\mathbb{E}_2 = \left\{ I \in \mathbb{I}_{p,q} \;\middle|\; \begin{matrix}\text{I is a line segment} \\ \text{or a rectangle}\end{matrix} \right\}, \qquad \#\mathbb{E}_2 = \tbinom{p}{2} \cdot q + \tbinom{q}{2} \cdot p + \tbinom{p}{2} \cdot \tbinom{q}{2},$$

$$\mathbb{E}_3 = \left\{ I \in \mathbb{I}_{p,q} \;\middle|\; \#E(I) = 3 \right\}, \qquad \#\mathbb{E}_3 = \tfrac{pq}{18} \cdot (p^2-1) \cdot (q^2-1).$$

Note that vertices are not considered line segments or rectangles in $\mathbb{E}_2$. The three terms in the expression for $\#\mathbb{E}_2$ represent the number of horizontal line segments, vertical line segments, and rectangles, respectively. For $\#\mathbb{E}_3$, we can count the ways of cutting a smaller rectangle from a larger non-degenerate rectangle of size subject to the condition that either the top-right or the bottom-left vertices of both rectangles coincide. This enumeration is formulated by the sum $\sum_{h=2}^{q}\sum_{w=2}^{p} 2 \cdot \underbrace{(p-w+1)\cdot(q-h+1)}_{\#\text{larger rectangles of size } w \times h} \cdot \underbrace{(w-1)\cdot(h-1)}_{\#\text{smaller rectangles}}$, which then reduces to the expression above. We can also verify that $\#\mathbb{E}_3$ is also equal to $2 \cdot \binom{p+1}{3} \cdot \binom{q+1}{3}$, leading to

another way to compute $\#\mathbb{E}_3$ by considering the three essential vertices $v_i := (x_i, y_i)$ that define the intervals. Assuming the vertices are ordered from left to right (so that $x_1 \le x_2 \le x_3$). Now, we count the ways to choose coordinates for these vertices. The binomial coefficient $\binom{p+1}{3} = \binom{p}{3} + \binom{p}{2}$ corresponds to the number of ways to choose three increasing x-coordinates, where $\binom{p}{3}$ is for the strictly increasing case and $\binom{p}{2}$ for the case with one equality. Similarly, the number of ways of choosing y-coordinates is $\binom{q+1}{3}$. We also notice that there are two ways to assign the y-values, and they have to satisfy either $y_1 \le y_3 \le y_2$ or $y_2 \le y_1 \le y_3$, which corresponds to the coefficient 2. This combinatorial explanation ensures that all configurations are accounted for, and it provides a systematic way to calculate the total number of intervals with three essential vertices.

Recall the definitions of cover and join from Definition 3.23. For a subset $\mathbb{J}$ of $\mathbb{I}_{p,q}$, we define $\mathsf{Cov}_{\mathbb{J}} J$ as the cover of J induced by the partial order on $\mathbb{J}$ for each $J \in \mathbb{J}$. Likewise, given an interval $J \in \mathbb{J}$ and a subset $S \subseteq \mathsf{Cov}_{\mathbb{J}} J$, we use $\bigvee_{\mathbb{J}} S$ to denote the join of S under the induced partial order, assuming it exists. We can now generalize the concept of interval approximation from Definition 3.25 by broadening the criteria for intervals to be considered.

Definition 3.33 (Partial Interval Approximation)**.** Consider a representation $M \in \mathbf{rep}(\vec{G}_{p,q})$, a set $\mathbb{J} \subseteq \mathbb{I}_{p,q}$, and an essential assignment ξ defined on $\mathbb{J}$. A *partial interval approximation* of M by $\mathbb{J}$ via ξ-compressed multiplicities is defined as an integer-valued function ${}_{\mathbb{J}}\delta_M^{\xi}$ defined on intervals of $\mathbb{J}$ that satisfies the following equation for any $I \in \mathbb{J}$:

$$c_M^{\xi}(I) = \sum_{I \le J \in \mathbb{J}} {}_{\mathbb{J}}\delta_M^{\xi}(J).$$

Remark 3.34. In parallel to Remark 3.26, ${}_{\mathbb{J}}\delta_M^{\xi}(J)$ can be built up by firstly setting ${}_{\mathbb{J}}\delta_M^{\xi}(J) := c_M^{\xi}(J)$ for each J that is a maximal element of $\mathbb{J}$, then tracing down along the cover relations in iterative steps by setting ${}_{\mathbb{J}}\delta_M^{\xi}(J) := c_M^{\xi}(J) - \sum_{J < I \in \mathbb{J}} {}_{\mathbb{J}}\delta_M^{\xi}(I)$. Similarly, if $\mathsf{Cov}_{\mathbb{J}} J$ and $\bigvee_{\mathbb{J}} S$ are well-defined for any $J \in \mathbb{J}$ and $S \subseteq \mathsf{Cov}_{\mathbb{J}} J$, we can use the Möbius inversion to express the partial interval approximation as:

$${}_{\mathbb{J}}\delta_M^{\xi}(J) = \sum_{S \subseteq \mathsf{Cov}_{\mathbb{J}} J} (-1)^{\#S} \cdot c_M^{\xi}(\bigvee_{\mathbb{J}} S).$$

Remark 3.35. We refer to the partial interval approximation ${}_{\mathbb{E}_{\le 2}}\delta_M^{\xi}(J)$ as the *rectangle approximation*.

Definition 3.36 (Rank Invariant)**.** Consider a representation M in $\mathbf{rep}(\vec{G}_{p,q})$ and a subset of intervals $\mathbb{J} \subseteq \mathbb{I}_{p,q}$. A partial interval approximation ${}_{\mathbb{J}}\delta_M^{\xi}$ is said to be *rank invariant* if the rank of M over any path w in $\vec{G}_{p,q}$ can be expressed as the following weighted sum:

$$\mathsf{rank}\big(M(w)\big) = \sum_{J \in \mathbb{J}} {}_{\mathbb{J}}\delta_M^{\xi}(J) \cdot \mathsf{rank}\big(V_J(w)\big).$$

Example 3.37. Any interval approximation δ_M^ξ is rank invariant, as shown by Theorem 3.29.

The compressed multiplicity function $c_M^\xi(J)$ offers more flexibility compared to the rank function, stemming from the freedom to select J and ξ. This flexibility permits the selection of a subset $\mathbb{J}$ of intervals $\mathbb{I}_{p,q}$ for approximation, leading to a generalization of the rank invariant property.

Definition 3.38 (k-rank Invariant)**.** Let k be a fixed non-negative integer. A partial interval approximation ${}_{\mathbb{J}}\delta_M^\xi$ is said to be *k-rank invariant* if the following equation holds for any $I \in \mathbb{E}_{\leq k+1}$:

$$c_M^\xi(I) = \sum_{J \in \mathbb{J}} {}_{\mathbb{J}}\delta_M^\xi(J) \cdot c_{V_J}^\xi(I).$$

We now establish the equivalence between rank invariance and 1-rank invariance. Consider a path $s \xrightarrow{\alpha_l \cdots \alpha_1} t$ in $\vec{G}_{p,q}$ and the rectangle interval I bounded by vertices s and t. By invoking Lemma 3.28, we obtain:

$$c_M^\xi(I) = d_{\mathrm{tour}_{\xi(I)}(M)}\big(\mathrm{tour}_{\xi(I)}(V_I)\big) = \mathrm{rank}\big(M(s \xrightarrow{\alpha_l \cdots \alpha_1} t)\big).$$

Meanwhile, Proposition 3.21 indicates that $c_{V_J}^\xi(I)$ is equal to $\mathrm{rank}\big(V_J(s \xrightarrow{\alpha_l \cdots \alpha_1} t)\big)$. Substituting these two equations back into the defining equation of being 1-rank invariant completes the statement.

Remark 3.39. We observe that 0-rank invariance is equivalent to preserving the dimension vector of the original representation. As discussed above, 1-rank invariance ensures that the rank of paths is maintained. Furthermore, 2-rank invariance preserves information about more complex shapes, such as the L-shaped regions depicted in $\mathbb{E}_3$ of Example 3.32.

Theorem 3.40. *Let M be a representation of $\vec{G}_{p,q}$. If $\mathbb{E}_{\leq k+1} \subseteq \mathbb{J}$, then the partial interval approximation ${}_{\mathbb{J}}\delta_M^\xi$ is k-rank invariant. In particular, the interval approximation $\delta_M^\xi = {}_{\mathbb{E}_{\leq\infty}}\delta_M^\xi$ is k-rank invariant with respect to all non-negative integers k.*

Proof. Consider the defining equation $c_M^\xi(I) = \sum_{I \leq J \in \mathbb{J}} {}_{\mathbb{J}}\delta_M^\xi(J)$. Given $c_{V_J}^\xi(I) = \begin{cases} 1 & I \leq J \\ 0 & \text{otherwise} \end{cases}$ by Proposition 3.21, we can incorporate a multiplier $c_{V_J}^\xi(I)$ for each summand, and then change the summation range to $J \in \mathbb{J}$. This adjusted summation aligns with the definition of being k-rank invariant, concluding the proof. □

Corollary 3.41. *If $\mathbb{E}_{\leq 2} \subseteq \mathbb{J}$, then ${}_{\mathbb{J}}\delta_M^\xi$ is rank invariant. As a result, the rectangle approximation ${}_{\mathbb{E}_{\leq 2}}\delta_M^\xi$ as defined in Remark 3.35 is also rank invariant.*

Here, we show that rectangle approximations of a 2D persistence module are equivalent to 1D affine slices as described in RIVET [31]. We use $\overset{t}{\underset{s}{\square}}$ in $\mathbb{E}_{\leq 2}$ to denote the rectangle interval bounded by the two vertices s and t if there exists a path from

s to t. Consider the slice along the line connecting u_1 and u_n in Figure 3.5, and let A_n denote the type $\mathbb{A}_n$ quiver defined by the slice. We denote the interval of A_n connecting s and t as $[s,t]$. The multiplicity of $V_{[u_b,u_d]}$ in the compressed representation $\mathsf{tour}_{\xi^{ss}(u_1 \square^{u_n})}(M) \in \mathbf{rep}(A_n)$ can be calculated as:

$$\begin{aligned}
&d_{\mathsf{tour}_{\xi^{ss}(u_1 \square^{u_n})}(M)}\big(V_{[u_b,u_d]}\big)\\
=&\,\mathsf{rank}\big(M(u_b \to u_d)\big) - \mathsf{rank}\big(M(u_{b-1} \to u_d)\big)\\
&- \mathsf{rank}\big(M(u_b \to u_{d+1})\big) + \mathsf{rank}\big(M(u_{b-1} \to u_{d+1})\big)\\
=&\, c_M^{\xi^{ss}}(u_b \square^{u_d}) - c_M^{\xi^{ss}}(u_{b-1} \square^{u_d}) - c_M^{\xi^{ss}}(u_b \square^{u_{d+1}}) + c_M^{\xi^{ss}}(u_{b-1} \square^{u_{d+1}}).
\end{aligned}$$

The multiplicity of $V_{[u_b,u_d]}$ in the compressed representation $\mathsf{tour}_{\xi^{ss}(u_1 \square^{u_n})}(M)$ is equal to the multiplicity of the interval $[u_b, u_d]$ in the persistence diagram of the slice, therefore, both the rectangle approximation and RIVET's persistence diagram are determined by $\{ c_M^{\xi^{ss}}(I) \}_{I \in \mathbb{I}_{\leq 2}}$.

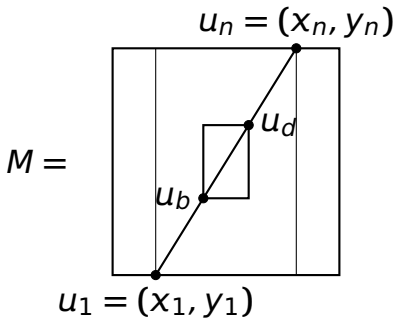

Figure 3.5: Illustration of a 1D affine slice in a 2D grid.

Based on these observations, we construct an approximation series on $\vec{G}_{p,q}$ employing the stratification provided by k-essential intervals, depicted in Figure 3.6. The top row displays the order of the interval count for each corresponding set below. The third row lists partial interval approximations, the fourth row shows names for specific invariants, and the bottom row illustrates the change in resolution.

It is worth noting that for any fixed $\vec{G}_{p,q}$, this approximation series stabilizes because the number of k-essential intervals in $\mathbb{I}_{p,q}$ is finite. The series starts with the dimension vector and ends with the interval approximation. RIVET's persistence diagram/rectangle approximation is located just to the right of the dimension vector. As the series progresses, the corresponding partial interval approximation provides more information about the morphisms of the representation M since more intervals are included at the cost of higher computational demands.

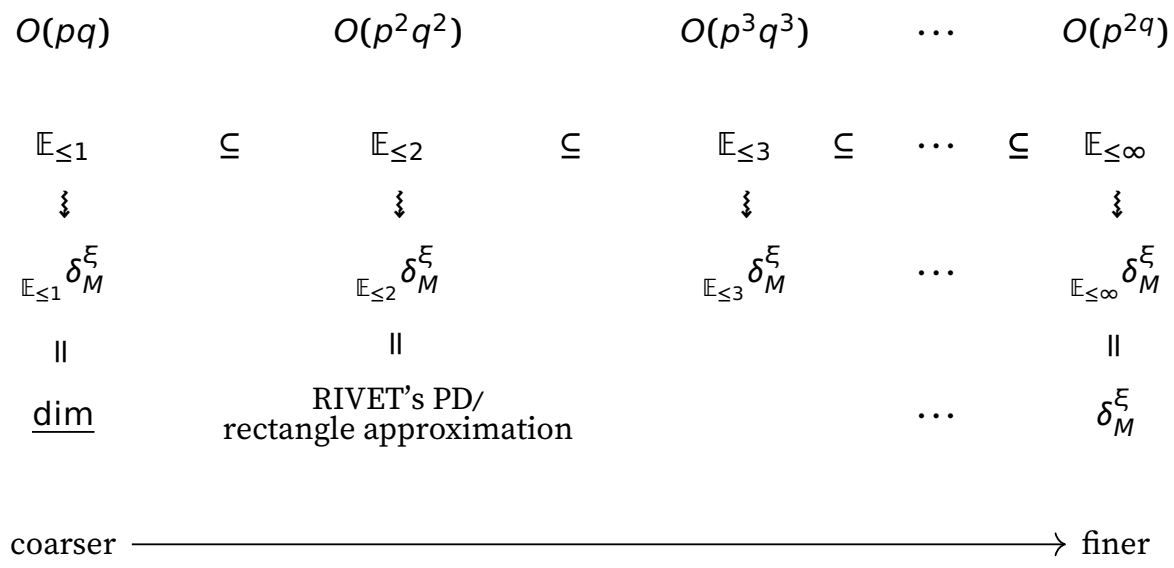

Figure 3.6: Partial interval approximation series constructed from an increasing sequence of k-essential intervals.

4 Topological Invariants for Commutative Ladders

In this section, we validate the effectiveness of our theoretical framework by addressing specific challenges associated with commutative ladders. We first devise an algorithm that efficiently computes the indecomposable decomposition of any representation of an equi-oriented finite-type commutative ladder, then extend persistence diagrams to infinite-type cases. While our focus here is primarily on the equi-oriented cases, both approaches can seamlessly extend to an arbitrary orientation τ_n.

4.1 Finite-Type Commutative Ladders: Indecomposable Decomposition

Consider a finite-type commutative ladder $\mathsf{CL}(n)$. Let $\mathcal{L}$ be a complete set of representatives of the isomorphism classes of indecomposable $\mathsf{CL}(n)$-modules. Our objective is to compute the persistent homology of a $\mathsf{CL}(n)$-filtration X, represented as $M := H_k(X)$. This amounts to determine the multiplicity function $d_M(L)$ for every $L \in \mathcal{L}$. While existing theoretical frameworks such as [4, Theorem 3.4] and [18, Section 4] can handle this, they both require the explicit representation of M and the determination of a common basis for the hom-sets between multiple vector spaces, which can be computationally intensive.

In contrast, our algorithm circumvents the direct use of M and instead utilizes the filtration X. This approach transforms the original computation into numerous computations of zigzag persistent homology, a tool where mature and fast algorithms are already available [11]. As a result, we can significantly reduce computational demands and make it more tractable for practical implementations.

Let $G = (Q, R)$ be a fully commutative quiver and $\mathcal{L}$ be a finite subset of a complete set of representatives of the isomorphism classes of indecomposables in $\mathbf{rep}(G)$. We say a representation $M \in \mathbf{rep}(G)$ is *$\mathcal{L}$-decomposable* if every indecomposable direct summand of M is isomorphic to an element in $\mathcal{L}$. For any $\mathcal{L}$-decomposable representation

$M \in \mathbf{rep}(G)$ with $M = H_k(X)$, Theorem 2.19 guarantees the following decomposition:

$$M \cong \bigoplus_{L \in \mathcal{L}} L^{d_M(L)}.$$

Consider a family of functions $\{ f_j \}_{j \in J}$ on $\mathbf{rep}(G)$ that are compatible with direct sum operations and isomorphism (referred to as the *compatibility condition* in the subsequent discussion). Applying these functions to the decomposition of M yields the following set of equations:

$$f_j(M) = \sum_{L \in \mathcal{L}} f_j(L) \cdot d_M(L), \quad \forall j \in J.$$

These equations can be summarized into a matrix expression (assuming the column vector convention):

$$\Big(f_j(M)\Big)_{j \in J} = \Big(f_j(L)\Big)_{\substack{j \in J \\ L \in \mathcal{L}}} \cdot \Big(d_M(L)\Big)_{L \in \mathcal{L}}.$$

The coefficient matrix has $|J|$ rows and $|\mathcal{L}|$ columns, where we can assume $|J| = |\mathcal{L}|$ [1] . If its rank is equal to $|\mathcal{L}|$, then there exists a left inverse to it, from which the multiplicity functions can be solved as

$$\Big(d_M(L)\Big)_{L \in \mathcal{L}} = \Big(f_j(L)\Big)^{-1}_{\substack{L \in \mathcal{L} \\ j \in J}} \cdot \Big(f_j(M)\Big)_{j \in J}.$$

Notice that the inverse of the coefficient matrix is independent of the knowledge about M. For each new filtration X and the associated $H_k(X)$, we only need to recompute the vector $\Big(f_j(M)\Big)_{j \in J} = \Big(f_j \circ H_k(X)\Big)_{j \in J}$.

Example 4.1. This example examines the finite-type commutative ladder $\mathsf{CL}(3)$. Let $\mathcal{L}$ denote a complete set of representatives of isomorphism classes of $\mathbf{rep}\big(\mathsf{CL}(3)\big)$, where $|\mathcal{L}| = 29$ by [18]. Denoting the vertex set of $\mathsf{CL}(3)$ as $V := \{ 11, 21, 31, 12, 22, 32 \}$, each representation M can be formulated as:

$$\begin{array}{ccccc} M_{12} & \longrightarrow & M_{22} & \longrightarrow & M_{32} \\ \uparrow & & \uparrow & & \uparrow \\ M_{11} & \longrightarrow & M_{21} & \longrightarrow & M_{31} \end{array}.$$

Consider the following functions defined on $\mathbf{rep}\big(\mathsf{CL}(3)\big)$:

- $f_x(M) := d_{M_x}(\Bbbk) = \dim M_x$ for $x \in V$;
- $f_{x,y}(M) := d_{M_x \to M_y}(\Bbbk \xrightarrow{\mathrm{id}} \Bbbk) = \mathrm{rank}\big(M_x \to M_y\big)$ for $x \neq y \in V$ if there exists a path from x to y;

[1] To solve this linear system, a coefficient matrix of rank $|\mathcal{L}|$ is required. If $|J| < |\mathcal{L}|$, this system is underdetermined, and we need to add more functions. If $|J| > |\mathcal{L}|$, we can remove surplus functions from $\{ f_j \}_{j \in J}$ to equate $|J|$ and $|\mathcal{L}|$.

- $f_{x,y,z}(M) := d_{M_x \to M_y \leftarrow M_z}(\Bbbk \xrightarrow{\mathrm{id}} \Bbbk \xleftarrow{\mathrm{id}} \Bbbk)$ for distinct $x, y, z \in V$ if there exists a course $(C = \underset{a}{\bullet} \to \underset{b}{\bullet} \leftarrow \underset{c}{\bullet}, F)$ on $\mathsf{CL}(3)$ such that $F(a) = x,\ F(b) = y,\ F(c) = z$;

- $g_{x,y,z}(M) := d_{M_x \leftarrow M_y \to M_z}(\Bbbk \xleftarrow{\mathrm{id}} \Bbbk \xrightarrow{\mathrm{id}} \Bbbk)$ for distinct $x, y, z \in V$ if there exists a course $(C = \underset{a}{\bullet} \leftarrow \underset{b}{\bullet} \to \underset{c}{\bullet}, F)$ on $\mathsf{CL}(3)$ such that $F(a) = x,\ F(b) = y,\ F(c) = z$;

- $f_{x,y,z,w}(M) := d_{M_x \to M_y \leftarrow M_z \to M_w}(\Bbbk \xrightarrow{\mathrm{id}} \Bbbk \xleftarrow{\mathrm{id}} \Bbbk \xrightarrow{\mathrm{id}} \Bbbk)$ for distinct $x, y, z, w \in V$ if there exists a course $(C = \underset{a}{\bullet} \to \underset{b}{\bullet} \leftarrow \underset{c}{\bullet} \to \underset{d}{\bullet}, F)$ on $\mathsf{CL}(3)$ such that $F(a) = x,\ F(b) = y,\ F(c) = z,\ F(d) = w$.

All these functions meet the compatibility condition. The linear space spanned by the family of functions of form f_x and $f_{x,y}$ on $\mathcal{L}$ has a dimension of 16. This dimension increases to 26 by including all functions defined by type $\mathbb{A}_3$ courses (*i.e.*, functions of the form $f_{x,y,z}$ and $g_{x,y,z}$), and further to $|\mathcal{L}|$=29 upon adding three linearly independent functions of the form $f_{x,y,z,w}$[2]. This yields a coefficient matrix that can be used to compute the indecomposable decomposition of any representation of $\mathsf{CL}(3)$.

Definition 4.2 (Zigzag Course with an Alternating Orientation)**.** A course (C, F) is called a *zigzag course with an alternating orientation* if C is a type $\mathbb{A}_n$ quiver with orientation $\tau = (fbfbfb\cdots)$. This definition accommodates the general one-parameter cases with any orientation since consecutive arrows pointing in the same direction can be composed together, and if the first arrow points backward, it can be repeated twice. For brevity, we use the term "alternating zigzag course" to refer to such a course.

Example 4.3. Consider a course $(\underset{x}{\bullet} \leftarrow \underset{y}{\bullet} \to \underset{z}{\bullet}, F)$ with orientation type (bf). To transform it into an alternating zigzag course starting with a forward arrow, we build a type $\mathbb{A}_4$ course $(\underset{a}{\bullet} \to \underset{b}{\bullet} \leftarrow \underset{c}{\bullet} \to \underset{d}{\bullet}, \widetilde{F})$, with the labeling map below:

$$\widetilde{F}(a) := F(y),\ \widetilde{F}(b) := F(x),\ \widetilde{F}(c) := F(y),\ \widetilde{F}(d) := F(z).$$

This modified course effectively prepends the map $\underset{y}{\bullet} \to \underset{x}{\bullet}$ to the original course, and it satisfies the definition of an alternating zigzag course. It can be easily verified that all computations using it in the ξ-compressed multiplicity yield the same results as those obtained from the original course based on the definition.

Remark 4.4. Recall that $\mathfrak{s}$ and $\mathfrak{t}$ assign the start and target of a path. For $n \geq 2$, a sequence of paths $(p_1, \ldots, p_{n-1})$ determines an alternating zigzag course (C, F) of type $\mathbb{A}_n$ if it meets one of the following conditions:

- If $n = 2$, then the path p_1 always determines an alternating zigzag course, which is given by $C = \underset{1}{\bullet} \to \underset{2}{\bullet}$ and $F(1) = \mathfrak{s}(p_1)$, $F(2) = \mathfrak{t}(p_1)$.

[2]One possible choice is to set (x, y, z, w) as in $\{\ (12, 22, 21, 31), (11, 31, 21, 22), (21, 22, 12, 32)\ \}$.

- If $n > 2$, then it determines an alternating zigzag course if and only if the pattern below is satisfied:

$$\underset{1}{\bullet} \xrightarrow{p_1} \underset{2}{\bullet} \xleftarrow{p_2} \underset{3}{\bullet} \xrightarrow{p_3} \cdots \xleftrightarrow{p_{n-1}} \underset{n}{\bullet},$$

  where p_{n-1} points forwards if n is even, and backwards if n is odd. This condition can be expressed as:

  - $\mathfrak{t}(p_i) = \mathfrak{t}(p_{i+1})$ for odd i with $1 \le i \le n-2$;
  - $\mathfrak{s}(p_i) = \mathfrak{s}(p_{i+1})$ for even i with $2 \le i \le n-2$.

  The alternating zigzag course (C, F) can be easily read from the graphic pattern above.

Given an alternating zigzag course (C, F), recall that V_C denotes the longest interval representation in $\mathbf{rep}(C)$. We associate this course with the following function on $\mathbf{rep}(G)$:

$$f_{(C,F)}(M) := d_{\mathsf{tour}_{(C,F)}(M)}(V_C). \tag{4.1}$$

Notice that it satisfies the compatibility condition. In particular, although the representation M appears in the subscript, representation $\mathsf{tour}_{(C,F)}(M) = \mathsf{tour}_{(C,F)}\big(H_k(X)\big)$ is always of type $\mathbb{A}_n$. Therefore, we do not need to compute the representation M in advance, significantly speeding up the computation.

Our current objective is to identify a sufficient number of alternating zigzag courses that can induce linearly independent functions. To achieve this, we need to determine the labeling map

$$F\colon (A_n)_0 \to G_0$$

via a sequence of (non-trivial) paths $p_1, \ldots, p_{n-1}$ that form an alternating zigzag course (A_n, F) for $n \le N$, where N is a preset limit. Since G is a finite acyclic quiver, the count of alternating zigzag courses (hence labeling maps) is finite for any fixed positive integer n. This allows for an exhaustive search for all courses. Appendix A.1 provides an illustrative enumeration algorithm and Appendix A.2 shows a more efficient breadth-first search algorithm.

After gathering all alternating zigzag courses up to length N, we associate each course with a function defined by (4.1). Notice that multiple courses can result in the same function, and the generated functions can be linearly dependent (for example, the first path in an alternating zigzag course can be repeated twice, similar to the steps described in Example 4.3). An algorithm of this process is provided in Appendix A.3.

We execute the algorithms on $\mathsf{CL}(n)$ for $n = 2, 3, 4$ and successfully find sufficient linearly independent functions to solve their indecomposable decompositions. Specifically, for $\mathsf{CL}(4)$, choosing $N = 6$ serves as an adequate preset limit, and a detailed list of the obtained 76 alternating zigzag courses can be found in [23]. As an illustration, we show five such courses in Figure 4.1. The vertices in each course are labeled with letters, while those in $\mathsf{CL}(4)$ are labeled with their Cartesian coordinates. Several alternating zigzag courses in this figure do not belong to the three types of compressions defined in [3], demonstrating the capability of our framework to extract deeper insights compared to the existing methods.

Alternating zigzag course	Type	Labeling map	Graphic diagram
	$\mathbb{A}_3$	$a\mapsto(1,2)$, $b\mapsto(4,2)$ $c\mapsto(2,1)$	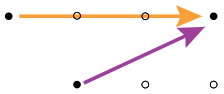
	$\mathbb{A}_4$	$a\mapsto(1,2)$, $b\mapsto(2,2)$ $c\mapsto(2,1)$, $d\mapsto(4,2)$	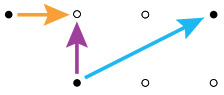
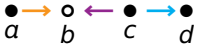	$\mathbb{A}_4$	$a\mapsto(2,1)$, $b\mapsto(3,2)$ $c\mapsto(1,2)$, $d\mapsto(4,2)$	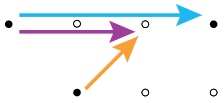
	$\mathbb{A}_5$	$a\mapsto(2,1)$, $b\mapsto(4,2)$ $c\mapsto(1,2)$, $d\mapsto(3,2)$ $e\mapsto(3,1)$	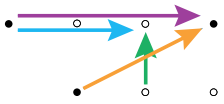
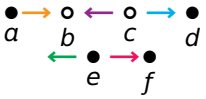	$\mathbb{A}_6$	$a\mapsto(2,1)$, $b\mapsto(4,1)$ $c\mapsto(3,1)$, $d\mapsto(3,2)$ $e\mapsto(1,2)$, $f\mapsto(4,2)$	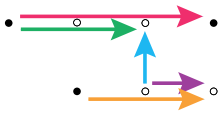

Figure 4.1: Five alternating zigzag courses used for solving the indecomposable decomposition of representations in $\mathsf{CL}(4)$. They are essential courses in the interval depicted in Figure 3.2, with essential vertices shown as solid dots.

4.2 Infinite-Type Commutative Ladders: Connected Persistence Diagram

Our discussion in the previous subsection relies on the $\mathcal{L}$-decomposability condition with a predetermined finite set of isomorphism classes $\mathcal{L}$, where the finiteness requirement cannot be generalized to representations of a general $\mathsf{CL}(n)$. To broaden our framework's applicability, we introduce a novel invariant crafted specifically for general commutative ladders by leveraging their unique two-row structure. This invariant captures the topological information in the two rows extractable via one-parameter persistence in the horizontal direction and measures the vertical persistence of generators along these two rows, using a selected essential assignment.

By setting the parameters in (2.2) to $p = n, q = 2$ and categorizing intervals into subsets based on their support, we can obtain an indexing for intervals in $\mathsf{CL}(n)$ as below:

$$\begin{aligned}\mathbb{I} := \mathbb{I}_{n,2} = &\{\, [b_1, d_1]_1 \mid 1 \le b_1 \le d_1 \le n \,\} \\ &\sqcup \{\, [b_2, d_2]_2 \mid 1 \le b_2 \le d_2 \le n \,\} \\ &\sqcup \{\, [b_1, d_1]_1 \sqcup [b_2, d_2]_2 \mid 1 \le b_2 \le b_1 \le d_2 \le d_1 \le n \,\} \\ &= \mathbb{I}_1 \sqcup \mathbb{I}_2 \sqcup \mathbb{I}_{2/1},\end{aligned} \tag{4.2}$$

where $\mathbb{I}_1$ contains all intervals entirely supported in the lower row, $\mathbb{I}_2$ contains all intervals entirely supported in the upper row, and $\mathbb{I}_{2/1}$ contains intervals with support that bridges the two rows. An element of form $[b_i, d_i]_i$ in $\mathbb{I}_1$ or $\mathbb{I}_2$ has type $\mathbb{A}_{d_i - b_i + 1}$, and a typical

element in $\mathbb{I}_{2/1}$ is shown below:

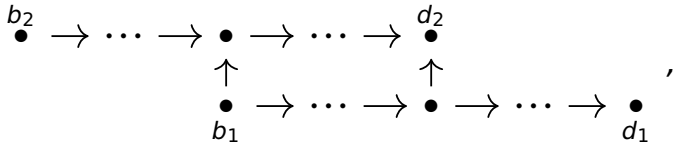

where vertices b_1 and b_2 can share a column, as can d_1 and d_2.

Definition 4.5. Consider an essential assignment ξ on $\mathbb{I}$ and a persistence module M of $\mathsf{CL}(n)$ as:

$$M := \begin{array}{ccccccc} M_{(1,2)} & \longrightarrow & M_{(2,2)} & \longrightarrow & \cdots & \longrightarrow & M_{(n,2)} \\ \uparrow & & \uparrow & & & & \uparrow \\ M_{(1,1)} & \longrightarrow & M_{(2,1)} & \longrightarrow & \cdots & \longrightarrow & M_{(n,1)} \end{array} . \tag{4.3}$$

We define an auxiliary function $\widetilde{\delta}^{\xi}_{M} : \mathbb{I} \to \mathbb{Z}$ constructed from the interval approximation δ^{ξ}_{M}, as per the steps delineated below.

- For intervals in $\mathbb{I}_1$, with fixed indices b_1 and d_1, we define

$$\widetilde{\delta}^{\xi}_{M}([b_1, d_1]_1) = \delta^{\xi}_{M}([b_1, d_1]_1) + \sum_{[b_2,d_2]_2 \sqcup [b_1,d_1]_1 \in \mathbb{I}_{2/1}} \delta^{\xi}_{M}([b_2, d_2]_2 \sqcup [b_1, d_1]_1).$$

- For intervals in $\mathbb{I}_2$, given b_2 and d_2, we define

$$\widetilde{\delta}^{\xi}_{M}([b_2, d_2]_2) = \delta^{\xi}_{M}([b_2, d_2]_2) + \sum_{[b_2,d_2]_2 \sqcup [b_1,d_1]_1 \in \mathbb{I}_{2/1}} \delta^{\xi}_{M}([b_2, d_2]_2 \sqcup [b_1, d_1]_1).$$

- For intervals in $\mathbb{I}_{2/1}$, we define

$$\widetilde{\delta}^{\xi}_{M}([b_2, d_2]_2 \sqcup [b_1, d_1]_1) := \delta^{\xi}_{M}([b_2, d_2]_2 \sqcup [b_1, d_1]_1).$$

Notice that the original interval approximation can be retrieved from the associated $\widetilde{\delta}^{\xi}_{M}$. The following proposition explains the summations involved in the definition. It shows that $\widetilde{\delta}^{\xi}_{M}$ encodes all the information available in the corresponding multiplicity functions when we only look at the upper or lower row.

Proposition 4.6. *Let ξ be an essential assignment and M be a persistence module of $\mathsf{CL}(n)$. Referring to (4.3), we denote the lower and upper rows of M as*

$$\underline{M} := M_{(1,1)} \to M_{(2,1)} \to \cdots \to M_{(n,1)} \quad \textit{and} \quad \overline{M} := M_{(1,2)} \to M_{(2,2)} \to \cdots \to M_{(n,2)} ,$$

respectively. Both $\underline{M}$ and $\overline{M}$ are one-parameter persistence modules over quiver $\vec{A}_n$. Define $\mathcal{V}$ as the function mapping intervals in $\mathbb{I}_1 \sqcup \mathbb{I}_2$ to representations of $\vec{A}_n$:

$$\begin{aligned} \mathcal{V} \colon \mathbb{I}_1 \sqcup \mathbb{I}_2 &\to \mathbf{rep}(\vec{A}_n) \\ I &\mapsto V_I. \end{aligned}$$

Then, the following equations hold:

$$d_{\underline{M}} \circ \mathcal{V} = \widetilde{\delta}^{\xi}_{M}\big|_{\mathbb{I}_1} \qquad \text{and} \qquad d_{\overline{M}} \circ \mathcal{V} = \widetilde{\delta}^{\xi}_{M}\big|_{\mathbb{I}_2}.$$

In other words, for any interval $I \in \mathbb{I}_1 \sqcup \mathbb{I}_2$, its multiplicity in $\widetilde{\delta}^{\xi}_{M}$ aligns with its multiplicity in the corresponding one-parameter persistence module, irrespective of the choice of ξ.

Proof. We here only show the statement for $d_{\overline{M}} \circ \mathcal{V}$. By padding the persistence module M with zero vector spaces on both sides (which ensures that $M_{(x,1)} = \mathbf{0}$ and $M_{(x,2)} = \mathbf{0}$ for $x < 1$ or $x > n$), rank calculations involving indices outside of the range $x \in [1, n]$ become well-defined. Consider an interval $[b, d]_2 \in \mathbb{I}_2$, the multiplicity of its associated interval module is

$$\begin{aligned} d_{\overline{M}} \circ \mathcal{V}\big([b, d]_2\big) &= d_{\overline{M}}(V_{[b,d]_2}) \\ &= \operatorname{rank}\Big(M\big((b, 2) \to (d, 2)\big)\Big) \\ &\quad - \operatorname{rank}\Big(M\big((b-1, 2) \to (d, 2)\big)\Big) - \operatorname{rank}\Big(M\big((b, 2) \to (d+1, 2)\big)\Big) \\ &\quad + \operatorname{rank}\Big(M\big((b-1, 2) \to (d+1, 2)\big)\Big). \end{aligned}$$

By Theorem 3.29, this equation rearranges to:

$$\begin{aligned} &\sum_{I \in \mathbb{I}} \delta^{\xi}_{M}(I) \cdot \operatorname{rank}\Big(V_I\big((b, 2) \to (d, 2)\big)\Big) \\ -&\sum_{I \in \mathbb{I}} \delta^{\xi}_{M}(I) \cdot \operatorname{rank}\Big(V_I\big((b-1, 2) \to (d, 2)\big)\Big) - \sum_{I \in \mathbb{I}} \delta^{\xi}_{M}(I) \cdot \operatorname{rank}\Big(V_I\big((b, 2) \to (d+1, 2)\big)\Big) \\ +&\sum_{I \in \mathbb{I}} \delta^{\xi}_{M}(I) \cdot \operatorname{rank}\Big(V_I\big((b-1, 2) \to (d+1, 2)\big)\Big). \end{aligned}$$

We define an alternating sum function $\Omega_{[b,d]_2}$ on the set of intervals $\mathbb{I}$:

$$\begin{aligned} \Omega_{[b,d]_2}(I) \coloneqq &\operatorname{rank}\Big(V_I\big((b, 2) \to (d, 2)\big)\Big) \\ &- \operatorname{rank}\Big(V_I\big((b-1, 2) \to (d, 2)\big)\Big) - \operatorname{rank}\Big(V_I\big((b, 2) \to (d+1, 2)\big)\Big) \\ &+ \operatorname{rank}\Big(V_I\big((b-1, 2) \to (d+1, 2)\big)\Big). \end{aligned}$$

It is easy to verify the following relations:

$$\Omega_{[b,d]_2}(I) = \begin{cases} 1 & \text{if } I = [b, d]_2 \\ 1 & \text{if } I \text{ is of form } [b, d]_2 \sqcup [b_1, d_1] \\ 0 & \text{otherwise.} \end{cases}$$

The original equation can be further reduced to:

$$\begin{aligned} d_{\overline{M}} \circ \mathcal{V}\big([b,d]_2\big) &= \sum_{I \in \mathbb{I}} \delta_M^{\xi}(I) \cdot \Omega_{[b,d]_2}(I) \\ &= \sum_{\substack{I \in \mathbb{I} \\ \Omega_{[b,d]_2}(I)=1}} \delta_M^{\xi}(I) \cdot \Omega_{[b,d]_2}(I) \\ &= \delta_M^{\xi}\big([b,d]_2\big) + \sum_{I=[b,d]_2 \sqcup [b_1,d_1]_1 \in \mathbb{I}_{2/1}} \delta_M^{\xi}(I) \\ &= \widetilde{\delta}_M^{\xi}\big([b,d]_2\big). \end{aligned}$$

□

To visualize $\widetilde{\delta}_M^{\xi}$, we first adopt an approach that retains a clear relationship to standard persistence diagrams by plotting within two complementary isosceles right triangles that together form a square. We introduce the following points and line segments in $\mathbb{Z}^2$ for upcoming discussions:

- $\mathbb{T}_1 := \{\, (d,b) \in \mathbb{Z}_+ \times \mathbb{Z}_+ \mid d > b \,\}$, the lower triangular region in the first quadrant;
- $\mathbb{T}_2 := \{\, (b,d) \in \mathbb{Z}_+ \times \mathbb{Z}_+ \mid b < d \,\}$, the upper triangular region in the first quadrant;
- $\mathbb{T}_{2/1} := \left\{ \big((b_2,d_2),(d_1,b_1)\big) \in \mathbb{T}_2 \times \mathbb{T}_1 \;\middle|\; -1 \le \frac{d_2-b_1}{b_2-d_1} \le 0 \right\}$, the set of line segments connecting points from $\mathbb{T}_2$ and $\mathbb{T}_1$ with slope[3] within the range $[-1, 0]$.

Definition 4.7 (Connected Persistence Diagram)**.** Let ξ be an essential assignment and M be a persistence module of $\mathsf{CL}(n)$. A *connected persistence diagram* of M, denoted as $\mathfrak{D}^{\xi}(M)$, visualizes the interval approximation δ_M^{ξ} via $\widetilde{\delta}_M^{\xi}$ in the two-dimensional integer lattice $\mathbb{Z}^2$ as a multiset comprising both points and line segments, where the multiplicity of an element can be negative. Represented as a function, elements with a non-trivial multiplicity are given by:

$$\begin{aligned} \mathfrak{D}^{\xi}(M) \colon \mathbb{T}_1 \sqcup \mathbb{T}_2 \sqcup \mathbb{T}_{2/1} &\to \mathbb{Z} \\ \mathbb{T}_1 \ni (d,b) &\mapsto \widetilde{\delta}_M^{\xi}\big|_{\mathbb{I}_1}\big([b,d-1]_1\big) \\ \mathbb{T}_2 \ni (b,d) &\mapsto \widetilde{\delta}_M^{\xi}\big|_{\mathbb{I}_2}\big([b,d-1]_2\big) \\ \mathbb{T}_{2/1} \ni \big((b_2,d_2),(d_1,b_1)\big) &\mapsto \widetilde{\delta}_M^{\xi}\big([b_2,d_2-1]_2 \sqcup [b_1,d_1-1]_1\big). \end{aligned}$$

[3]This condition on the slope of the line segment results from the index condition of intervals in $\mathbb{I}_{2/1}$ specified in (4.2).

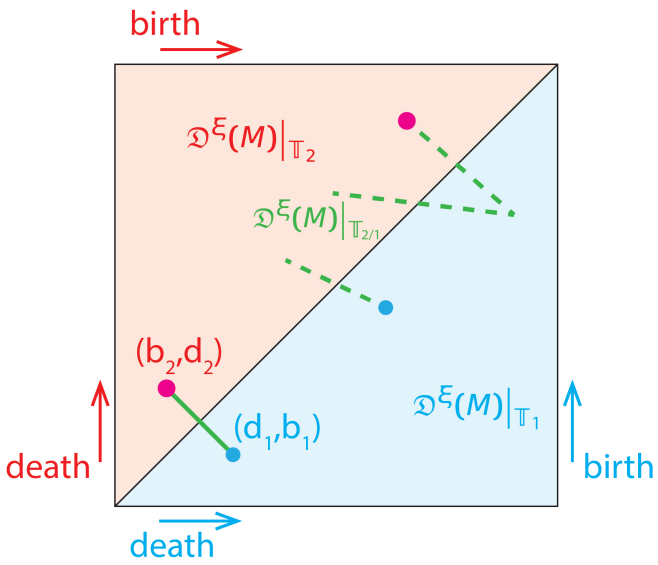

Figure 4.2: Schematic illustration of a connected persistence diagram. A dashed line indicates negative multiplicity.

Remark 4.8. In a connected persistence diagram, multiplicities on $\mathbb{T}_1$ and $\mathbb{T}_2$ measure the horizontal persistence, and multiplicities on $\mathbb{T}_{2/1}$ can measure the vertical persistence, which is crucial for revealing information that is not accessible via only one-parameter persistent homology on the two rows. Notice that the two endpoints of a line segment in $\mathbb{T}_{2/1}$ often coincide with points from both $\mathbb{T}_1$ and $\mathbb{T}_2$. However, as illustrated in Figure 4.2, this overlap is not requisite.

Remark 4.9. We choose the source-sink essential assignment ξ^{ss} for our subsequent computations since its simplicity makes it an ideal starting point. We note that other essential assignments could offer more refined or specific insights. A visualization of ξ^{ss} on representatives of intervals classified by the number of essential vertices is provided in Figure 4.3.

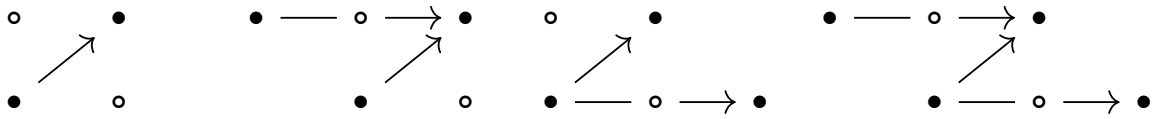

Figure 4.3: Illustration of intervals $I \in \mathbb{I}_{2/1}$ and the courses defined by $\xi^{ss}(I)$. Solid dots represent essential vertices, with the number of essential vertices ranging from 2 to 4 in each example.

Example 4.10. To highlight the effectiveness of connected persistence diagrams, we present two configurations with topological structures that are distinguishable by connected persistence diagrams but not by standard persistence diagrams at any homology dimension. Figure 4.4 depicts each configuration as a filtration of Čech complexes in the horizontal direction. For clarity, we omit the associated disks and display all simplicial

complexes at four critical radii. We also directly use the radius as our parameter instead of indexing them with natural numbers. The symbol x^- denotes a value infinitesimally less than x for $x \in \mathbb{R}$.

Let the two representations be $M_a := H_1(X_a)$ and $M_b := H_1(X_b)$, and the connected persistence diagrams be $D_a := \mathfrak{D}^{\xi^{\mathrm{ss}}}(M_a)$ and $D_b := \mathfrak{D}^{\xi^{\mathrm{ss}}}(M_b)$. In both cases, the only interval in $\mathbb{I}_{2/1}$ that might yield a non-zero value under the map of D_a or D_b is $I_0 := [\sqrt{3}, 2^-]_2 \sqcup [\sqrt{3}, 2^-]_1$. It is easy to verify that $\mathsf{Cov} I_0 = \{ [(\sqrt{3})^-, 2^-]_2 \sqcup [\sqrt{3}, 2^-]_1, [\sqrt{3}, 2^-]_2 \sqcup [\sqrt{3}, 2]_1 \}$. Applying the definition of the connected persistence diagram yields

$$\begin{aligned} D_c(I_0) =& \delta_{M_c}^{\xi^{\mathrm{ss}}}(I_0) \\ =& \sum_{S \subseteq \mathsf{Cov} I_0} (-1)^{\#S} c_{M_c}^{\xi^{\mathrm{ss}}}(\bigvee S) \\ =& c_{M_c}^{\xi^{\mathrm{ss}}}(I_0) - c_{M_c}^{\xi^{\mathrm{ss}}}([(\sqrt{3})^-, 2^-]_2 \sqcup [\sqrt{3}, 2^-]_1) \\ & - c_{M_c}^{\xi^{\mathrm{ss}}}([\sqrt{3}, 2^-]_2 \sqcup [\sqrt{3}, 2]_1) + c_{M_c}^{\xi^{\mathrm{ss}}}([(\sqrt{3})^-, 2^-]_2 \sqcup [\sqrt{3}, 2]_1). \end{aligned}$$

The last three terms all vanish in both cases, because either $(M_c)_{((\sqrt{3})^-, 2)} = \mathbf{0}$ or $(M_c)_{(2,1)} = \mathbf{0}$. Continuing with the computation, we find that $D_c(I_0) = c_{M_c}^{\xi^{\mathrm{ss}}}(I_0) = d_{\mathsf{tour}_{\xi^{\mathrm{ss}}(I_0)}(M_c)}\big(\mathsf{tour}_{\xi^{\mathrm{ss}}(I_0)}(V_{I_0})\big) = d_{(M_c)_{(\sqrt{3},1)} \to (M_c)_{(2^-,2)}}(\Bbbk \xrightarrow{\mathrm{id}} \Bbbk)$. This yields a value of 1 when $c = a$ and 0 when $c = b$.

Another visualization method to consider is the *layered presentation* of the connected persistence diagram. This approach overlays the two standard persistence diagrams, and line segments are also drawn in the upper triangular region. Although superimposed generators become less discernible, this method offers a clearer insight into how specific generators persist in the vertical direction in certain contexts. We further illustrate this method in Section 6.3.1.

Remark 4.11. The *extended diagram* presented in [15] also utilizes two triangular regions. Although visually similar, this structure differs from the connected persistence diagram, and they are not directly related.

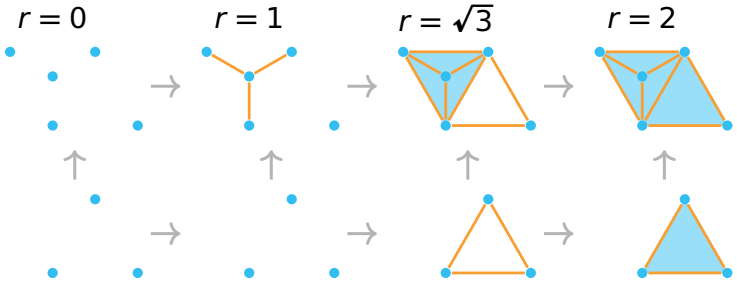

(a-1) Filtration X_a.

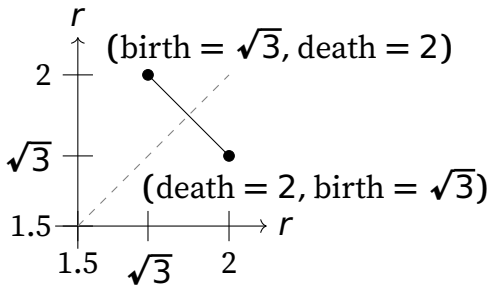

(a-2) Connected persistence diagram D_a.

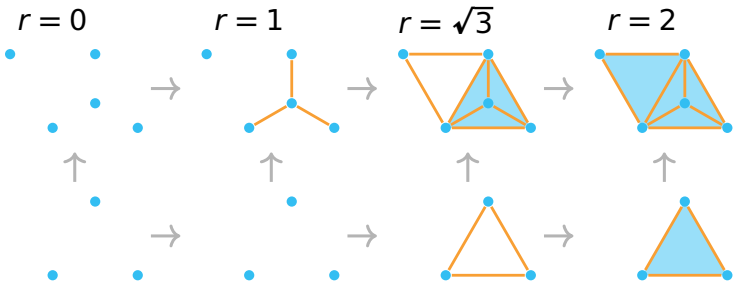

(b-1) Filtration X_b.

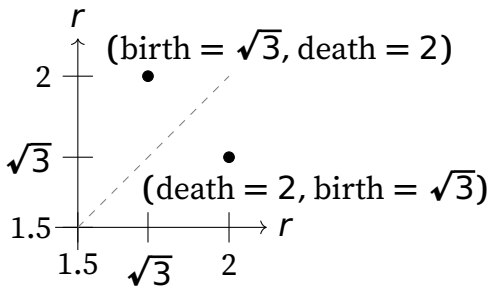

(b-2) Connected persistence diagram D_b.

Figure 4.4: (a-1) A $\mathsf{CL}(n)$-filtration at critical radii, where all arrows indicate inclusion maps. (a-2) The upper and lower triangular regions represent persistence diagrams at dimension one for respective rows. The connecting line is consistent with the observation that the two generators share a homologous cycle. (b-1) In this filtration, the generator in the lower row becomes a boundary when mapped to the upper row. (b-2) The two generators corresponding to the cycles in the upper row and lower row are disconnected, indicating that they are irrelevant cycles.

5 Models for Commutative Ladder Filtrations of Simplicial Complexes

In this part, we introduce models to construct commutative ladder filtrations at the simplicial complex level, enhancing the applicability of the topological invariants discussed in the prior section.

5.1 A General Model

A *filtered simplicial complex* is a pair (K, f), where K is a simplicial complex and $f : K \to \overline{\mathbb{R}} := \{ \mathbb{R}, \pm\infty \}$ is a *filter* satisfying:

$$f(\tau) \leq f(\sigma) \text{ if } \tau \text{ is a face of } \sigma.$$

Every number $r_i \in \overline{\mathbb{R}}$ can be associated with a simplicial complex through the preimage $f^{-1}\big((-\infty, r_i]\big)$. For a strictly increasing sequence $r_1 < r_2 < \cdots < r_n$ in $\overline{\mathbb{R}}$, this yields a sequence of simplicial complexes:

$$f^{-1}\big((-\infty, r_1]\big) \subseteq f^{-1}\big((-\infty, r_2]\big) \subseteq \cdots \subseteq f^{-1}\big((-\infty, r_n]\big),$$

which forms a filtration of sublevel sets.

We now consider a simplicial complex K equipped with two filters f_1 and f_2, subject to the condition $f_1(\sigma) \geq f_2(\sigma)$ for any $\sigma \in K$. Given a sequence $r_1 < r_2 < \cdots < r_n$, the pair (K, f_y) with $y \in \{ 1, 2 \}$ yields a sequence as above by defining $X_{(i,y)} := f_y^{-1}\big((-\infty, r_i]\big)$. They play the role of the lower and upper rows in a $\mathsf{CL}(n)$-filtration, respectively. The condition $f_1 \geq f_2$ ensures the vertical inclusions and the commutativity can also be verified. Finally, the $\mathsf{CL}(n)$-filtration specified by the triplet (K, f_1, f_2) can be formulated as

$$X := \begin{array}{ccccccc} X_{(1,2)} & \longrightarrow & X_{(2,2)} & \longrightarrow & \cdots & \longrightarrow & X_{(n,2)} \\ \uparrow & & \uparrow & & & & \uparrow \\ X_{(1,1)} & \longrightarrow & X_{(2,1)} & \longrightarrow & \cdots & \longrightarrow & X_{(n,1)} \end{array} . \tag{5.1}$$

5.2 Thinning Models for Point Cloud Data

Let P be a point cloud and P' be a subset of P. Let $\check{C}(P, r)$ denote the Čech complex constructed on the point cloud P with ball radius r. For a sequence $r_1 < r_2 < \cdots < r_n$ in $\overline{\mathbb{R}}$, we have the following filtration:

$$\begin{array}{ccccccc} \check{C}(P, r_1) & \longrightarrow & \check{C}(P, r_2) & \longrightarrow & \cdots & \longrightarrow & \check{C}(P, r_n) \\ \uparrow & & \uparrow & & & & \uparrow \\ \check{C}(P', r_1) & \longrightarrow & \check{C}(P', r_2) & \longrightarrow & \cdots & \longrightarrow & \check{C}(P', r_n) \end{array}, \tag{5.2}$$

where the definition of the Čech complex guarantees the commutativity. To incorporate this construction into the general model introduced above, we set the simplicial complex K to be $\check{C}(P, r_n)$, and define the induced filter f_2 for $\sigma \in K$ as:

$$f_2(\sigma) = \min \left\{ r_i \in \overline{\mathbb{R}} \,\middle|\, \sigma \in \check{C}(P, r_i) \right\}.$$

Given that each simplex σ can be expressed in the form $\{ v_0, v_1, \ldots, v_d \}$ with each $v_i \in P$, the filter f_1 on K can be defined as:

$$f_1(\sigma) = \begin{cases} f_2(\sigma) & \sigma \subseteq P', \\ +\infty & \sigma \nsubseteq P'. \end{cases}$$

The filtration (5.2) can then be retrieved from the triplet (K, f_1, f_2) following the steps in Section 5.1.

Remark 5.1. Thinning in topological data analysis, introduced in [25], can incorporate a variety of patterns, such as removing points forming certain shapes or employing a density function. An example can be found in Section 6.3.2. Besides what is described here, there exist other methods for creating a filtration from a point cloud P, including non-constant point removal or removing higher-dimensional simplices. The multi-cover method described in [39] can also generate a $\mathsf{CL}(n)$-filtration consistent with our general model.

5.3 Two Models from Random Simplicial Complexes

5.3.1 Clique Complex Model

Our first random model employs the Erdős-Rényi random graph process for generating commutative ladders. Consider the complete graph with m vertices, denoted by $K_m = (V_m, E_m)$, where V_m is the set of vertices and E_m is the set of edges. We associate each edge $e \in E_m$ with two independent random variables T_e and $\widetilde{T}_e$, both follow the standard uniform distribution $U(0, 1)$. Given $t \in [0, 1]$, we define the following two increasing stochastic processes of subgraphs of K_m:

$$K_m^1(t) := \big(V_m, \{ e \in E_m \mid T_e \le t \}\big), \qquad K_m^2(t) := \big(V_m, \{ e \in E_m \mid T_e \cdot \widetilde{T}_e \le t \}\big).$$

The stochastic process K_m^1 is called the Erdős-Rényi random graph process [17]. Recall that the clique complex $\Delta(G)$ of a graph G is the abstract simplicial complex that includes all cliques (*i.e.* complete subgraphs) of G. The two stochastic processes defined above induce two increasing stochastic processes of simplicial complexes $\Delta(K_m^1)$ and $\Delta(K_m^2)$. Notice that the condition $\Delta(K_m^1)(t) \subseteq \Delta(K_m^2)(t)$ holds for any $t \in [0, 1]$, as ensured by the multiplication in K_m^2's definition. By selecting n values $t_1 < t_2 < \cdots < t_n \in [0, 1]$ and setting $X_{(i,j)} := \Delta(K_m^j)(t_i)$, we obtain a random $\mathsf{CL}(n)$-filtration.

To fit it into (5.1) in the general model, we set K to be $\Delta(K_m)$. For $j = 1, 2$, each filter f_j on K is defined as below for $\sigma = \{ v_0, \ldots, v_d \}$:

$$f_1(\sigma) := \max_{0 \le < p < q \le d} t_{v_p v_q} \qquad \text{and} \qquad f_2(\sigma) := \max_{0 \le < p < q \le d} t_{v_p v_q} \cdot \widetilde{t}_{v_p v_q}.$$

In this formulation, the subscript $v_p v_q$ represents the edge incident to vertices v_p and v_q. The terms t_e and $\widetilde{t}_e$ are realizations of T_e and $\widetilde{T}_e$, respectively.

5.3.2 d-Linial-Meshulam Model

We introduce another model adapted from the d-Linial-Meshulam process [26, 33]. This stochastic process can be seen as a generalization of the Erdős-Rényi random graph process. It begins with a skeleton of a simplicial complex and then progressively adds simplices that are one-dimensional higher than the initial skeleton. We outline the components required for this model as follows.

- A vertex set $[m] := \{ 1, \ldots, m \}$.
- The largest abstract simplicial complex over $[m]$, denoted as $\Delta := \Delta_{m-1}$, which has dimension $m - 1$.
- A chosen dimension d where $1 \le d \le m - 1$.
- The $(d-1)$-skeleton of Δ, denoted as $\Delta^{(d-1)}$, comprising all simplices in Δ having a dimension no greater than $d - 1$.
- The set of all d-simplices in Δ, represented as Δ_d.
- Each $\sigma \in \Delta_d$ is associated with two independent random variables T_σ and $\widetilde{T}_\sigma$ that follow the standard uniform distribution $U(0, 1)$.
- Two increasing stochastic processes of simplicial complexes:

$$\mathcal{K}_1^{(d)}(t) := \Delta^{(d-1)} \sqcup \{ \sigma \in \Delta_d \mid T_\sigma \le t \}, \; \mathcal{K}_2^{(d)}(t) := \Delta^{(d-1)} \sqcup \left\{ \sigma \in \Delta_d \;\middle|\; T_\sigma \cdot \widetilde{T}_\sigma \le t \right\}.$$

For both $j = 1, 2$, we have $\mathcal{K}_j^{(d)}(0) = \Delta^{(d-1)}$ at the start of each filtration almost surely and $\mathcal{K}_j^{(d)}(1) = \Delta^{(d)}$ at the end. Analogous to the previous model, selecting n values $t_1 < t_2 < \cdots < t_n$ in $[0, 1]$ and setting $X_{(i,j)} := \mathcal{K}_j^{(d)}(t_i)$ yields a random $\mathsf{CL}(n)$-filtration. A realization of this random $\mathsf{CL}(n)$-filtration can be established using the triplet (K, f_1, f_2) as outlined in the general model similarly.

6 Experiments and Analysis

This section discusses computational results regarding the newly introduced invariants. We begin by providing several quantities for measuring non-intervals, then analyze the occurrence of non-intervals in the three different models outlined in the previous section. Finally, we show our findings by applying our tools to material structures.

6.1 Invariants for Measuring Non-intervals

The under-investigated realm of non-interval representations within multiparameter persistence represents a fertile ground for exploration. This subsection provides several preliminary tools for extracting and interpreting information about these non-intervals.

Finite-type Commutative Ladders

Recall from Theorem 2.23 that the representation type of $\mathsf{CL}(n)$ is finite when $n \leq 4$. We will focus on $\mathsf{CL}(4)$ because any representation of $\mathsf{CL}(1)$ or $\mathsf{CL}(2)$ is interval-decomposable, and the non-interval representations of $\mathsf{CL}(3)$ can be embedded into $\mathbf{rep}\big(\mathsf{CL}(4)\big)$. Let $\mathcal{L}$ be a complete set of representatives of the isomorphism classes of indecomposables in $\mathbf{rep}\big(\mathsf{CL}(4)\big)$. The Auslander-Reiten quiver [1] reveals that there are 21 non-intervals and 55 intervals in $\mathcal{L}$ [18, Fig. 17]. Non-intervals and some intervals are indexed as shown in Figure 6.1 for easier reference in subsequent discussions, where each class is represented by its dimension vector.

Remark 6.1. There are two non-interval representatives of isomorphism classes in $\mathsf{CL}(3)$, represented by dimension vectors $\begin{pmatrix} 1 & 2 & 1 \\ 0 & 1 & 1 \end{pmatrix}$ and $\begin{pmatrix} 1 & 1 & 0 \\ 1 & 2 & 1 \end{pmatrix}$. They can be embedded into either $N1$ and $N9$ or $N13$ and $N21$ in $\mathbf{rep}\big(\mathsf{CL}(4)\big)$, as shown in Figure 6.1.

Infinite-type Commutative Ladders

[1] The Auslander-Reiten quiver of $\mathbf{rep}\big(\mathsf{CL}(4)\big)$ consists of elements in $\mathcal{L}$ as vertices and irreducible morphisms among them as arrows. We use it to represent elements in $\mathcal{L}$. See [5, Chapter 4] for details.

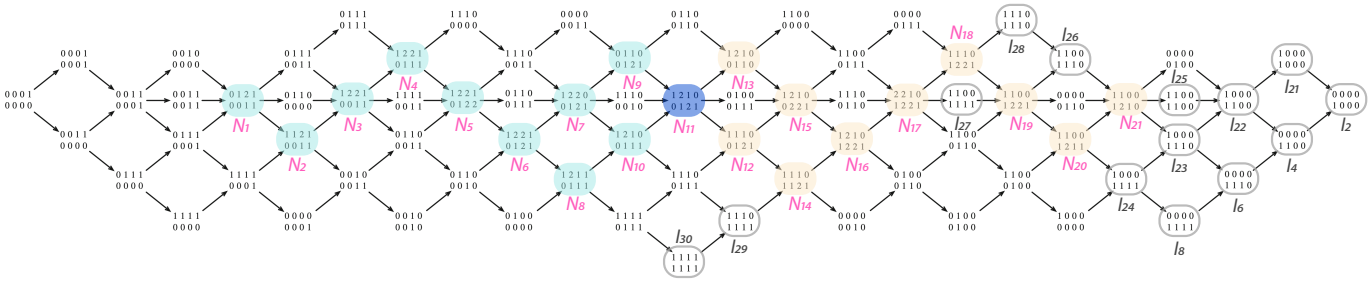

Figure 6.1: The 76 representatives in $\mathcal{L}$. Non-intervals are numbered such that N_{11-i} is isomorphic to the dual of N_{11+i} for $i \in \{0, \dots, 10\}$.

Unlike the scenario in the finite-type cases, our understanding of non-intervals in infinite-type cases is limited. First, we show that the property below establishes a negative multiplicity as an indicator of the presence of non-interval summands.

Proposition 6.2. *Let M be a representation of $\mathsf{CL}(n)$. If there exists an essential assignment ξ and an interval I of $\mathsf{CL}(n)$ such that $\delta_M^\xi(I) < 0$, then M has an indecomposable non-interval direct summand.*

Proof. The negativity of $\delta_M^\xi(I)$ implies $d_M(V_I) \neq \sum_{S \subseteq \mathrm{Cov} I} (-1)^{\#S} c_M^\xi(\bigvee S)$ by Remark 3.26. Therefore, M is not an interval-decomposable representation by Theorem 3.24. □

Next, we provide finer invariants for measuring non-intervals. Let $\mathcal{L}$ be a complete set of isomorphism classes of $\mathbf{rep}(\mathsf{CL}(n))$. We write it as $\mathcal{I} \sqcup \mathcal{N}$, the disjoint union of the collection of interval isomorphism classes $\mathcal{I}$ and the collection non-interval isomorphism classes $\mathcal{N}$. A representation M can be written as a direct sum of interval indecomposable summands and non-interval indecomposable summands as below:

$$M \cong \bigoplus_{L \in \mathcal{L}} L^{d_M(L)} = \bigoplus_{I \in \mathcal{I}} I^{d_M(I)} \oplus \bigoplus_{N \in \mathcal{N}} N^{d_M(N)} = M_I \oplus M_N, \tag{6.1}$$

where M_I denotes the interval part of M, and M_N denotes the non-interval part of M. We note that although the representation type of $\mathsf{CL}(n)$ is wild in general, there is only a finite number of non-vanishing summands as M is finite-dimensional.

Definition 6.3. Let M be a representation of $\mathsf{CL}(n)$. The *aggregate dimension* of M is the one-norm of its dimension vector:

$$\mathsf{agg}(M) := \|\underline{\dim} M\|_1$$

To quantify the position of M in the spectrum of being more interval-like or non-interval like, we introduce a weight function $w \colon \mathcal{L} \to \mathbb{R}_{>0}$, and define a non-interval score for M:

$$\text{n-score}(M; w) := \frac{\sum_{N \in \mathcal{N}} d_M(N) \cdot w_N \cdot \mathsf{agg}(N)}{\sum_{L \in \mathcal{L}} d_M(L) \cdot w_L \cdot \mathsf{agg}(L)}. \tag{6.2}$$

This thesis will consider the following two weight functions for our analysis.

1. The constant function $w \equiv 1$. In this case, (6.2) can be simplified as

$$\text{n-Score}_c := \text{n-Score}(M; \text{const}) = \frac{\text{agg}(M_N)}{\text{agg}(M)}, \tag{6.3}$$

   where the letter c in the subscript stands for constant.

2. The logistic function $w_L := \frac{1}{1+\exp(-(\text{agg}(L)-d_0))}$. It assigns greater weight to summands with larger aggregate dimensions. The parameter $d_0 \geq 0$ is a constant offset dimension, allowing us to distribute less weight to any indecomposable summand with an aggregate dimension below it. We denote this non-interval score as n-Score_l, where the letter l in the subscript stands for logistic.

Irrespective of the weight function, the non-interval score satisfies the following condition:

- when $\text{n-Score}(M; w) = 0$, the representation M is interval-decomposable;
- when $\text{n-Score}(M; w) = 1$, the representation M does not contain any interval summands.

The non-interval scores are not computable in general. To obtain a computable alternative, we consider an interval resolution of representation M as proposed in [2, Proposition 4.5]:

$$0 \to \bigoplus_{J\in\mathbb{I}} V_J^{d_J^{(r)}} \xrightarrow{f_r} \cdots \xrightarrow{f_2} \bigoplus_{J\in\mathbb{I}} V_J^{d_J^{(1)}} \xrightarrow{f_1} \bigoplus_{J\in\mathbb{I}} V_J^{d_J^{(0)}} \xrightarrow{f_0} M \to 0. \tag{6.4}$$

Here $\mathbb{I}$ is the set of interval subquivers of $\text{CL}(n)$. It is easy to verify that if M is interval-decomposable, then $d_J^{(i)} = 0$ for any $J \in \mathbb{I}$ and $r > 0$. This resolution can be decomposed as a direct sum of a resolution for M_I and a resolution for M_N. Assuming [2, Conjecture 4.11] and consider an interval resolution for M_N. Then (6.4) can be written as the exact sequence (see [2, Remark 3.2]) below:

$$0 \to \bigoplus_{J\in\mathbb{I}} V_J^{d_J^{(2)}} \xrightarrow{f_2} \bigoplus_{J\in\mathbb{I}} V_J^{d_J^{(1)}} \xrightarrow{f_1} \bigoplus_{J\in\mathbb{I}} V_J^{d_J^{(0)}} \xrightarrow{f_0} M_N \to 0. \tag{6.5}$$

By the rank-nullity theorem and the exactness, we can reformulate the numerator of $\mathsf{n\text{-}Score}_c(M)$ in (6.3) as below:

$$\begin{aligned}
\operatorname{agg}(M_N) &= \operatorname{agg}(\operatorname{Im} f_0) \\
&= \operatorname{agg}(\bigoplus_{J\in\mathbb{I}} V_J^{d_J^{(0)}}) - \operatorname{agg}(\operatorname{Ker} f_0) \\
&= \operatorname{agg}(\bigoplus_{J\in\mathbb{I}} V_J^{d_J^{(0)}}) - \operatorname{agg}(\operatorname{Im} f_1) \\
&= \operatorname{agg}(\bigoplus_{J\in\mathbb{I}} V_J^{d_J^{(0)}}) - \big[\operatorname{agg}(\bigoplus_{J\in\mathbb{I}} V_J^{d_J^{(1)}}) - \operatorname{agg}(\operatorname{Ker} f_1)\big] \\
&= \operatorname{agg}(\bigoplus_{J\in\mathbb{I}} V_J^{d_J^{(0)}}) - \operatorname{agg}(\bigoplus_{J\in\mathbb{I}} V_J^{d_J^{(1)}}) + \operatorname{agg}(\operatorname{Im} f_2) \\
&= \operatorname{agg}(\bigoplus_{J\in\mathbb{I}} V_J^{d_J^{(0)}}) - \operatorname{agg}(\bigoplus_{J\in\mathbb{I}} V_J^{d_J^{(1)}}) + \operatorname{agg}(\bigoplus_{J\in\mathbb{I}} V_J^{d_J^{(2)}}).
\end{aligned}$$

Currently, there is no efficient way to compute all terms in this equation. But for $\operatorname{agg}(\bigoplus_{J\in\mathbb{I}} V_J^{d_J^{(1)}})$, a lower bound estimation can be obtained in some cases. If the essential assignment used in the computation of connected persistence diagrams is ξ_I as defined at the beginning of [2, Section 5.1], then the values of interval approximations satisfy the following equation by [2, Corollary 5.7]:

$$\begin{aligned}
\delta_M^{\xi_I}(J) &= \sum_{i=0}^{r} (-1)^i d_J^{(i)},\ \forall J \in \mathbb{I} \\
&= d_J^{(0)} - d_J^{(1)} + d_J^{(2)},\ \forall J \in \mathbb{I},
\end{aligned}$$

where we used the conjecture mentioned above to impose $r = 2$. If $\delta_M^{\xi_I}(J) \geq 0$, it is hard to estimate the values for $d_J^{(i)}$. But when $\delta_M^{\xi_I}(J) < 0$, we know $d_J^{(1)} > 0$ as each $d_J^{(i)}$ is non-negative. In particular, this negativity necessitates the appearance of the corresponding $V_J^{d_J^{(i)}}$ in the resolution for M_N. In this case the absolute value $\left|\delta_M^{\xi_I}(J)\right|$ is equal to $d_J^{(1)} - (d_J^{(0)} + d_J^{(2)})$, from which we derive $\left|\delta_M^{\xi_I}(J)\right| < d_J^{(1)}$. This inequality allows us to compute the following quantity:

$$\operatorname{agg}\Big(\bigoplus_{J\in\mathbb{I}} V_J^{\left|\delta_M^{\xi_I}(J)\right|\cdot \mathbf{1}_{\delta_M^{\xi_I}(J)<0}}\Big) = \sum_{\substack{J\in\mathbb{I} \\ \delta_M^{\xi_I}(J)<0}} \operatorname{agg}(V_J^{\left|\delta_M^{\xi_I}(J)\right|}) < \operatorname{agg}(\bigoplus_{J\in\mathbb{I}} V_J^{d_J^{(1)}}).$$

We define a computable non-interval score $\mathsf{n\text{-}Score}_c'$ for $M \in \mathbf{rep}(\mathsf{CL}(n))$ with respect to any essential assignment ξ:

$$\mathsf{n\text{-}Score}_c'(M) := \frac{\sum_{J \in \mathbb{I}} \mathsf{agg}(V_J^{\left|\delta_M^{\xi_I}(J)\right|})^{\delta_M^{\xi}(J)<0}}{\mathsf{agg}(M)},$$

referred to as the *inferred non-interval score (with the constant weight function)*. Figure 6.6 shows that this quantity is positively correlated with $\mathsf{n\text{-}Score}_c(M)$ statistically in the $\mathsf{CL}(4)$ case for the models we explored.

6.2 Non-intervals in Three Different Models

6.2.1 On Point Cloud Model and Clique Complex Model

We demonstrate a comparative analysis of the results from the Point Cloud Model in Section 5.2 and the Clique Complex Model in Section 5.3.1. Throughout this discussion, we maintain the notations established in the individual model's specification. Implementation details for building filtrations are listed below.

Point Cloud Model	**Clique Complex Model**
• Construct a set P comprising uniformly randomly distributed points confined in the unit cube of $\mathbb{R}^2$ or $\mathbb{R}^3$, where the number of points ranges from 5 to 30. Subsequently, create a point cloud P' by randomly choosing a non-empty proper subset of P.	• Construct a complete graph with m vertices where $m \in [4, 30]$. Subsequently, generate samples of the random variables T_e and $\widetilde{T}_e$ for $e \in E_m$.
• Set the homology dimension d as 1 if $P \subseteq \mathbb{R}^2$. Otherwise, assign d as either 1 or 2. Apply one-parameter persistent homology H_d functor on $\check{C}(P)$ and $\check{C}(P')$ to get their critical filtration values. Collect these values and denote their disjoint union with duplicates removed as $\mathscr{V} := \{ t_1, t_2, \ldots, t_{\lvert\mathscr{V}\rvert} \}$. Discard this configuration if $\lvert\mathscr{V}\rvert < 4$.	• Assign the homology dimension d to be 1 or 2. Apply one-parameter persistent homology H_d functor on $\Delta(K^1_m)$ and $\Delta(K^2_m)$ to get their critical filtration values. Collect these values and denote their disjoint union with duplicates removed as $\mathscr{V} := \{ t_1, t_2, \ldots, t_{\lvert\mathscr{V}\rvert} \}$. Discard this configuration if $\lvert\mathscr{V}\rvert < 4$.
• For the finite-type cases, choose four radii randomly from $\mathscr{V}$. For the infinite-type cases, select an integer n such that $4 \leq n \leq \min(\lvert\mathscr{V}\rvert, 50)$, and build a $\mathrm{CL}(n)$-filtration by choosing n radii randomly.	• As detailed in the corresponding entry in the left column.

Ideally, we want to analyze the $\mathrm{CL}(\lvert\mathscr{V}\rvert)$ representation obtained from the $\mathrm{CL}(\lvert\mathscr{V}\rvert)$-filtration of simplicial complexes using all radii. However, due to escalating computational demands (in the order of $O(\lvert\mathscr{V}\rvert^4)$ by Theorem 3.30), we limit the ladder length to a maximum of 50. This is realized by choosing a random subset of the critical radii, where the subset size n is less than 50. The representation is then defined by the critical radii selected and the homology dimension used to compute the homology module. The value n is set to start from 4, as this is when a total decomposition can be obtained. Therefore, we can compare results using different tools. We begin by examining the interval-decomposability of non-trivial representations. For a representation of $\mathrm{CL}(4)$, its indecomposable decomposition is computed to identify the presence of any non-interval components. This allows us to determine the proportion of the number of representations that are not interval-decomposable compared to the total number of non-trivial representations. For a general representation of $\mathrm{CL}(n)$, we turn to its connected persistence diagram and look for the presence of negative multiplicities, providing a lower bound estimate of the aforementioned proportion. Table 6.1 presents the proportions obtained

from various settings, using either CL(4) (for indecomposable decomposition) or cPD (for connected persistence diagram) as specified above.

	Point Cloud Model: $\mathbb{R}^2$		Point Cloud Model: $\mathbb{R}^3$		Clique Complex Model	
	CL(4)	cPD	CL(4)	cPD	CL(4)	cPD
H_1	0.034%	3.38%	0.097%	8.83%	1.727%	34.74%
H_2	N/A	N/A	0.042%	1.25%	0.001%	0.037%

Table 6.1: The proportion or its lower-bound of non-trivial representations that are not interval-decomposable for the Point Cloud Model embedded in $\mathbb{R}^2$, $\mathbb{R}^3$, and the Clique Complex Model. Tools used are indicated in the second row. [2]

Upon comparing the data from both models in homology dimension one using CL(4), it is evident that the Point Cloud Model exhibits a significantly lower proportion of non-interval-decomposable representations compared to the Clique Complex Model. This relatively infrequent occurrence of non-intervals in the Point Cloud Model can be primarily attributed to the geometry of Čech complexes, as illustrated in Figure 6.2. Additionally, it is worth noting that the proportion of non-interval-decomposable representations in $\mathbb{R}^3$ is higher than that in $\mathbb{R}^2$, which is likely due to increased tolerance for perturbations in $\mathbb{R}^3$ owing to its additional degree of freedom.

The comparative analysis reveals that the lower bound obtained using cPD is significantly higher than that obtained using the CL(4) method. This discrepancy arises from the CL(4) method's selection of merely four radii, which inadvertently omits many critical radii in a typical configuration. Such an omission leads to an incomplete profile of the topological persistence, where homology generators can be born and then die without being detected. Despite the current absence of an efficient tool to compute the indecomposable of a general CL(n) representation, the cPD method provides a better estimation in discerning the presence of non-interval components within a representation.

Besides the differences in interval-decomposability, non-intervals also exhibit an uneven distribution across the set of all 21 representatives in different models. Figure 6.3 illustrates the proportion of each representative's sum of multiplicities, normalized against the total multiplicity of all the non-intervals.

In the Point Cloud Model, only eight distinct representatives appear among all representatives. Non-intervals predominantly concentrate on $N13$, which has one of the lowest 1-norms of the dimension vector among all representatives. In contrast, in the Clique Complex Model, the diversity of non-intervals increases, and they are also less concentrated. All 21 representatives are observed, with no apparent preference towards representatives possessing the lowest 1-norms of dimension vectors.

[2]The number of total non-trivial representations in the row with H_1 are 132k, 132k, 66k, 66k, 211k, 221k respectively, and 49k, 50k, 141k, 142k for the row with H_2.

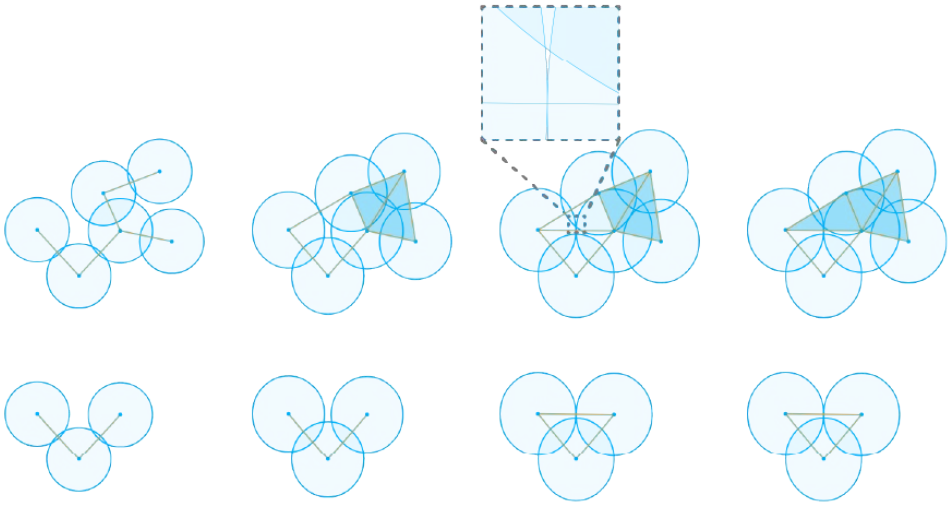

Figure 6.2: An example of a $\mathsf{CL}(4)$-filtration. Its one-dimensional homology module corresponds to $N1$ in Figure 6.1. The new hole, encased in the square, is crucial for this non-interval despite its extremely short lifetime. While the generator in the lower row also has a very short lifetime, it slightly outlives the prior generator, leading to a non-interval component. This fragile structure is prone to perturbations, explaining the infrequent occurrence of non-intervals in the Point Cloud Model.

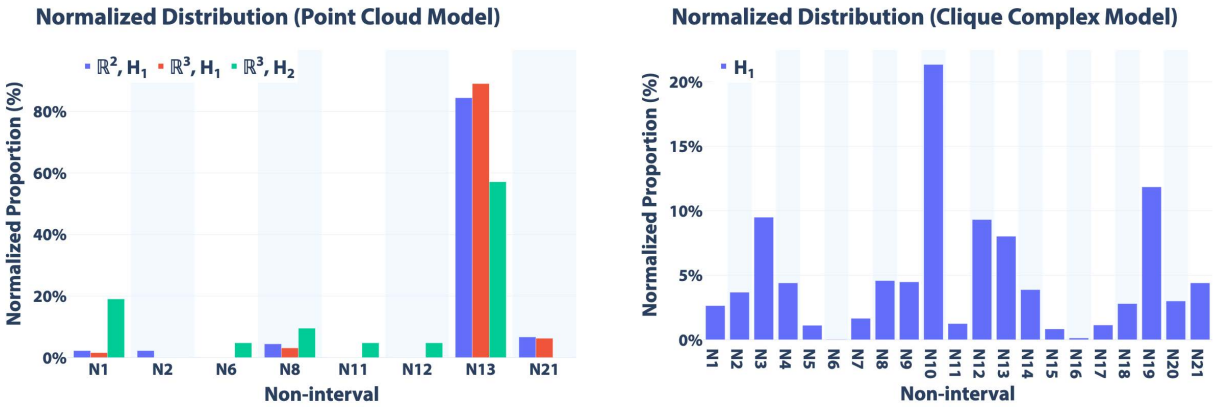

(a) (b)

Figure 6.3: Normalized proportions are presented across various settings, only showing non-interval representatives observed in the computational results. (a) The distribution of non-intervals in the Point Cloud Model. (b) The distribution of non-intervals in the Clique Complex Model with homology dimension one. [3]

Next, we look at the effect of ladder length n on the detectability of a non-interval component. Figure 6.4 shows the ratios of the connected persistence diagrams with a negative multiplicity.

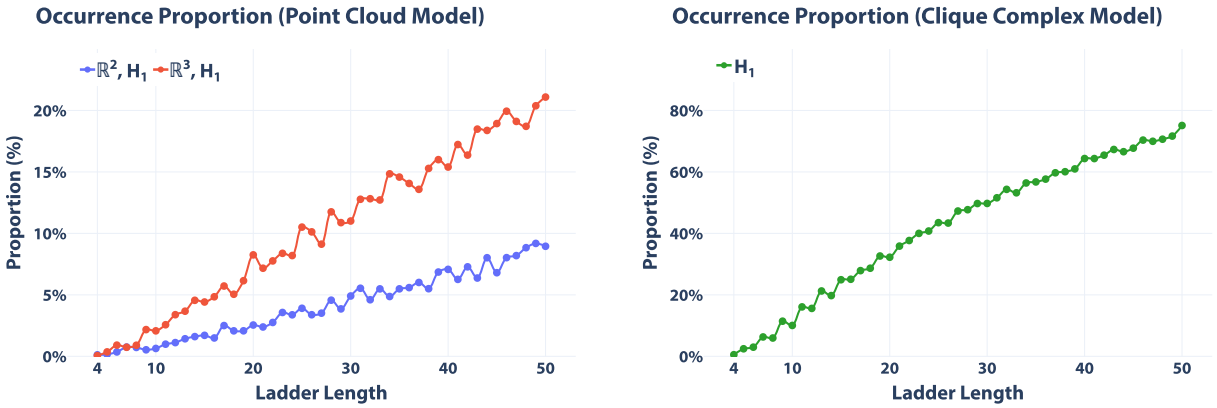

(a) (b)

Figure 6.4: Occurrence proportions of negative multiplicities in connected persistence diagrams of homology dimension one. (a) For the Point Cloud Model in $\mathbb{R}^2$ and $\mathbb{R}^3$. (b) For the Clique Complex Model. [4]

With shorter ladder lengths, many details in the original representation are lost, leading to a lower proportion of the occurrence of negative multiplicities. On the other hand, as we increase the length, more topological information is being scrutinized, increasing the likelihood of finding a negative multiplicity. We also see that the Clique Complex Model demonstrates a much higher proportion than the Point Cloud Model, aligning with the observation obtained using indecomposable decomposition.

The analysis thus far focused on the distribution and existence of non-intervals in data. To further understand the significance of these non-intervals, we employ non-interval scores. Figure 6.3a indicates that in $\mathbb{R}^3$ with homology dimension 2, more complex (characterized by larger aggregate dimension) non-intervals appear. This behavior is captured by the mean of $\mathsf{n\text{-}Score}_l$ computed from representations that are not interval decomposable, where we use an increasing offset dimension d_0 as in the weight function $w_L := \frac{1}{1+\exp(-(\mathrm{agg}(L)-d_0))}$ in Figure 6.5. As d_0 increases, more weight is placed on indecomposable summands with higher aggregate dimensions. From a data analysis point of view, this corresponds to viewing indecomposables with smaller aggregate dimensions as noise and regarding those with larger aggregate dimensions as signals.

In Figure 6.5, all curves go upwards as the offset dimension increases as expected, reflecting the fact that non-interval summands have an averagely higher aggregate dimension than interval summands. The order of curves in Figure 6.5a behaves in a way suggesting that representations in the case $(\mathbb{R}^3, H_2)$ are more non-interval like, *i.e.*, with

[3]Among all the 141k non-trivial representations obtained using H_2, only one representation is not interval-decomposable, consisting of an $N14$ as its summand.

[4]Results for homology dimension two in both the Point Cloud Model and the Clique Complex Model are omitted due to insufficient data points after grouping by ladder length.

fewer interval summands. This observation aligns with the distribution shown in Figure 6.3a, where the case $(\mathbb{R}^3, H_2)$ also exhibits more complex non-intervals, reflected in the highest mean of $\mathsf{n\text{-}Score}_l$ both after and before offsetting. In comparison, Figure 6.5b displays a broader range of mean values. This difference suggests that representations in the Clique Complex Model with non-intervals often come with a larger proportion of intervals accompanying it, as opposed to those in the Point Cloud Model.

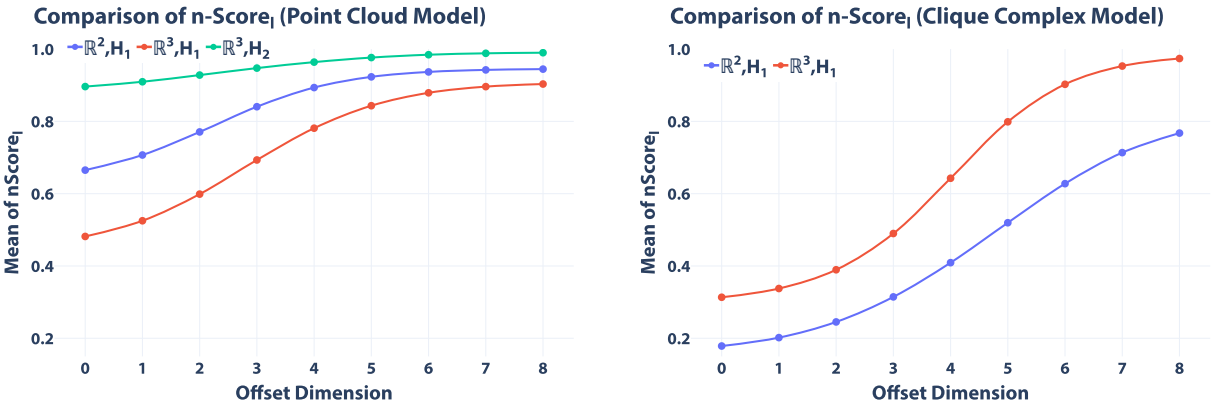

(a) (b)

Figure 6.5: Mean of $\mathsf{n\text{-}Score}_l$ with increasing offset dimensions in the weight function. (a) For the Point Cloud Model. (b) For the Clique Complex Model.

In the previous subsection, we introduce the concept of the inferred non-interval score, $\mathsf{n\text{-}Score}_c'$, as a computable proxy to the non-interval score $\mathsf{n\text{-}Score}_c$ in order to circumvent the computational challenges. Figure 6.6 shows our findings for the $\mathsf{CL}(4)$ case, where $\mathsf{n\text{-}Score}_c$ is computable. Our computation reveals a statistically significant positive correlation between $\mathsf{n\text{-}Score}_c'$ and $\mathsf{n\text{-}Score}_c$ in both models. This observation suggests that $\mathsf{n\text{-}Score}_c'$ could be used in the general $\mathsf{CL}(n)$ cases as an estimator for to what extent a persistence module exhibits non-interval characteristics.

6.2.2 On d-Linial-Meshulam Model

This part analyzes the d-Linial-Meshulam Model outlined in Section 5.3.2, with the homology dimension fixed at $d-1$. Our numerical computations focus on cases where $d=2$ and $d=3$, with the number of vertices m varying between 4 and 20. The methodology for creating a commutative ladder filtration is similar to the approaches used in the prior two models. Figure 6.7 summarizes the proportions of each representative's sum of multiplicities within the indecomposable decomposition obtained using $\mathsf{CL}(4)$. Two immediate observations from the computational outcomes are:

1. There exist only interval indecomposable components.
2. All present intervals are anchored at the bottom-left vertex of $\mathsf{CL}(4)$ (refer to Figure 6.1 for details).

[5]Computed on 15k 2-LM Model instances and 14k 3-LM Model instances

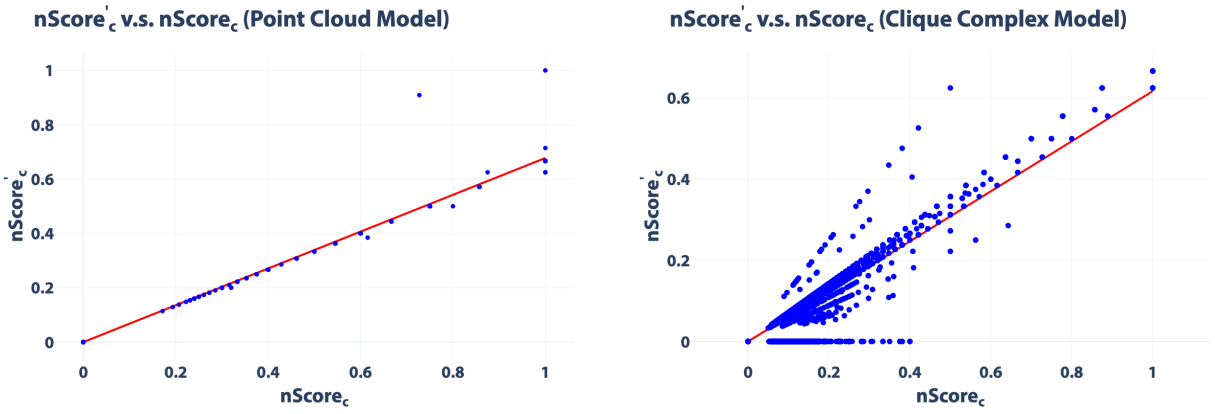

(a) (b)

Figure 6.6: Scatter plot illustrating the correlation between $\text{n-Score}'_c$ and n-Score_c. (a) In the Point Cloud Model. (b) In the Clique Complex Model.

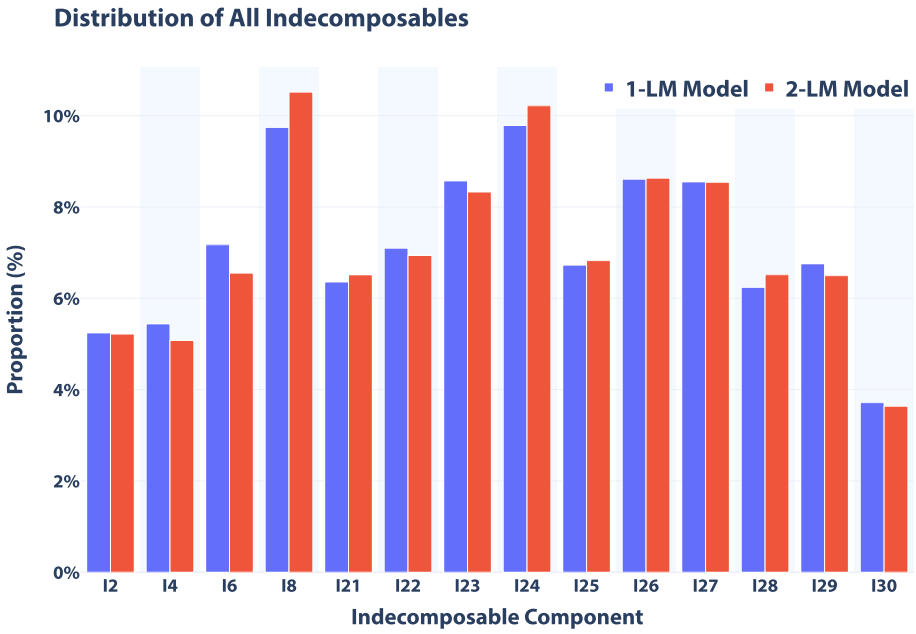

Figure 6.7: The distribution of non-vanishing indecomposable components in the computational results.[5]

This is not merely a coincidence but an inherent characteristic of the d-Linial-Meshulam Model. In the construction process, we always start with a $(d-1)$ skeleton $\Delta^{(d-1)}$, this implies that all the $(d-1)$-homologous cycles of Δ are present at critical value $t = 0$. Throughout the stochastic process, d-simplices from Δ_d are being incorporated, which only serves to fill $(d-1)$-cycles without introducing new ones. It is easy to see that homologous cycles neither merge nor split during this process. Consequently, all representations created from this process are interval-decomposable and, in particular, pivoted at the bottom left vertex. Therefore, the inherent structure of the d-Linial-Meshulam Model

makes it a systematic approach to generate interval-decomposable representations pivoted at the left bottom vertex.

6.3 On Exploring Material Structures

This subsection uses connected persistence diagrams to uncover the topological properties inherent in amorphous and crystalline structures. Our analysis offers a unique perspective on the topological characteristics of material structures, highlighting features invisible to one-parameter persistent homology.

6.3.1 Silica Thinning Analysis

In this example, we examine the atomic arrangement of amorphous silica using the layered presentation of connected persistence diagrams. Our dataset is a point cloud representing silicon and oxygen atoms in silica [30], as depicted in Figure 6.8a. The ring formations in this structure [22] motivate us to apply the constant thinning model from Section 5.2. Specifically, we selectively remove atoms to perturb the structured arrangement and then employ connected persistence diagrams to evaluate the structural changes. We work in homology dimension one throughout this example.

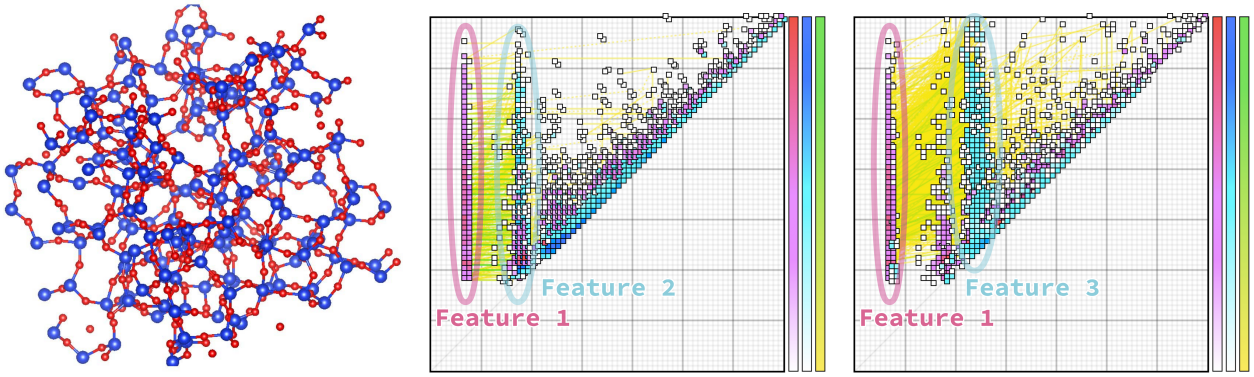

(a) (b) (c)

Figure 6.8: (a) Atomic representation of silica with chemical bonds illustrated. Blue balls represent silicon atoms, and red balls represent oxygen atoms. (b) The connected persistence diagram of the configuration with all silicon atoms removed. (c) The connected persistence diagram of the configuration with half of the oxygen atoms removed.

Let M be a persistence module of $\mathsf{CL}(n)$ obtained from a thinning model. Recall that a connected persistence diagram directly visualizes $\widetilde{\delta}_M$ (where the superscript for the essential assignment is omitted). Each layered presentation in Figure 6.8 is plotted following the rules below:

- $\widetilde{\delta}_M\big|_{\mathbb{I}_1}$: corresponds to the standard persistence diagram of the post-thinning point cloud, visualized with the middle color bar where color saturation indicates multiplicity values.

- $\widetilde{\delta}_M\big|_{\mathbb{I}_2}$: corresponds to the standard persistence diagram of the original silica molecules, visualized with the left color bar.

- $\widetilde{\delta}_M\big|_{\mathbb{I}_{2/1}}$: corresponds to vertical persistence between generators, visualized with the right color bar, with dashed lines implying negative multiplicity and the color saturation signifying the absolute value of multiplicity.

Although generators near the diagonal line overlap, the main features in the diagrams remain clear.

Case 1: Removing All Silicon Atoms

This scenario assesses topological changes when all silicon atoms are removed while oxygen atoms are left intact. The most prominent features before and after the thinning are labeled as Feature 1 and 2 in Figure 6.8b. These two features appear to persist through the thinning process, but that cannot be justified using the standard persistence diagrams alone. This observation is confirmed here by the numerous horizontal green connecting lines between the two features. Therefore, we conclude that the main feature's birth is delayed, with its basic structure maintained.

Case 2: Thinning Out Oxygen Atoms at a 50% Rate

Half of the oxygen atoms are removed in this case, while silicon atoms are untouched. This amounts to a similar number of atoms being removed compared with Case 1. Contrary to the first case, the primary topological feature shows significant deformation, as can be seen by many more line segments emanating from Feature 1 but not terminating within Feature 3. For those line segments connecting Feature 1 and Feature 3, we observe that the transition distance is much longer, and the angles are steeper, reflecting delayed birth and death, exhibiting a more substantial structural disruption.

This comparative analysis demonstrates that the connected persistence diagrams effectively reveal how different thinning strategies affect the structure.

6.3.2 Face-Centered Cubic and Hexagonal Close Packing

Face-centered cubic (FCC) and hexagonal close packing (HCP) are two packings of equal spheres in three-dimensional space, seen in various materials. These two packings share many common properties and cannot be distinguished using standard persistence diagrams in any dimension. This challenge has sparked numerous research efforts within the community. Hiraoka et al. [25] demonstrated that the persistence diagrams of the two structures after a thinning process are topologically distinct. Meanwhile, Osang et al. [39] proposed k-fold covers, which modify the growing-radius ball model typically used to obtain a filtration of simplicial complexes from a given point cloud, to distinguish these two structures.

Figure 6.9a illustrates one layer of a packing. If this layer serves as the base 2D plane, the relative position of any succeeding layer is determined by projecting the center of any sphere from that layer onto this base. We label potential projection points as A, B, and C. If the next layer projects at B, then the third layer could be A or C. Maintaining a periodic packing pattern up until now across all layers, a choice of C for the third layer results in a layer sequence ABCABC. . ., characteristic of FCC packing. Conversely, choosing position

A for the third layer yields a layer sequence ABABAB. . ., referred to as HCP. For the subsequent discussion, we assume spheres with a radius of one and a homology dimension of two.

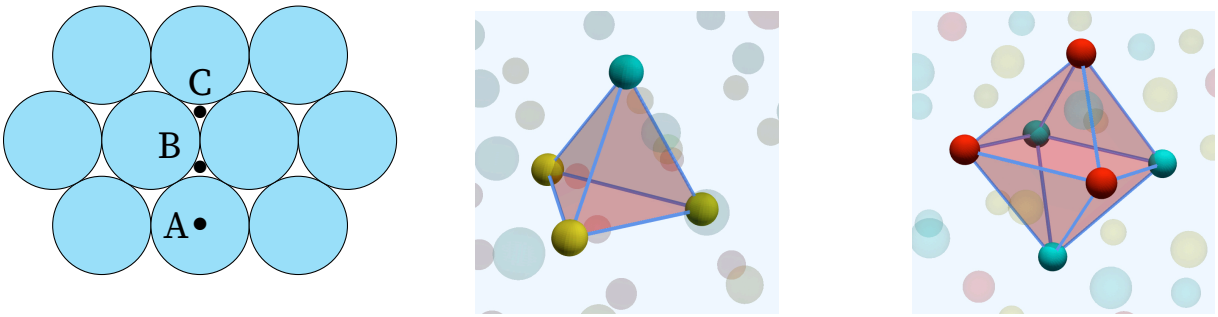

(a) (b) (c)

Figure 6.9: (a) Single layer illustration of a close packing. (b) A two-dimensional homology generator in FCC with spheres colored by layer. Its HCP counterpart shares the same shape. (c) Another type of homology generator in FCC. Notice that only two adjacent layers are involved, so we also have this in HCP.

The standard persistence diagrams of FCC and HCP are identical to the upper half triangular region of Figure 6.10a and 6.10b respectively. The generator closer to the diagonal line arises from tetrahedron structures formed by four neighboring atoms, as illustrated in Figure 6.9b. Another generator corresponds to the octahedron shown in Figure 6.9c. We utilize a patterned thinning model as discussed in Section 5.2 to discern the subtle topological differences between these two packings. Specific to this context, we remove tetrahedral structures randomly to create a $\mathsf{CL}(n)$-filtration, and we restrict to removing only one such structure to make the explanation more intuitive.

Figure 6.10 shows the resulting connected persistence diagrams and the homology generators post-thinning obtained via inverse analysis [38]. Notice that the deaths of the two labeled generators in the diagrams are different [6]. We represent each such generator as a brown cage in Figure 6.10c and 6.10d, where faces are omitted for visual clarity. The red points within each cage represent the tetrahedron structure removed during the thinning, and we depict how each large cage can contain one original octahedron generator once embedded back into the upper row in the $\mathsf{CL}(n)$-filtration. This relation is reflected in the connected persistence diagram via the connecting line between the octahedron generator and the cage generator.

[6] We record the numerical values of birth and death obtained in the experiment, but their analytical values are also computable. The one for FCC is $(\frac{2\sqrt{3}}{3}, \frac{\sqrt{22}}{2})$, and for HCP it is $(\frac{2\sqrt{3}}{3}, \frac{11\sqrt{6}}{12})$.

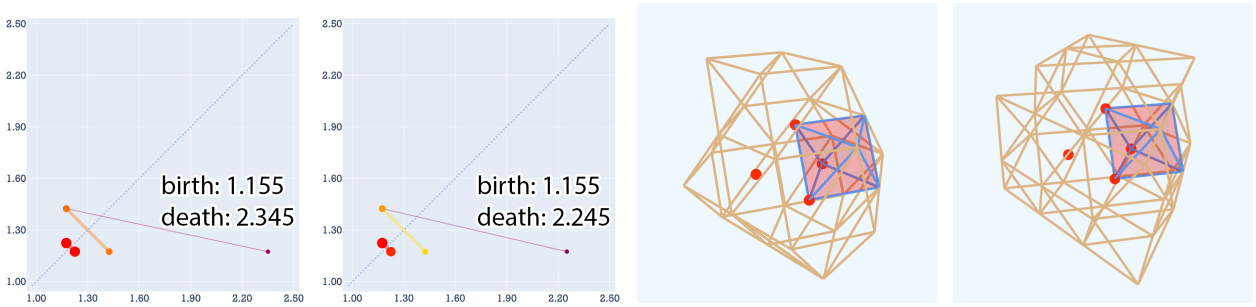

(a) (b) (c) (d)

Figure 6.10: (a) The connected persistence diagram for the FCC configuration. (b) The connected persistence diagram for the HCP configuration. (c) The new generator post-thinning in FCC. (d) The new generator post-thinning in HCP.

7 Concluding Remarks

Refining interval approximations has led to notable advancements. The novel framework has broadened the scope of defining invariants on a given interval via accommodating courses of diverse and valid shapes. This discovery reveals hidden complexities within intervals and unlocks the potential for discovering intricate non-interval structures. Furthermore, the partial interval approximation offers a practical invariant for general commutative grids. When applied to the commutative ladders, our framework yields an efficient method for the indecomposable decomposition of finite-type commutative ladders. The algorithm, as detailed in Section 4.1, can potentially be instrumental in computing the decomposition of broader cases beyond its current application, especially when decomposability is restricted to a finite set. This indicates a vast horizon of unexplored courses, hinting at the potential discovery of more intricate non-interval structures. For general commutative ladders, the introduction of the connected persistence diagram facilitates the simultaneous visualization of horizontal and non-horizontal persistence, addressing a critical need in the field. Based on the new toolkit and proposed models for the construction of commutative ladder filtrations, we provided insights that stand among the early works analyzing the behavior of non-intervals, and employed connected persistence diagrams to unveil hidden topological information in material structures.

The future of this work is rich with possibilities. Research on vectorizing interval approximations through kernel embedding, aiming to catalyze further integration with machine learning techniques, is ongoing. Connected persistence diagrams offer a versatile tool for studying configurations adaptable to commutative ladder filtrations. Along with enriched thinning techniques, they can evaluate the robustness of topological features in point clouds against the removal of a designated type of structure, termed a "topological attack" on the original point cloud. Additionally, the sublevel set model, used for generating commutative ladder filtrations, has broader applications beyond point cloud thinning. It can be instrumental in analyzing relationships between different multi-covers, as discussed in Edelsbrunner's work [16], and in investigating the changes in topological properties of neural networks during pruning processes. Overall, this work has pushed the boundaries of persistent homology by offering a framework for uncovering intricate topological structures and paving the way for future discoveries in diverse domains.

A Appendices

A.1 Enumeration Algorithm for Finding Alternating Zigzag Courses

Algorithm 1 is an enumeration algorithm that illustrates the procedures for discovering alternating zigzag courses. This approach involves examining all type $\mathbb{A}_n$ courses with an increasing number of paths up to a predetermined threshold value N.

Algorithm 1: Searching for all type $\mathbb{A}_n$ alternating zigzag courses with $n \leq N$ (via enumeration)

Data: a fully commutative quiver G
Result: a list of all type $\mathbb{A}_n$ alternating zigzag courses in G with $n \leq N$

$P \leftarrow$ the set of all non-trivial paths in G `// P is finite as G is finite and acyclic`
$J \leftarrow \{ \left(A_1 = \underset{1}{\bullet}, F\colon 1 \mapsto v\right) \mid v \in G_0 \}$ `// initialize with type` $\mathbb{A}_1$ `courses`
for n *in* $\{ 2, \ldots, N \}$ **do**
  for $(p_1, \ldots, p_{n-1})$ *in* $\underbrace{P \times P \times \cdots \times P}_{n-1}$ **do**
    `// iterate over all` $(n-1)$`-tuples of paths in` P
    if $(p_1, \ldots, p_{n-1})$ *determines an alternating zigzag course* (A_n, F) `// see Remark 4.4`
    then
      add (A_n, F) to J
    end
  end
end
return J

A.2 BFS Algorithm for Finding Alternating Zigzag Courses

Algorithm 2 provides a more efficient algorithm to find alternating zigzag courses using a breadth-first search (BFS) approach.

Algorithm 2: Searching for all type $\mathbb{A}_n$ alternating zigzag courses with $n \leq N$ (via BFS)

Data: a fully commutative quiver G
Result: a list of all type $\mathbb{A}_n$ alternating zigzag courses on G for $n \leq N$

$startsFrom \leftarrow$ a hash map
$endsAt \leftarrow$ a hash map
for v *in* G_0 **do**
    $startsFrom(v) \leftarrow$ the set of non-trivial paths in G that start from v
    $endsAt(v) \leftarrow$ the set of non-trivial paths in G that end at v
end
$J \leftarrow \{ \left(A_1 = \underset{1}{\bullet}, F\colon 1 \mapsto v\right) \mid v \in G_0 \}$ `// initialize with type` $\mathbb{A}_1$ `zigzag courses`
$queue \leftarrow \{ \left(A_1 = \underset{1}{\bullet}, F\colon 1 \mapsto v\right) \mid v \in G_0 \}$ `// initialize the queue for BFS`
while $queue$ *is not empty* **do**
    $currentCourse \leftarrow queue.popleft()$
    $n \leftarrow n$ as the value in $currentCourse$ being a type $\mathbb{A}_n$ course
    if $n + 1 > N$ **then**
        break `// break loop since all required alternating zigzag courses have been processed`
    end
    $lastVertex \leftarrow$ the last vertex in $currentCourse$ `// this vertex can be obtained as` $F(n)$
    if $n \mod 2 == 1$ **then**
        $pathsToBeAttached = startsFrom(lastVertex)$ `// attach rightward paths`
    else
        $pathsToBeAttached = endsAt(lastVertex)$ `// attach leftward paths`
    end
    for $newPath$ *in* $pathsToBeAttached$ **do**
        $newCourse \leftarrow appendTo(currentCourse, newPath)$ `// form a longer alternating zigzag course by appending` $newPath$ `to` $currentCourse$
        add $newCourse$ to J
        $queue.append(newCourse)$
    end
end
return J

A.3 Algorithm for Extracting Linearly Independent Functions

Algorithm 3 obtains a linearly independent set from the associated functions of a set of alternating zigzag courses. When a function is evaluated on the pre-determined set $\mathcal{L}$, it provides a new row for our coefficient matrix. Each entry in this row is the multiplicity of the longest interval in a zigzag persistence module, which can be calculated using existing software packages such as [11] and [36]. This algorithm then iteratively appends rows to the coefficient matrix until the matrix's rank reaches $|\mathcal{L}|$ or all potential candidates have been considered.

Algorithm 3: Extracting linearly independent functions from a set of alternating zigzag courses

Data: a fully commutative quiver G; a finite subset $\mathcal{L}$ of the isomorphism classes; a base field $\Bbbk$ for the path algebra; a set J of alternating zigzag courses
Result: a rank $|\mathcal{L}|$ coefficient matrix C if it exists

$C \leftarrow$ an empty matrix // initialize the coefficient matrix
$r \leftarrow 0$ // for keeping track of the rank
for (A_n, F) *in* J **do**
  $f(-) \leftarrow d_{\mathrm{tour}_{(A_n,F)}(-)}(V_{A_n})$ // multiplicity of the longest interval in $\mathrm{tour}_{(A_n,F)}(-)$.
  $C_{\mathrm{new}} \leftarrow \begin{pmatrix} C \\ \hline \{f(L)\}_{L\in\mathcal{L}} \end{pmatrix}$ // add a new row to C by incorporating the new function
  $r_{\mathrm{new}} \leftarrow \mathrm{rank}(C_{\mathrm{new}})$
  if $r_{new} > r$ // update the coefficient matrix only if the new function increases the rank
  then
    $C \leftarrow C_{\mathrm{new}}$
    $r \leftarrow r_{\mathrm{new}}$
  end
  if $r == |\mathcal{L}|$ **then**
    return C
  end
end
raise Exception("Insufficient courses in the input to solve a general $\mathcal{L}$-decomposition.")

References

[1] Asashiba, H., Buchet, M., Escolar, E. G., Nakashima, K., and Yoshiwaki, M.: On interval decomposability of 2D persistence modules. *Computational Geometry* (2022). https://doi.org/10.1016/j.comgeo.2022.101879

[2] Asashiba, H., Escolar, E. G., Nakashima, K., and Yoshiwaki, M.: Approximation by interval-decomposables and interval resolutions of persistence modules. *Journal of Pure and Applied Algebra* (2023). https://doi.org/10.1016/j.jpaa.2023.107397

[3] Asashiba, H., Escolar, E. G., Nakashima, K., and Yoshiwaki, M.: On approximation of 2D persistence modules by interval-decomposables. *Journal of Computational Algebra* (2023). https://doi.org/10.1016/j.jaca.2023.100007

[4] Asashiba, H., Nakashima, K., and Yoshiwaki, M.: Decomposition theory of modules: the case of Kronecker algebra. *Japan Journal of Industrial and Applied Mathematics* (2017). https://doi.org/10.1007/s13160-017-0247-y

[5] Assem, I., Skowronski, A., and Simson, D.: *Elements of the Representation Theory of Associative Algebras: Techniques of Representation Theory*. Cambridge University Press, Cambridge (2006). https://doi.org/10.1017/CBO9780511614309

[6] Betti, E.: Sopra gli spazi di un numero qualunque di dimensioni. *Annali di Matematica Pura ed Applicata (1867-1897)* (1870). https://doi.org/10.1007/BF02420029. https://doi.org/10.1007/BF02420029

[7] Carlsson, G.: Topology and data. *Bulletin of the American Mathematical Society* (2009). https://doi.org/10.1090/S0273-0979-09-01249-X

[8] Carlsson, G. and Silva, V. de: Zigzag Persistence. *Foundations of Computational Mathematics* (2010). https://doi.org/10.1007/s10208-010-9066-0. https://doi.org/10.1007/s10208-010-9066-0

[9] Carlsson, G. and Zomorodian, A.: The theory of multidimensional persistence. *Discrete & Computational Geometry* (2009). https://doi.org/10.1007/s00454-009-9176-0

[10] Chung, M. K., Bubenik, P., and Kim, P. T.: Persistence Diagrams of Cortical Surface Data. *Information Processing in Medical Imaging* (2009). https://doi.org/10.1007/978-3-642-02498-6_32

[11] Dey, T. K. and Hou, T.: Fast Computation of Zigzag Persistence. *30th Annual European Symposium on Algorithms (2022)*. https://doi.org/10.4230/LIPIcs.ESA.2022.43

[12] Dey, T. K., Kim, W., and Mémoli, F.: Computing Generalized Rank Invariant for 2-Parameter Persistence Modules via Zigzag Persistence and Its Applications. *38th International Symposium on Computational Geometry (2022)*. https://doi.org/10.4230/LIPIcs.SoCG.2022.34

[13] Giunti, B., Lazovskis, J., and Rieck, B.: *DONUT: Database of Original & Non-Theoretical Uses of Topology*. 2022 (2022). https://donut.topology.rocks

[14] Edelsbrunner, H., Letscher, D., and Zomorodian, A.: Topological Persistence and Simplification. In: *Proceedings of the 41st Annual Symposium on Foundations of Computer Science (2000)*. https://dl.acm.org/doi/10.5555/795666.796607

[15] Edelsbrunner, H. and Harer, J.: *Computational Topology: An Introduction*. American Mathematical Society, Providence (2010). https://doi.org/10.1090/mbk/069

[16] Edelsbrunner, H. and Osang, G.: The Multi-Cover Persistence of Euclidean Balls. *Discrete & Computational Geometry* (2021). https://doi.org/10.1007/s00454-021-00281-9

[17] Erdős, P. and Rényi, A.: On the evolution of random graphs. In: *A Magyar Tudományos Akadémia. Matematikai Kutató Intézetének Közleményei* (1960). https://static.renyi.hu/~p_erdos/1960-10.pdf

[18] Escolar, E. G. and Hiraoka, Y.: Persistence modules on commutative ladders of finite type. *Discrete & Computational Geometry* (2016). https://doi.org/10.1007/s00454-015-9746-2

[19] Euler, L.: Solutio problematis ad geometriam situs pertinentis. In: *Commentarii academiae scientiarum Petropolitanae* (1741). https://archive.org/details/commentariiacade08impe/page/128/mode/2up

[20] Frosini, P.: Measuring shapes by size functions. *Intelligent Robots and Computer Vision X: Algorithms and Techniques (1992)*. International Society for Optics and Photonics. https://doi.org/10.1117/12.57059

[21] Gabriel, P.: Unzerlegbare Darstellungen I. *manuscripta mathematica* (1972). https://doi.org/10.1007/BF01298413

[22] Hiraoka, Y., Nakamura, T., Hirata, A., Escolar, E. G., Matsue, K., and Nishiura, Y.: Hierarchical structures of amorphous solids characterized by persistent homology. *Proceedings of the National Academy of Science* (2016). https://doi.org/10.1073/pnas.1520877113

[23] Hiraoka, Y., Nakashima, K., Obayashi, I., and Xu, C.: *Online Supplement for "Interval Approximations for Fully Commutative Quivers and Their Applications"*. https://ladder-invariants.netlify.app (2023). Accessed 06 October 2023

[24] Hiraoka, Y., Nakashima, K., Obayashi, I., and Xu, C.: Refinement of Interval Approximations for Fully Commutative Quivers. *arXiv e-prints* (2023). https://doi.org/10.48550/arXiv.2310.03649

[25] Hiraoka, Y., Obayashi, I., and Akagi, K.: Persistent Homology and Structural Analysis in Materials Science. *Journal of the Japanese Society for Artificial Intelligence* (2019). https://doi.org/10.11517/jjsai.34.3_330

[26] Hiraoka, Y. and Shirai, T.: Minimum spanning acycle and lifetime of persistent homology in the Linial-Meshulam process. *Random Structures & Algorithms* (2017). https://doi.org/10.1002/rsa.20718

[27] Hong, S. and Kim, D.: Medium-range order in amorphous ices revealed by persistent homology. *Journal of Physics: Condensed Matter* (2019). https://doi.org/10.1088/1361-648X/ab3820

[28] Kim, W. and Mémoli, F.: Generalized persistence diagrams for persistence modules over posets. *Journal of Applied and Computational Topology* (2021). https://doi.org/10.1007/s41468-021-00075-1

[29] Kim, W. and Moore, S.: Bigraded Betti numbers and Generalized Persistence Diagrams. *arXiv e-prints* (2021). https://doi.org/10.48550/arXiv.2111.02551

[30] Le Roux, S. and Petkov, V.: *ISAACS* – interactive structure analysis of amorphous and crystalline systems. *Journal of Applied Crystallography* (2010). https://doi.org/10.1107/S0021889809051929

[31] Lesnick, M. and Wright, M.: Interactive Visualization of 2-D Persistence Modules. *arXiv e-prints* (2015). https://doi.org/10.48550/arXiv.1512.00180

[32] Li, M., An, H., Angelovici, R., Bagaza, C., Batushansky, A., Clark, L., Coneva, V., Donoghue, M. J., Edwards, E., Fajardo, D., Fang, H., Frank, M. H., Gallaher, T., Gebken, S., Hill, T., Jansky, S., Kaur, B., Klahs, P. C., Klein, L. L., Kuraparthy, V., Londo, J., Migicovsky, Z., Miller, A., Mohn, R., Myles, S., Otoni, W. C., Pires, J. C., Rieffer, E., Schmerler, S., Spriggs, E., Topp, C. N., Van Deynze, A., Zhang, K., Zhu, L., Zink, B. M., and Chitwood, D. H.: Topological Data Analysis as a Morphometric Method: Using Persistent Homology to Demarcate a Leaf Morphospace. *Frontiers in Plant Science* (2018). https://doi.org/10.3389/fpls.2018.00553

[33] Linial, N. and Meshulam, R.: Homological connectivity of random 2-complexes. *Combinatorica* (2006). https://doi.org/10.1007/s00493-006-0027-9

[34] Listing, J. B.: *Vorstudien zur Topologie*. German. Digitized in 2009, Available at: http://resolver.sub.uni-goettingen.de/purl?PPN575020857. Vandenhoeck and Ruprecht, Göttingen (1848)

[35] McGuirl, M. R., Volkening, A., and Sandstede, B.: Topological data analysis of zebrafish patterns. *Proceedings of the National Academy of Sciences* (2020). https://doi.org/10.1073/pnas.1917763117

[36] Morozov, D.: *Dionysus 2, a library for computing persistent homology*. https://www.mrzv.org/software/dionysus2 (2023). Accessed 06 October 2023

[37] Nicolau, M., Levine, A. J., and Carlsson, G.: Topology based data analysis identifies a subgroup of breast cancers with a unique mutational profile and excellent survival. *Proceedings of the National Academy of Sciences* (2011). https://doi.org/10.1073/pnas.1102826108

[38] Obayashi, I., Nakamura, T., and Hiraoka, Y.: Persistent Homology Analysis for Materials Research and Persistent Homology Software: HomCloud. *Journal of the Physical Society of Japan* (2022). https://doi.org/10.7566/JPSJ.91.091013

[39] Osang, G., Edelsbrunner, H., and Saadatfar, M.: Topological signatures and stability of hexagonal close packing and Barlow stackings. *Soft Matter* (2021). https://doi.org/10.1039/D1SM00774B

[40] Oudot, S. Y.: *Persistence Theory - From Quiver Representations to Data Analysis.* American Mathematical Society, Providence (2015). https://bookstore.ams.org/surv-209

[41] Oyama, A., Hiraoka, Y., Obayashi, I., Saikawa, Y., Furui, S., Shiraishi, K., Kumagai, S., Hayashi, T., and Kotoku, J.: Hepatic tumor classification using texture and topology analysis of non-contrast-enhanced three-dimensional T1-weighted MR images with a radiomics approach. *Scientific Reports* (2019). https://doi.org/10.1038/s41598-019-45283-z

[42] Patel, A.: Generalized persistence diagrams. *Journal of Applied and Computational Topology* (2018). https://doi.org/10.1007/s41468-018-0012-6

[43] Poincaré, H.: Analysis Situs. In: *Journal de l'École Polytechnique* (1895). https://gallica.bnf.fr/ark:/12148/bpt6k4337198/f7.image

[44] Pranav, P., Adler, R. J., Buchert, T., Edelsbrunner, H., Jones, B. J. T., Schwartzman, A., Wagner, H., and Weygaert, R. van de: Unexpected topology of the temperature fluctuations in the cosmic microwave background. *Astronomy & Astrophysics* (2019). https://doi.org/10.1051/0004-6361/201834916

[45] Pranav, P., Edelsbrunner, H., Weygaert, R. van de, Vegter, G., Kerber, M., Jones, B. J. T., and Wintraecken, M.: The topology of the cosmic web in terms of persistent Betti numbers. *Monthly Notices of the Royal Astronomical Society* (2016). https://doi.org/10.1093/mnras/stw2862

[46] Rabadán, R., Mohamedi, Y., Rubin, U., Chu, T., Alghalith, A. N., Elliott, O., Arnés, L., Cal, S., Obaya, Á. J., Levine, A. J., and Cámara, P. G.: Identification of relevant genetic alterations in cancer using topological data analysis. *Nature Communications* (2020). https://doi.org/10.1038/s41467-020-17659-7

[47] Riemann, B.: Theorie der Abel'schen Functionen. In: (1857). https://www.emis.de/classics/Riemann/AbelFn.pdf

[48] Robins, V.: Towards Computing Homology from Finite Approximations. In: *Topology Proceedings* (1999). Electronic version appeared 5 March 2001. https://topology.nipissingu.ca/tp/reprints/v24/tp24222.pdf

[49] Sørensen, S. S., Biscio, C. A. N., Bauchy, M., Fajstrup, L., and Smedskjaer, M. M.: Revealing hidden medium-range order in amorphous materials using topological data analysis. *Science Advances* (2020). https://doi.org/10.1126/sciadv.abc2320

[50] Xia, K. and Wei, G.-W.: Persistent homology analysis of protein structure, flexibility, and folding. *International Journal for Numerical Methods in Biomedical Engineering* (2014). https://doi.org/https://doi.org/10.1002/cnm.2655

[51] Xu, X., Cisewski-Kehe, J., Green, S. B., and Nagai, D.: Finding cosmic voids and filament loops using topological data analysis. *Astronomy and Computing* (2019). https://doi.org/10.1016/j.ascom.2019.02.003

[52] Zomorodian, A. and Carlsson, G.: Computing Persistent Homology. *Proceedings of the Twentieth Annual Symposium on Computational Geometry (2004)*. https://doi.org/10.1145/997817.997870